Published on p.25-94 of S. Kalliadasis and U. Thiele (eds.), Thin films of soft matter. Springer Wien / New York, ISBN 978-3-211-69807-5 (2007).

Structure formation in thin liquid films

Uwe Thiele

Max-Planck-Institut für Physik komplexer Systeme, Nöthnitzer Str. 38, D-01187 Dresden, Germany

Abstract

We outline some recent developments in the theoretical description of structure formation in thin liquid films. The main focus lies on systems involving a single layer of liquid on a solid substrate that can be described using an evolution equation for the film thickness profile. Reviewing the history of the subject we sketch important experimental and theoretical results and practical applications. After establishing the systematics of the present text we introduce the common mathematical framework for studies of thin films of soft matter, namely by deriving the generic evolution equation for such films from the Navier-Stokes equations. In the main part we first introduce the different possible geometries and the transitions between them, i.e. from homogeneous to inhomogeneous substrates, or from horizontal to inclined substrates. We then present the physical questions posed by the individual systems and discuss approaches and results for

- Dewetting on a horizontal homogeneous substrate. We investigate the solution structure and its consequences for the system behaviour. For the initial film rupture we distinguish nucleation-dominated and instability-dominated behaviour for linearly unstable thin films.
- Dewetting on a horizontal inhomogeneous substrate. The solution structure of the governing equation is analysed in dependence of the strength of a chemical heterogeneity. We describe a pinning-coarsening transition with a large range of multistability, implying a large hysteresis and strong dependence on initial conditions and noise.
- Heated thin films on a horizontal homogeneous substrate. We discuss nucleation and drop solutions and show that it is possible to construct all drop solutions separated by dry regions. Incorporating a disjoining pressure allows to study the coarsening behaviour of the drop pattern.
- Sliding drops on an inclined homogeneous substrate. Using a model that incorporates a disjoining pressure allows to calculate the usually used ad-hoc parameters of models for moving contact lines from surface chemistry. The involved transition from a Cahn-Hilliard-like to a Kuramoto-Sivashinsky-like dynamics that occurs for increasing inclination angle is discussed in passing for heated films.
- Transversal instabilities of a liquid ridge are discussed encompassing all the above geometries. Particular interest lies on the stabilisation of such an instability due to stripe-like heterogeneities for a resting ridge on a horizontal substrate and on the drastic change in the mode type when inclining the substrate. It changes from a symmetric varicose mode (horizontal substrate) via

Manuscript —- contact: thiele@pks.mpg.de – http://www.uwethiele.de – 10th March 2006

Published on p.25-94 of S. Kalliadasis and U. Thiele (eds.), Thin films of soft matter. Springer Wien / New York, ISBN 978-3-211-69807-5 (2007).

an asymmetric varicose mode via an asymmetric zigzag mode to decoupled front and back modes.

Finally, we shortly discuss extensions of thin film studies beyond the case of a single evolution equation. In particular, we introduce two different models based on two coupled evolution equations describing the dynamics of dewetting of a two-layer thin film and the chemically driven self-propelled movement of droplets, respectively.

Contents

Manuscript —- contact: thiele@pks.mpg.de – http://www.uwethiele.de – 10th March 2006

Published on p.25-94 of S. Kalliadasis and U. Thiele (eds.), Thin films of soft matter. Springer Wien / New York, ISBN 978-3-211-69807-5 (2007).

Manuscript —- contact: thiele@pks.mpg.de – http://www.uwethiele.de – 10th March 2006

1 Introduction

1.1 History

For centuries thin liquid films have attracted the interest of scientists and layman alike due to their fascinating behaviour and presence in everyday life. The most prominent example are probably soap films whose beauty is appreciated by almost everyone. Their properties were investigated by scientists like (Newton, 1730, Book II, Part 1, Obs. 17-19), Thomson (1887) or Plateau (1873).

Beside these freely suspended films also thin liquid layers between two solid substrates were studied very early. Films and drops between two parallel plates were used to investigate capillary effects also already by (Newton, 1730, Book III, Part 1, Querie 31) (following the experimentalist Hauksbee (1708, 1710)). However, our understanding is rather based on the explanations given later by Young (1805) and Laplace (1806). The physical principles of the use of thin films for lubrication purposes were analysed by Reynolds (1886). He laid the foundation for their description as slow viscous flow in lubrication approximation that was later built on by Sommerfeld (1904) and others.

Intermediate between the free films and the films between two solid supports one encounters liquid films that are bounded on one side by a solid substrate but have a free surface on the other side. This type of films will concern us here. They were mentioned early in connection with liquid flow driven by surface tension gradients by Thomson (1855) in his description of the phenomenon of the tears of wine, and also by Tomlinson (1870) and Marangoni (1871) referring to experiments on the spreading of surface active substances on thin films of water[1]. Free surface thin films are also the basis for studying surface waves and localized structures at the surface of a thin viscous layer flowing down an inclined plate. Starting with the experiments by the Kapitzas (Kapitza, 1949; Kapitza and Kapitza, 1949) the system became paradigmatic for the study of this type of structure formation (see the review by Chang (1994) and the beginning of Section 5.2).

Nowadays, thin liquid films on solid substrates are studied in a wide range of fields and have numerous applications. The spectrum ranges from films of sub-micrometer thickness (Ruckenstein and Jain, 1974; Kheshgi and Scriven, 1991) to studies of lava flows (Huppert, 1982; Balmforth et al., 2004). This indicates that 'thin' does not refer to an absolute film thickness, but rather to the fact that the films are thin as compared to typical length-scales parallel to the substrate. Representatives of medical interest are the tear film in the eye (Lin and Brenner, 1982; Sharma and Ruckenstein, 1985) and the aqueous lung lining (Gaver and Grotberg, 1990). Heat and mass transfer devices, like falling film evaporators rely on the heat-transfer properties and stability of falling thin liquid films (Bankoff, 1994). Thin films also gained increasing importance in coating technology. Beside the use as protective and aesthetic coatings that favours stable homogeneous films also the capacity of the films to structure themselves in the nanometer range renewed the interest in the dynamics of such films. The importance of structured and non-structured coatings in many fields of modern technology led to a still growing series of studies of the structuring process of ultrathin films with thicknesses below 100 nm

[1] The history of the study of capillary phenomena (Hardy, 1922; Millington, 1945; Scriven and Sternling, 1960) offers more examples involving thin films.

Manuscript — contact: thiele@pks.mpg.de – http://www.uwethiele.de – 10th March 2006

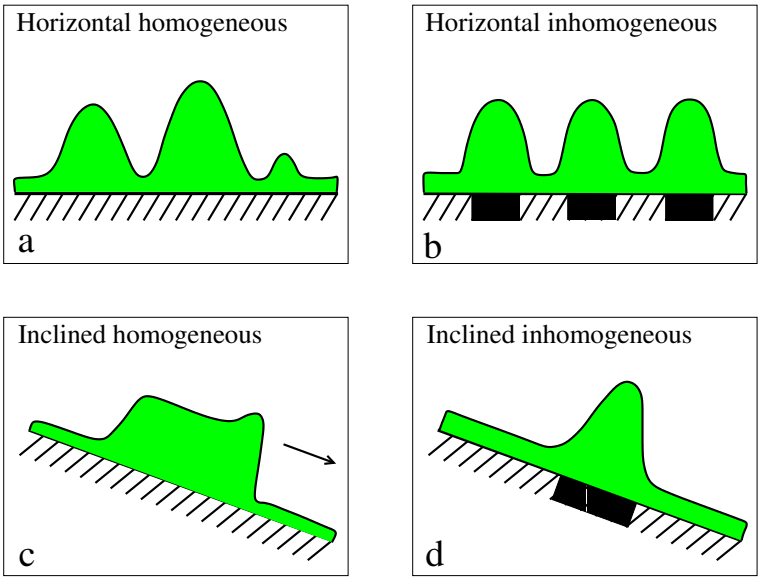

Figure 1. Sketch of the four basic geometries involving a single liquid layer on a solid substrate.

that are unstable due to effective molecular forces. These experiments on dewetting were pioneered by Reiter (1992) using polymer films and are continued by a number of groups (for a review see Thiele (2003a) and the chapter by Seemann et al. in the present book). Thereby all phases of the process are of interest (Brochard-Wyart and Daillant, 1989; Brochard-Wyart et al., 1992): the initial film rupture (Reiter, 1992; Seemann et al., 2001a), the growth of individual holes in the film (Redon et al., 1991; Seemann et al., 2001b), the evolution of the resulting hole pattern (Sharma and Reiter, 1996), and the stability of the individual dewetting fronts (Brochard-Wyart and Redon, 1992; Reiter and Sharma, 2001). The cursory overview of the literature given at this point is supplemented by more detailed synopses in the presentations of the specific physical situations below.

1.2 Systematics

In Sections 1 and 2 we introduce the general subject of thin liquid films whereas the following Sections are devoted to more detailed presentations of the specific models used and the individual physical situations studied. We do not discuss every situation individually, but group them according to their symmetry properties to emphasize that these mainly determine the qualitative behaviour. Based on substrate properties and acting forces one can distinguish four basic geometries as sketched in Fig. 1:

(a) A film on a horizontal homogeneous substrate is in a situation of maximal sym-

metry. The situation is invariant with respect to translation along the substrate and reflection at a plane orthogonal to the substrate[2]. This type of films will be introduced in Section 3 using the examples of dewetting on a smooth homogeneous substrate (Reiter, 1992) and of the pattern formation of a thin film on a homogeneously heated substrate (VanHook et al., 1997).

There are three ways to break these symmetries to arrive at the less symmetric situations (b) to (d):

(b) The translational symmetry is broken for a film on a horizontal inhomogeneous substrate as encountered for dewetting on a physically or chemically patterned substrate (Rehse et al., 2001) or for a film on an inhomogeneously heated plate (Burelbach et al., 1990; Tan et al., 1990). The heterogeneity especially influences processes where translational modes are involved as is the case in coarsening. This case is introduced in Section 4.

(c) The reflection symmetry is broken if an additional force is acting parallel to the substrate as for a flowing film or sliding droplet on an inclined homogeneous substrate (Kapitza and Kapitza, 1949; Podgorski et al., 2001) where the driving force is gravitation. Also a temperature or chemical gradient along the substrate leads to this situation (Brochard, 1989). Here we will use the inclined case as example to discuss moving drops and unstable fronts. It is introduced in Section 5.

(d) Both, the translational and reflection symmetry are broken on an inclined inhomogeneous substrate as encountered for films flowing on an inclined locally heated plate (Kabov and Marchuk, 1998) or droplets pinned by heterogeneities on an incline (Quéré et al., 1998).

All the situations covered by (a) to (d) can be described by a single partial differential equation for the evolution of the film thickness profile. This allows to move freely between the different geometries and to draw on results from the respective 'neighboring' ones. Excluding evaporation and condensation processes the governing equation is of the most general type for the evolution of a single conserved order parameter field (Langer, 1992). The basic formalism is introduced in Section 2, whereas Sections 3 to 5 are devoted to the above introduced situations (a) to (c). Situation (d) will only be mentioned in passing at the end of Section 5. Section 6 is devoted to the question of transversal contact line instabilities that are important in all the situations (a) to (d).

Finally, in Section 7 we leave the framework of a single evolution equation by focusing our interest on situations involving thin films where more degrees of freedom have to be taken into account. In the simplest case, two order parameter fields instead of only one are needed to model the dynamics. On general grounds one can distinguish two situations: (i) The second field beside the film thickness profile represents also a conserved order parameter like for a two-layer ultrathin film studied in Section 7.1 or (ii) the second field corresponds to a non-conserved order parameter like for the chemically driven droplets discussed in Section 7.2. In Section 8 we draw some conclusions, discuss open questions and give an outlook.

[2]Note, that the symmetry does not refer to the thickness profile of the film itself because it may evolve towards less symmetric states.

Manuscript —– contact: thiele@pks.mpg.de – http://www.uwethiele.de – 10th March 2006

1.3 Theoretical Approaches

A well established approach to determine the shape and stability of static fronts, droplets and ridges on homogeneous or heterogeneous substrates is based on variations of a suitable free energy functional (de Gennes, 1985; Sekimoto et al., 1987; Lenz and Lipowsky, 1998; Bauer et al., 1999; Bauer and Dietrich, 2000; Brinkmann and Lipowsky, 2002). It has the advantage that it is not restricted to small equilibrium contact angles. However, it is not suited to describe dynamic phenomena or 'dynamic aspects' of the static problem like, for instance, the most dangerous mode for the Rayleigh-like instability of a liquid ridge on a horizontal substrate (cp. results of Sekimoto et al. (1987) and Thiele and Knobloch (2003)).

The theoretical description of the dynamics of thin films with a free surface goes back half a century. Beside modelling the full Navier-Stokes (Salamon et al., 1994; Krishnamoorthy et al., 1995) or Stokes (Boos and Thess, 1999) equations with moving boundaries one can derive a reduced model based on long-wave approximation (Oron et al., 1997). The latter can be applied to all the structuring processes covered here, because the films are thin as compared to the lateral extension of the evolving long-wave structures. The occurrence of short-wave structures whose lateral extension is of the order of the film thickness as convection cells in films heated from below – as described by Bénard (1900) and Rayleigh (1916) – is avoided by choosing parameters properly. Also the interaction of short-wave and long-wave structures is not subject of our presentation (but see Golovin et al. (1994); VanHook et al. (1997)).

The long-wave approximation was used to derive dynamical equations for the evolution of the film thickness profile for falling films by Benney (1966), for free films by Vrij (1966)[3], for films on a heated horizontal substrate by Burelbach et al. (1988), for films on heated slightly inclined plates by Oron and Rosenau (1992), and for ultrathin films on a horizontal substrate by Ruckenstein and Jain (1974). In the latter case the films may be unstable due to acting effective molecular interactions that are incorporated in form of an additional pressure term into the governing equations. This so-called disjoining pressure was introduced by Derjaguin and coworkers in connection with work on the forces acting between two solid plates separated by a thin film (Derjaguin et al., 1987; Dzyaloshinskii et al., 1960). In the simplest case the disjoining pressure only results from the apolar London–van der Waals dispersion forces (Ruckenstein and Jain, 1974), but there may be additional polar short-range contributions (Sharma, 1993b). Mitlin (1993) established the analogy between the surface instability observed for ultrathin films, called spinodal dewetting, and spinodal decomposition studied by Cahn and Hilliard (1958)[4]. Consequently, most results obtained for the decomposition of a binary mixture have a counterpart in the evolution of thin films on horizontal substrates and *vice versa*. One can generally say, that thin films on horizontal substrates follow a Cahn-Hilliard-like dynamics.

Inclining the substrate strongly, inertia has to be taken into account leading in the simplest case to the Benney equation (Benney, 1966). This equation was extended to

[3]Note, that there only the linear stage of the evolution is covered.

[4]However, already Vrij (1966) noted the formal equivalence of the equation for free films to the equation of Cahn (1965) for concentration fluctuations in solutions.

Manuscript —- contact: thiele@pks.mpg.de – http://www.uwethiele.de – 10th March 2006

include the effect of a heated substrate by Joo et al. (1991). Such Benney-like equations were used to perform linear stability analysis (Benjamin, 1957; Yih, 1963), weakly non-linear analysis (Benney, 1966; Gjevik, 1970; Shkadov, 1967), fully non-linear analysis (Joo et al., 1991), to study sideband instabilities (Lin, 1974) and solitary waves (Pumir et al., 1983). The small amplitude limit of the falling film equations corresponds to the Kuramoto-Sivashinsky equation (Kuramoto and Tsuzuki, 1976; Sivashinsky, 1977). Here, we will discuss Benney-type equations only in passing, but will elucidate in Section 5.3 that already for slightly inclined plates, where no inertia is included in the description, Kuramoto-Sivashinsky-type dynamics can be found.

2 The derivation of the film thickness evolution equation

2.1 General approach

A layer of liquid on a solid substrate with a free surface is called a *thin film* if its thickness is small compared to all relevant length scales parallel to the substrate. This refers to substrate properties like length scales of a heterogeneity as well as to typical lateral extensions of the surface profile of the film itself. The latter implies that the slope of the profile has to be small, but does not restrict the amplitude of its modulations. In consequence, *thin film* does by no means refer to some absolute thickness measure but has to be defined individually for each physical situation studied.

In principle, all situations pictured in Fig. 1 are governed by the Navier-Stokes equations with adequate boundary conditions at the substrate and the free surface, i.e. the liquid-gas interface. Usually, at the liquid-gas interface the balance of the stress-tensors is used assuming the gas to be passive. At the substrate usually the no-slip condition is applied. However, also a variety of slip conditions like, for instance, the Navier slip condition are used (Oron et al., 1997; Münch, 2005). For the thin film geometry the velocities parallel to the substrate are large compared to the ones orthogonal to the substrate. Continuity then implies that the gradients orthogonal to the substrate are large compared to the ones parallel to the substrate. This allows to simplify the governing equations using long-wave or lubrication approximation (Oron et al., 1997). A kinematic boundary condition for the free surface asures that the material boundary moves with the velocity of the liquid at the boundary. Putting all this together one derives a fourth order nonlinear partial differential equation describing the time evolution of the film thickness profile. For simplicity we restrict ourselves here to a physically two-dimensional situation where the film thickness $h(t, x)$ depends on the coordinate x only [5].

[5] Note, that in the literature there exist two different ways to count the dimensions. On the one hand, one can derive the dimension from the physical situation, i.e. a drop on a plate represents a three-dimensional situation and an orthogonal cut through a liquid ridge represents a two-dimensional situation. This is what we use throughout the present work. On the other hand, one can base the dimension count on the spatial dimensions the film thickness profile depends on, i.e. drop and cut through a ridge are represented by two- and one-dimensional profiles, respectively.

Manuscript — contact: thiele@pks.mpg.de – http://www.uwethiele.de – 10th March 2006

2.2 Basic equations

The derivation of the thin film equation embarks from the transport equation for the momentum density (Navier-Stokes equations)

$$\varrho \frac{d\vec{v}}{dt} = \nabla \cdot \underline{\tau} + \vec{f} \tag{2.1}$$

where $\vec{v}(x,z)$ and $\vec{f}(x,z)$ are the velocity and a body force field, respectively. We use

$$\vec{v} = \begin{pmatrix} u \\ w \end{pmatrix}, \qquad \vec{f} = \begin{pmatrix} f_1 \\ f_2 \end{pmatrix} \qquad \text{and} \qquad \nabla = \begin{pmatrix} \partial_x \\ \partial_z \end{pmatrix}.$$

In the following we will denote partial derivatives with respect to i either by ∂_i or simply by the subscript i. The body force may be potential, i.e. given by $\vec{f} = -\nabla\phi$. The stress tensor writes

$$\underline{\tau} = -p\underline{I} + \eta(\nabla\vec{v} + (\nabla\vec{v})^T). \tag{2.2}$$

where $p(x,z)$ stands for the pressure field and $\underline{I}$ is the unity tensor. The material derivative is defined by

$$\frac{d}{dt} = \frac{\partial}{\partial t} + (\vec{v}\cdot\nabla). \tag{2.3}$$

The transport equation for the energy writes

$$\varrho c_p \frac{dT}{dt} = k_{th}\nabla^2 T + \frac{\eta}{2}\left[\nabla\vec{v} + (\nabla\vec{v})^T\right]^2 \tag{2.4}$$

where $T(x,z)$ is the temperature field. The last term corresponds to the mechanical work due to inner tensions $(\underline{\tau}\cdot\nabla)\cdot\vec{v}$. Due to its smallness it will be neglected in the following. Finally, for an incompressible liquid one has the continuity equation

$$\nabla\cdot\vec{v} = 0. \tag{2.5}$$

The parameters ρ, η, c_p, and k_{th} are the density, dynamic viscosity, specific heat and thermal conductivity of the liquid, respectively. The kinematic viscosity is $\nu = \eta/\varrho$ whereas the thermal diffusivity is $\kappa_{th} = k_{th}/\varrho c_p$.

2.3 Boundary conditions

The transport equations are accompanied by boundary conditions at the smooth solid substrate and the free surface. We assume for the velocity field at the substrate ($z = 0$) the no-slip and the no-penetration condition

$$\vec{v} = 0. \tag{2.6}$$

At the free surface [$z = h(t,x)$] one has the kinematic condition (surface follows flow field)

$$w = \partial_t h + u\partial_x h \tag{2.7}$$

Manuscript —- contact: thiele@pks.mpg.de – http://www.uwethiele.de – 10th March 2006

and the force equilibrium

$$(\underline{\tau} - \underline{\tau}_{air}) \cdot \vec{n} = K\gamma\,\vec{n} + (\partial_s \gamma)\,\vec{t} \tag{2.8}$$

where the surface derivative is defined by $\partial_s = \vec{t} \cdot \nabla$ and we assume that the ambient air does not transmit any force ($\underline{\tau}_{\rm air} = 0$). The term $p_L = -\gamma K = \gamma \nabla \cdot \vec{n}/2$ corresponds to the Laplace or curvature pressure whereas $\partial_s \gamma$ results from the variation of the surface tension along the surface (caused, for instance, by solutal or thermal Marangoni effects). The latter is modelled in the simplest case by a linear dependence of the surface tension on temperature; $\gamma = \gamma_0 + \gamma_T(T_0 - T)$, where γ_0 is the surface tension at the reference temperature T_0 and $\gamma_T = d\gamma/dT$ at γ_0.

$$\vec{n} = \frac{(-\partial_x h, 1)}{\left(1 + (\partial_x h)^2\right)^{1/2}}, \quad \vec{t} = \frac{(1, \partial_x h)}{\left(1 + (\partial_x h)^2\right)^{1/2}}, \quad K = \frac{\partial_{xx} h}{\left(1 + (\partial_x h)^2\right)^{3/2}}$$

are the normal vector, tangent vector and curvature of the surface, respectively. The boundary condition (2.8) is of vectorial character, i.e. one can derive two scalar conditions by projecting it onto $\vec{n}$ and $\vec{t}$, respectively.

$$\vec{t}: \quad \eta\left[(u_z + w_x)(1 - h_x^2) + 2(w_z - u_x)h_x\right] = \partial_s \gamma (1 + h_x^2) \tag{2.9}$$

$$\vec{n}: \quad p + \frac{2\eta}{1 + h_x^2}\left[-u_x h_x^2 - w_z + h_x(u_z + w_x)\right] = -\frac{\gamma h_{xx}}{(1 + h_x^2)^{3/2}} \tag{2.10}$$

For the temperature field we will assume a constant temperature at the substrate and Newton's cooling law at the free surface, i.e.

$$\begin{aligned} T &= T_0 \qquad \text{at} \qquad z = 0 \\ \text{and} \qquad \kappa \vec{n} \cdot \nabla T + \alpha_{th}(T - T_\infty) &= 0 \qquad \text{at} \qquad z = h(x), \end{aligned}$$

respectively. The temperature of the ambient gas is T_∞ and α_{th} is the heat transfer coefficient.

2.4 Incorporation of interaction with the substrate

Interestingly, the above reviewed transport equations and boundary conditions of classical hydrodynamics are not sufficient to account for all situations involving thin films or drops. For a static droplet on a solid substrate (Fig. 2 (a)) in an isothermal situation, we have $\vec{v} = 0$ everywhere and Eq. (2.1) reduces to the static equation

$$-\nabla p + \vec{f} = 0 \tag{2.11}$$

Assuming an isothermal situation and neglecting hydrostatic effects and other body forces ($\vec{f} = 0$), the Laplace pressure (Eq. (th-hddf7)) determines the solution of (2.11) as a spherical cap-like droplet (or a flat film); see Fig. 2. However, even for a fixed volume the radius of the droplet is still a free parameter. One additionally needs a condition at the three-phase contact line. Such a condition can be derived from the involved interface

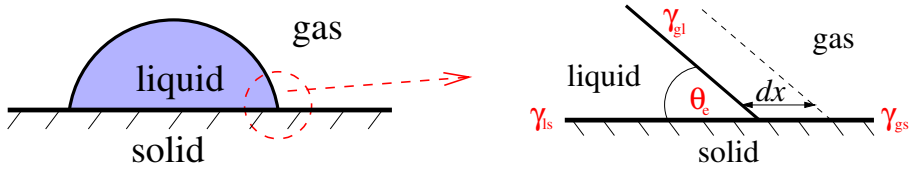

Figure 2. Sketch of a cap-like droplet and the geometry of a static three-phase contact line, indicating gas-solid (γ_{gs}), gas-liquid (γ_{gl}), and liquid-solid (γ_{ls}) interfacial tensions and the equilibrium contact angle θ_e.

energies using the invariance of the total energy with respect to translation (de Gennes, 1985). It is the well known Young-Laplace law

$$\gamma_{lg} \cos\theta_e = \gamma_{gs} - \gamma_{sl} \tag{2.12}$$

where θ_e is the equilibrium contact angle and the γ_{ij} are the interfacial tensions (see Fig. 2 (b)).

The Young-Laplace law does well describe situations of so-called partial wetting where $0 < \theta_e < \pi$, i.e. where $-1 < (\gamma_{gs} - \gamma_{sl})/\gamma_{lg} < 1$. Corresponding droplets are depicted in Fig. 3 (b). To also cover the remaining cases it is practical to introduce the spreading coefficient (de Gennes, 1985)

$$S = \gamma_{gs} - \gamma_{lg} - \gamma_{sl}, \tag{2.13}$$

that measures the energy difference of a dry substrate and a substrate with a liquid film. For partial wetting the combination with Eq. (2.12) yields

$$S = \gamma_{lg} (\cos\theta_e - 1) \tag{2.14}$$

implying $\theta_e = \sqrt{-2S/\gamma}$ for small equilibrium contact angles, i.e. in long-wave approximation.

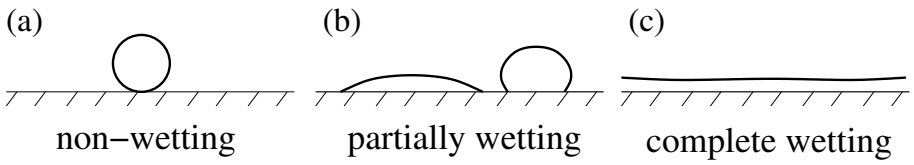

Figure 3. Sketches of the three qualitatively different wetting situations for a simple liquid on a smooth solid substrate: (a) non-wetting, (b) partially wetting, and (c) complete wetting.

The spreading coefficient also allows to quantify in a differentiated manner the non-wetting situation (Fig. 3 (a)) where always $\theta_e = \pi$ but S is only restricted by $S/\gamma_{lg} \leq -2$. The same is valid for the situation of complete wetting (Fig. 3 (c)) where always $\theta_e = 0$ (i.e. the liquid forms a film) but S is only restricted by $S \geq 0$. In this way static situations are well described.

However, a contact line still causes serious problems in hydrodynamics, especially in situations where it moves like for a droplet that slides down an incline. If the drop surface truly touches the substrate at the contact line and one does not relax the classical no-slip condition (Eq. (2.6)) then the viscous dissipation diverges at the contact line and it can not move (de Gennes, 1985).

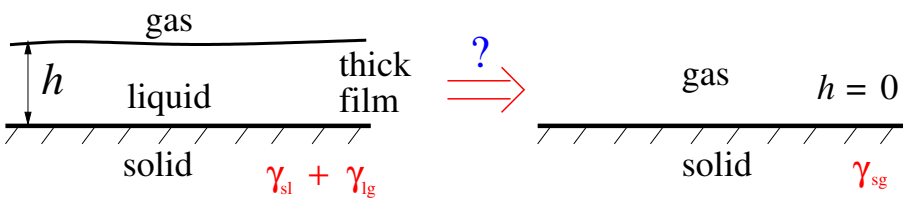

Figure 4. Sketch of the transition from a 'bulk film' to a dry substrate.

A second problem concerns ultrathin films of thicknesses below 100 nm. Normally, the energy of an interface between two substances, i.e. the interface tension, is calculated assuming both are bulk materials. This is still a very good approximation for a thick film depicted in Fig. 4 (a). There the overall interfacial energy is the sum of the solid-liquid one (γ_{sl}) and the liquid-gas one (γ_{lg}). Without film (Fig. 4 (b)) one only has the energy of the solid-gas interface (γ_{sg}). However, the question arises how does one model the transition from (a) to (b), i.e. what are the surface energies for situations where the film can not be regarded as a bulk volume.

Derjaguin and coworkers found that for ultrathin films there is an additional energy $V(h)$ depending on the thickness of the film (Dzyaloshinskii et al., 1960; Israelachvili, 1992). The thickness dependence leads to an additional attractive or repulsive force between the two film interfaces. This force is normally included into the hydrodynamic formalism as an additional pressure term $\Pi = -dV/dh$, the so-called disjoining or conjoining pressure (de Gennes, 1985; Teletzke et al., 1988; Oron et al., 1997). Is it introduced either in the normal force boundary condition supplementing the Laplace pressure

$$p_L \to p_L - \Pi(h)$$

or as an additional body force in the Navier Stokes equation (see de Gennes (1985)):

$$\vec{f}_{add} = -\nabla\phi_{add} \qquad \text{with} \qquad \phi_{add} = \Pi(z) - \Pi(h)$$

Both ways lead to the same result. Here we follow the first one.

The disjoining pressure can be calculated for specific intermolecular interactions. Assuming a long-range apolar van der Waals interaction one finds

$$\Pi_{vdW}(h) = \frac{2S_a d_0^2}{h^3} \tag{2.15}$$

where S_a is the apolar contribution to the spreading coefficient. The length d_0 is often introduced as a molecular cut-off the so-called Born repulsion length $d_{Born} = 0.158\,\text{nm}$

(Sharma, 1993b,a). $A = -12\pi S_a d_{Born}^2$ is the Hamaker constant that can be calculated from the optical indices of the involved materials (Israelachvili, 1992). For a short-range polar interaction (like, for instance, arising from the interaction of the electric double layers in a thin film of an electrolyte) one finds (Israelachvili, 1992; Probstein, 1994)

$$\Pi_p(h) = \frac{S_p}{l}\, e^{(d_0-h)/l} \tag{2.16}$$

where S_p is the polar contribution to the spreading coefficient and l is the correlation length of the polar interaction. One example of a commonly used expression for the disjoining pressure is the combination of the above long-range and short-range parts which writes in dimensionless form (Sharma, 1993b; Thiele et al., 2001a).

$$\Pi(h) = \frac{b}{h^3} \; - \; e^{-h} \tag{2.17}$$

where we introduced the ratio of apolar and polar interaction $b = 2S_a d_0^2/|S_p| l^2 e^{d_0/l}$ and assumed $S_a > 0$ and $S_p < 0$ (h is in units of l). Fig. 5 gives its dependence on film thickness for different values of b.

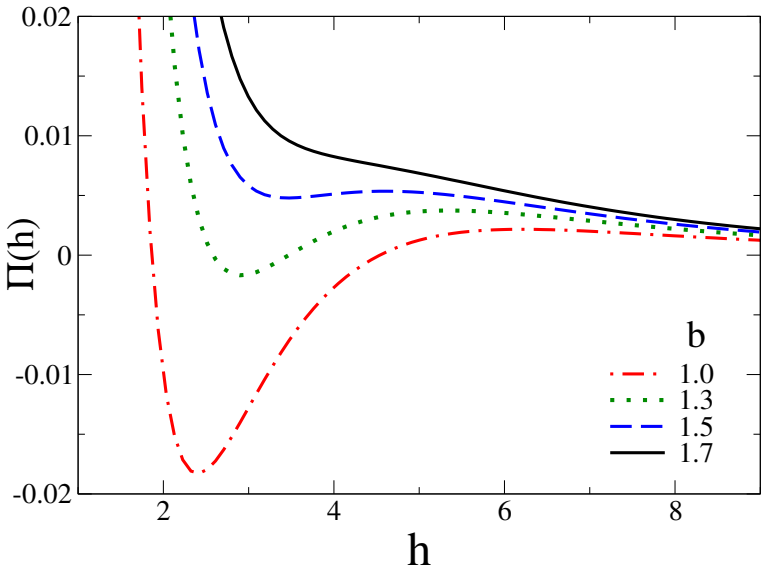

Figure 5. The disjoining pressure given by Eq. (2.17) for different values of the ratio of apolar and polar interactions b.

The choice of constants in Eqs. (2.15) and (2.16) asures that the total surface energy for a thin film $\gamma_{ls} + \gamma_{gl} + V(h)$ [where $V(h) = -\int \Pi(h) dh$] correctly interpolates between the thick film and the dry substrate, i.e. between the two situations depicted in Fig. 4. For thick films $h \to \infty$ and $V(h) \to 0$, the energy is $\gamma_{ls} + \gamma_{gl}$ as expected. At the cut-off

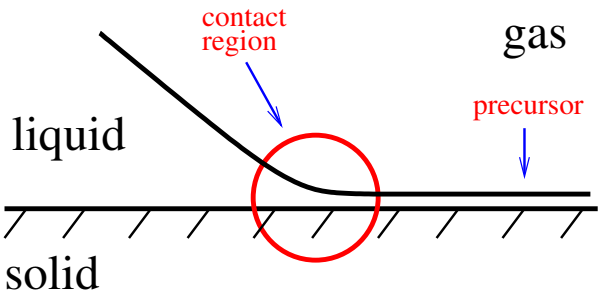

Figure 6. Sketch of a three-phase contact line with a precursor film on the 'dry' substrate.

height $h = d_0$ one has $V(d_0) = S_a + S_p = S$, i.e. taking into account Eq. (2.13) the surface energy is just γ_{gs}. Using Eq. (2.14) small contact angles are given by $\theta_e = \sqrt{-2V(d_0)/\gamma}$.

If the part of the interaction with the shortest range is stabilizing, a very thin precursor film of thickness h_p can be found on the macroscopically 'dry' parts of the substrate. The precursor film allows the contact line to move (see sketch in Fig. 6). However, the three-phase contact line has now to be seen as a contact region. Note, that with the disjoining pressure the precursor thickness is not an ad-hoc parameter but already a result of the model. If there exists no further equilibrium thickness beside h_p it is given by $\Pi(h_p) = 0$. Otherwise it can be obtained via a Maxwell construction (Mitlin, 1993; Thiele et al., 2001b).

As we will see later in section 3.1 in the former case the equilibrium contact angle can be identified with $\sqrt{-2V(h_p)/\gamma_{lg}}$. Consistency with the above expression implies $d_0 = h_p$. Then θ_e corresponds to the contact angle for the 'moist' case of de Gennes (1985). Keeping $d_0 = d_{Born} < h_p$, however, leads to the introduction of two different equilibrium contact angles; one for a truly dry substrate and one for the moist one (compare de Gennes (1985)).

Note finally, that for the disjoining pressure used here [Eqs. (2.15) and (2.16)] the choice $S_a > 0$ and $S_p < 0$ one usually describes verbally as a combination of a stabilizing long-range van der Waals and a destabilizing short-range polar interaction. However, this does not rflect the complete picture due to a subtle feature of the combination of exponential and power law. Combining a term $\sim 1/h^3$ and one $\sim \exp(-h)$ leads for a proper choice of parameters to a dominance of $1/h^3$ for large and very small h. The exponential term only dominates for intermediate thicknesses. This implies that the verbal description only covers part of the feature of the disjoining pressure and should be used with caution.

2.5 Dimensionless groups (numbers)

General In the next step we introduce suitable scales for space, time, pressure, velocity and temperature and write the governing equations and boundary condition in a dimensionless form. To find a suitable scaling is by no means a 'mechanical' task. To scale in an advantageous way corresponds to the determination of a 'good' minimal set

of parameters. At first one introduces a general rather abstract set of scales as follows

$$\begin{array}{ccc} \text{dimensionless} & \text{Scale} & \text{dimensional} \\ t' & t_0 = l/U_0 & t = t_0 t' \\ x',\, z' & l & x = lx',\, z = lz' \\ \vec{v}' & U_0 & \vec{v} = U_0 \vec{v}' \\ p' & P_0 = \varrho U_0^2 & p = P_0 p' \\ T' & \Delta T = T_0 - T_\infty & T = \Delta T T' + T_\infty \end{array} \tag{2.18}$$

The length l may be the mean film thickness, the precursor film thickness or another relevant vertical length scale. Introducing these scales, for instance, in the x-component of the momentum transport equations (2.1) and assuming $\vec{f} = \varrho\vec{g} = \varrho g\,(\sin\alpha, \cos\alpha)$ one obtains for a film on a incline

$$\varrho\frac{U_0^2}{l}(u'_{t'} + u'u'_{x} + w'u'_{z'}) = -\frac{\varrho U_0^2}{l}p'_{x'} + \eta\frac{U_0}{l^2}(u'_{x'x'} + u'_{z'z'}) + \varrho g\sin\alpha \tag{2.19}$$

where α is the inclination angle. For simplicity we drop the dashes and introduce the dimensionless numbers

$$\begin{aligned} \text{Reynolds number} \qquad & \mathrm{Re} = \frac{U_0 l \varrho}{\eta} \\ \text{Froude number} \qquad & \mathrm{Fr} = \frac{U_0^2}{lg} \end{aligned} \tag{2.20}$$

and get (now using both components of Eq. (2.1))

$$\begin{aligned} u_t + uu_x + wu_z &= -p_x + \frac{1}{\mathrm{Re}}(u_{xx} + u_{zz}) + \frac{\sin\alpha}{\mathrm{Fr}} \\ w_t + uw_x + ww_z &= -p_z + \frac{1}{\mathrm{Re}}(w_{xx} + w_{zz}) - \frac{\cos\alpha}{\mathrm{Fr}} \end{aligned} \tag{2.21}$$

The Reynolds number corresponds to the ratio of the selected velocity scale and the viscous one, whereas the Froude number corresponds to the squared ratio of the selected velocity scale to the gravitativ one. The general scaling says nothing about the 'driving force' or the interesting time scale. The scaling becomes specific if the used length l and velocity U_0 are identified. Note, that all scales in (2.20) are derived from the identical l and U_0. In general this is not required. For a film flowing on an incline we illustrate this point by presenting three scalings based on different choices for the velocity scale U_0. They lead to specific expressions for the dimensionless numbers. These are, first, the viscose scaling

$$U_0 = \frac{\eta}{\varrho l}, \qquad \frac{1}{\mathrm{Re}} \to 1, \qquad \frac{1}{\mathrm{Fr}} \to \frac{gl^3\varrho^2}{\eta^2} =: G \tag{2.22}$$

where G is the Galilei or Gravitation number; second, the falling film scaling

$$U_0 = \frac{\varrho g l^2 \sin\alpha}{\eta}, \qquad \frac{1}{\mathrm{Re}} \to \frac{1}{\mathrm{G}\sin\alpha}, \qquad \frac{1}{\mathrm{Fr}} \to \frac{1}{\mathrm{G}\sin\alpha}; \tag{2.23}$$

and third, the surface tension scaling

$$U_0 = \frac{\gamma}{\eta}, \qquad \frac{1}{\mathrm{Re}} \to \frac{\eta^2}{\varrho l \gamma} = \frac{1}{S}, \qquad \frac{1}{\mathrm{Fr}} \to \frac{lg\eta^2 \sin\alpha}{\gamma^2} = \frac{\mathrm{G}\sin\alpha}{S^2} \tag{2.24}$$

where S is the dimensionless surface tension. Inspecting (2.22) to (2.24) shows that the resulting sets of dimensionless numbers differ, and that different limits can be accessed with the different scalings. In the following we will always use the viscose scaling, i.e. we have as momentum equations

$$u_t + uu_x + wu_z = -p_x + u_{xx} + u_{zz} + G\sin\alpha \tag{2.25}$$
$$w_t + uw_x + ww_z = -p_z + w_{xx} + w_{zz} - G\cos\alpha. \tag{2.26}$$

For the temperature field we obtain the dimensionless equation

$$\frac{U_0 \varrho c_p \Delta T}{l}(T_t + uT_x + wT_z) = \frac{\kappa \Delta T}{l^2}(T_{xx} + T_{zz})$$

and after introducing the Péclet number

$$\mathrm{Pe} = \frac{U_0 l \varrho c_p}{k_{th}}$$

one gets

$$\mathrm{Pe}\,(T_t + uT_x + wT_z) = T_{xx} + T_{zz}. \tag{2.27}$$

Using again the viscous velocity scale the Péclet number becomes the Prantdl number $\mathrm{Pr} = \eta c_p/k_{th} = \nu/\kappa_{th}$. Beside the governing equations one also has to derive nondimensional boundary conditions from eqs. (2.6) to (2.3). Many variants exist in the literature. Here we consequently use viscous scales. Assuming furthermore a linear dependence of surface tension on temperature $\gamma = \gamma_0 - \gamma_T(T - T_\infty)$ where $\gamma_0 = \gamma(T_0)$ we find for the tangential stress condition

$$(u_z + w_x)(1 - h_x^2) + 2(w_z - u_x)h_x = -\,\mathrm{Ma}\,(T_x + h_x T_z)(1 + h_x^2)^{1/2} \tag{2.28}$$

where $\mathrm{Ma} = l\varrho\gamma_T \Delta T/\eta^2$ is the Marangoni number [as in Oron et al. (1997), not as in Joo et al. (1991)]. The normal stress condition is

$$p + \frac{2}{1 + h_x^2}[-u_x h_x^2 - w_z + h_x(u_z + w_x)] = -S\,\frac{h_{xx}}{(1 + h_x^2)^{3/2}} \;-\; \Pi \tag{2.29}$$

where $S = 1/\mathrm{Ca} = \gamma_0 l\varrho/\eta^2$ is the dimensionless surface tension (Joo et al., 1991) and Ca is the Capillary number (Oron et al., 1997). Note, that the use of γ_0 in the Laplace pressure term is only valid for $\gamma_0 \gg \gamma_T \Delta T$. The free surface boundary condition for the temperature field writes

$$(T_z - h_x T_x)(1 + h_x^2)^{-1/2} + \mathrm{Bi}\,T = 0 \tag{2.30}$$

where $\mathrm{Bi} = l\alpha_{th}/\kappa$ is the Biot number. The scaling of the remaining boundary conditions is trivial.

2.6 Long-wave scaling

The next step is crucial for the derivation of a simplification of the Navier-Stokes equation for the thin film geometry. It makes use of the observation that all length scales parallel to the substrate L like, for instance, periods of surface waves or drop length, are large as compared to the film thickness l, i.e.

$$l \ll L \quad \rightarrow \quad \epsilon = l/L$$

where we have introduced the smallness parameter ϵ. This allows to replace the scale l in (2.18) by two different scales for the x and the z coordinate, i.e.

$$x = Lx' = \frac{l}{\epsilon}x', \qquad z = lz'$$

In consequence of continuity also the velocity components are scaled differently using

$$u = U_0 u', \qquad w = \epsilon U_0 w'$$

In view of the kinematic boundary condition one also has to scale time as

$$t = \frac{L}{U_0} = \frac{l}{\epsilon U_0}\, t'.$$

Rescaling Eqs. (2.25)-(2.30) yields the transport and continuity equations

$$\begin{aligned}
\epsilon(u_t + uu_x + wu_z) &= -\epsilon p_x + \epsilon^2 u_{xx} + u_{zz} + G\sin\alpha \\
\epsilon^2(w_t + uw_x + ww_z) &= -p_z + \epsilon^3 w_{xx} + \epsilon w_{zz} - G\cos\alpha \\
\epsilon\,\mathrm{Pe}(T_t + uT_x + wT_z) &= \epsilon^2 T_{xx} + T_{zz} \\
u_x + w_z &= 0
\end{aligned} \tag{2.31}$$

and the boundary conditions at $z = h(x)$

$$\begin{aligned}
(u_z + \epsilon^2 w_x)(1 - \epsilon^2 h_x^2) + 2\epsilon^2(w_z - u_x)h_x &= -\mathrm{Ma}\,\epsilon(T_x + h_x T_z)(1 + \epsilon^2 h_x^2)^{1/2} \\
p + \frac{2}{1+\epsilon^2 h_x^2}[-\epsilon^3 u_x h_x^2 - \epsilon w_z + \epsilon h_x(u_z + \epsilon^2 w_x)] &= -\frac{1}{\mathrm{Ca}}\frac{\epsilon^2 h_{xx}}{(1+\epsilon^2 h_x^2)^{3/2}} \\
(T_z - \epsilon^2 h_x T_x)(1 + \epsilon^2 h_x^2)^{-1/2} + \mathrm{Bi}\,T &= 0 \\
w &= h_t + uh_x
\end{aligned} \tag{2.32}$$

The length scales l and L are still not specified. The mean film thickness and some wave period may be used but other candidates may also be suitable. The detailed scaling depends on the problem studied. However, it has always to be checked that the scales fulfill $l \ll L$.

2.7 Small inclination or horizontal substrate

All fields could now be written as series in ϵ to be able to solve Eqs. (2.31) to (2.32) order by order. Such a proceedure leads in $O(\epsilon)$ to the Benney equation (Benney, 1966; Joo et al., 1991). It has, however, the disadvantage to explicitely contain the smallness parameter ϵ, i.e. it consists of terms of different order. An alternative approach studies a situation where all physically interesting effects enter the lowest order equations. Mathematically this is achieved by rescaling the fields and dimensionsless numbers as follows (Oron and Rosenau, 1992).

For a small inclination ($\alpha \ll 1$) one introduces a new $O(1)$ variable $\alpha' = \alpha/\epsilon \approx \sin(\alpha)/\epsilon$. This implies $\sin\alpha \quad \rightarrow \quad \epsilon\alpha'$ and $\cos\alpha \rightarrow 1 - O(\epsilon^2)$. Furthermore one chooses $\mathrm{Ca}' = \mathrm{Ca}/\epsilon^2$ and accounts for the fact that for small inclinations all velocities are small, i.e. a new $\vec{v'} = \vec{v}/\epsilon$ is introduced. After dropping the dashes this leads in lowest order in ϵ to the transport equations

$$\begin{aligned} u_{zz} &= p_x - G\alpha, && (2.33)\\ p_z &= -G, && (2.34)\\ T_{zz} &= 0; && (2.35) \end{aligned}$$

the continuity equation $u_x + w_z = 0$ and the boundary conditions at $z = 0$

$$\begin{aligned} u &= w = 0, && (2.36)\\ T &= 1; && (2.37) \end{aligned}$$

and at $z = h(x)$

$$\begin{aligned} w &= \partial_t h + u\partial_x h, && (2.38)\\ u_z &= -\mathrm{Ma}\,(T_x + h_x T_z), && (2.39)\\ p &= -\frac{h_{xx}}{\mathrm{Ca}} - \Pi(h), && (2.40)\\ T_z &= -\mathrm{Bi}\,T; && (2.41) \end{aligned}$$

respectively. The resulting system can be readily solved. One obtains the fields

$$\begin{aligned} p(x,z) &= G(h-z) - \Pi(h) - \frac{h_{xx}}{\mathrm{Ca}}, && (2.42)\\ T(x,z) &= 1 - \frac{\mathrm{Bi}}{(1+\mathrm{Bi}\,h)} z, && (2.43) \end{aligned}$$

$$\text{and} \qquad u(x,z) = \left(\frac{z^2}{2} - zh\right)(p_x - G\alpha) + \frac{\mathrm{MaBi}\,h_x}{(1+\mathrm{Bi}\,h)^2}\, z. \qquad (2.44)$$

The kinematic boundary condition and continuity give

$$\partial_t h = -\partial_x \Gamma \qquad (2.45)$$

where $\Gamma = \int_0^h u dz$ is the flow in the laboratory frame.

Manuscript —- contact: thiele@pks.mpg.de – http://www.uwethiele.de – 10th March 2006

2.8 The film thickness evolution equation

Finally, using Eqs. (2.44) and (2.42) in Eq. (2.45) gives the evolution equation for the thickness profile of a film on a slightly inclined substrate

$$\partial_t h \;=\; -\partial_x \left\{ \frac{h^3}{3} \left[\partial_x \left(\frac{h_{xx}}{\mathrm{Ca}} - Gh - \Pi(h) \right) \;+\; \frac{3}{2h} \, \frac{\mathrm{Ma\,Bi}\, h_x}{(1+\mathrm{Bi}h)^2} \;+\; G\alpha. \right] \right\} \tag{2.46}$$

By a further rescaling we eliminate Ca and write in a more general form

$$\partial_t \, h \;=\; -\partial_x \, \{ Q(h) \, \partial_x \, [\partial_{xx} h - \partial_h f(h)] + \chi(h) \} \tag{2.47}$$

where $Q(h)$ is a mobility factor and $\chi(h)$ stands for a generalized driving parallel to the substrate. The use of slip boundary conditions at the substrate leads to different Q and χ but has no effect on the equation otherwise (Oron et al., 1997). The term in square brackets represents the negative of a pressure consisting of the Laplace term $\partial_{xx} h$ and an additional contribution $-\partial_h f(h)$ written as the derivative of a local free energy. The latter has to be specified for the respective studied problem. For the system presented here we have

$$\partial_h f(h) = -\Pi - Gh - \frac{3}{2} \mathrm{Ma\,Bi} \int \frac{dh}{h(1+\mathrm{Bi}\, h)^2}.$$

For inhomogeneous systems $f(h)$ may depend also on position. Eq. (2.47) can be written in a variational form

$$\partial_t \, h \;=\; \partial_x \left\{ Q(h) \, \partial_x \, \frac{\delta F[h]}{\delta h} \right\} \;-\; \partial_x \, \chi(h) \tag{2.48}$$

with $\delta / \delta h$ denoting functional variation with respect to h and the free energy functional

$$F[h] \;=\; \int \left[\frac{1}{2} \, (\partial_x h)^2 + f(h) \right] \, dx. \tag{2.49}$$

Without lateral driving, i.e. for $\chi = 0$, Eq. (2.48) corresponds to the simplest possible equation for the dynamics of a conserved order parameter field (Langer, 1992). In this case the system is variational (or relaxational) and $F(h)$ can be used as Lyapunov functional because it fulfills $dF/dt \leq 0$ (Langer, 1992; Mitlin, 1993; Oron and Rosenau, 1992). A prominent representative of this class of systems is the Cahn-Hilliard equation describing the evolution of a concentration field for a binary mixture (Cahn, 1965).

For $\chi \neq 0$, Eq. (2.48) does not represent a variational system any more, the dynamics is non-relaxational, i.e. $F[h]$ does not necessarily decrease in time. Representatives are, for example, the driven (or convective) Cahn-Hilliard equation (Golovin et al., 2001), the Kuramoto-Sivashinsky equation (Kevrekidis et al., 1990; Kuramoto and Tsuzuki, 1976; Sivashinsky, 1977), and also the Benney equation and their variants (Benney, 1966; Gjevik, 1970; Joo et al., 1991; Lin, 1974; Pumir et al., 1983; Scheid et al., 2005).

2.9 The additional pressure term

Equations like (2.47) can be used to study a wide variety of systems (Oron et al., 1997). Here we focus on two physical situations (i) ultrathin films below 100 nm thickness on

partially wettable substrates that undergo dewetting (Bischof et al., 1996; Brochard-Wyart and Daillant, 1989; de Gennes, 1985; Reiter, 1992; Thiele et al., 1998) and thin films below about 100 μm thickness heated from below. They may be unstable due to a long-wave Marangoni instability (Burelbach et al., 1988; Oron, 2000; Oron and Rosenau, 1992; VanHook et al., 1995, 1997). In the former case the additional pressure $-\partial_h f(h)$ in Eq. (2.47) corresponds to the disjoining pressure $\Pi(h)$ introduced above in Section 2.4 [$f(h)$ corresponds to $V(h)$]. Two forms of the pressure used here are

$$\partial_h f(h) = 2\kappa\, e^{-h}\left(1 - e^{-h}\right) + Gh \tag{2.50}$$

$$\text{and} \qquad \partial_h f(h) = \pm(-\frac{b}{h^3} + e^{-h}). \tag{2.51}$$

The first term of the form (2.50) was derived by Pismen and Pomeau (2000) combining the long wave approximation for thin films (Oron et al., 1997) with a diffuse interface model for the liquid-gas interface (Anderson et al., 1998). Also density variations close to the solid substrate enter their calculation in a natural way. The second term accounts for the hydrostatic pressure. Eq. (2.50) has the advantage of remaining finite even for vanishing film thickness. The parameter G is normally very small, however, it is possible to study the qualitative system behaviour using a small but not very small G.

Eq. (2.51) combines a long-range apolar van der Waals interaction and a short-range polar (electrostatic or entropic) interaction (Sharma, 1993a,b) as discussed above in Section 2.4. If the positive sign is used both disjoining pressures lead to qualitatively very similar results (Thiele et al., 2002b).

There exist various other forms of disjoining pressures used in the literature. Most results are valid in a similar form if the pressure in question describes a partially wetting situation and allows for a stable precursor film. Nondimensionalized examples for combinations of power laws are, for instance, $\partial_h f(h) = 1/h^3 - b_1/h^6$ derived from a diffuse interface theory with nonlocal interactions (Pismen, 2001; Pismen and Pomeau, 2004; Pismen and Thiele, 2006) and $\partial_h f(h) = 1/h^3 - b_1/(h + d_{co})^3 - b_2/h^9$ describing a film on a substrate with a coating of thickness d_{co} (Sharma and Reiter, 1996; Seemann et al., 2005). The b_i are dimensionless constants.

For the heated film the additional pressure $\partial_h f(h)$ results from the tangential stress condition at the free surface (Oron and Rosenau, 1992). It is given by

$$\partial_h f(h) = Gh - \frac{3}{2}\,\mathrm{Bi}\,\mathrm{Ma}\left[\log\left(\frac{h}{1+\mathrm{Bi}\,h}\right) + \frac{1}{1+\mathrm{Bi}\,h}\right]. \tag{2.52}$$

Beside these basic situations also combinations of the different pressure terms can be used. For example, supplementing Eq. (2.52) with a stabilising apolar interaction allows to study the long-time coarsening of a heated thin film (Bestehorn et al., 2003). To account for a chemically inhomogeneous substrate one can use a disjoining pressure that varies in space (Konnur et al., 2000; Thiele et al., 2003) For an inhomogeneous heating one modulates the Marangoni number in Eq. (2.52) (Scheid et al., 2002; Skotheim et al., 2003).

2.10 Analysis techniques

The analysis of the thin film equation (2.47) in the four different geometries rests on three columns: (1) analytical determination of fixed points, i.e. flat film solutions, and of their stability properties; (2) calculation of stationary solutions[6], their bifurcations and linear stability using continuation techniques; and (3) numerical integration in time. The majority of the presented results is based on continuation techniques (Doedel et al., 1991a,b, 1997).

With continuation techniques one can obtain solutions of a problem for a certain set of control parameters by iterative techniques from known solutions nearby in parameter space. Specifically, the film thickness equation written as a dynamical system, i.e. as a system of ordinary differential equations

$$u'(x) = f(u(x), p) \qquad \text{with} \qquad f, u\, in\, \mathbf{R}^n \tag{2.53}$$

where the dash indicates derivation with respect to x and p denotes the set of control parameters. Eq. (2.53) subject to boundary and integral conditions is discretized in space. The resulting algebraic system is solved iterativly. The package AUTO (Doedel et al., 1997) uses the method of Orthogonal Collocation for discretizing solutions, where the solution is approximated by piecewise polynomials with 2–7 collocation points per mesh interval. The mesh is adaptive as to equidistribute the discretization error. Starting from known solutions AUTO then tries to find nearby solutions to the discretized system, by using a combination of Newton and Chord iterative methods. Once the solution has converged AUTO proceeds along the solution branch by a small step in the parameter space defined by the free continuation parameters and restarts the iteration.

Boundary conditions and/or integral conditions require additional free parameters which are determined simultaneously and are part of the solution to the differential equation. The package AUTO is limited to the continuation of ordinary differential equations (ODE's), thus it can only be used to compute droplet solutions in two dimensions. As an example we consider the continuation of stationary surface waves or sliding drops steady in a comoving frame. After transforming Eq. (2.47) into the comoving frame with velocity v and integrating the resulting time-independent thin-film equation we have the system of ODE's

$$\begin{aligned} u_1' &= u_2 \\ u_2' &= u_3 \\ u_3' &= -\frac{\chi(u_1) + v u_1 - C_0}{Q(u_1)} + \partial_{u_1} f(u_1) \end{aligned} \tag{2.54}$$

where C_0 is an integration constant (see section 5). u_1, u_2 and u_3 denote h, $\partial_x h$ and $\partial_{xx} h$, respectively. The volume is conserved, thus we need to specify the integral condition

$$0 = \frac{1}{L} \int u_1 \, dx - \bar{h} \tag{2.55}$$

[6] We call stationary solutions, solutions that are steady in some co-moving frame of reference.

where L is the system length and $\bar{h}$ is the mean film thickness. We also use periodic boundary conditions

$$u_1(0) = u_1(L) \quad (2.56)$$
$$u_2(0) = u_2(L) \quad (2.57)$$
$$u_3(0) = u_3(L). \quad (2.58)$$

Translation of a solution along the substrate yields another valid solution. However, continuation along the 'trivial' families of solutions related through continuous symmetries of the system is not wanted. It is effectively forbidden by a pinning condition in the form of an additional boundary or integral condition. The number of boundary (NBCD) and integral conditions (NINT) determines the number of parameters (NPAR), that are varied during the continuation process. Specifically NPAR=NBCD+NINT-NDIM+1, where NDIM is the dimensionality of (2.53), i.e. here NDIM= 3 The resulting three free parameters are called continuation parameters and may, for instance, be the system size L, the integration constantC_0 and the velocity v.

The challenge is often to provide a starting solution for the continuation. For surface waves or sliding drops one can use analytically known surface waves obtained by a linear perturbation of the flat film. In other cases the initial solution is given numerically. Finally note, that continuation is not only used to determine families of stationary solutions (Thiele et al., 2001c,b), but also to follow their stability behaviour (Thiele and Knobloch, 2003) and bifurcations, like saddle-node bifurcations or branching points (Thiele and Knobloch, 2004; Scheid et al., 2005). This can be used to phase diagrams mapping the existence and stability of various solution types (John et al., 2005).

In general, details of the used techniques differ between the geometries. These are introduced were needed in the course of the following sections, that analyse specific physical situations corresponding to the different geometries shown in Fig. 1. However, many practically relevant thin film systems can not be modelled by a single evolution equation of the type of Eq. (2.47). Therefore, in Section 7 we extend the theory towards situations where two order parameter fields have to be taken into account.

3 Horizontal homogeneous substrate

3.1 General analysis

For the horizontal homogeneous substrate there exists no lateral driving force, i.e. $\chi(h) = 0$. Eq. (2.47) becomes

$$\partial_t h = -\partial_x \{Q(h)\, \partial_x [\partial_{xx} h - \partial_h f(h)]\} \quad (3.1)$$

Steady solutions To study steady solutions we set $\partial_t h = 0$ and integrate Eq. (3.1) to get

$$0 = \partial_{xxx} h - \partial_{hh} f(h)\, \partial_x h - \frac{C_0}{Q(h)}. \quad (3.2)$$

We look for periodic arrays of drops or holes, localized drops or holes, and flat film solutions. The reflection symmetry ($x \to -x$) with respect to the extrema of the solutions

or the flat film at infinity, respectively, implies $C_0 = 0$. Another way to see this is to interprete C_0 as the mean flow. Without an additional driving force no mean flow occurs, i.e. $C_0 = 0$.

A second integration yields

$$0 = \partial_{xx} h(x) - \partial_h f(h) + C_1. \tag{3.3}$$

The constant C_1 accounts for external conditions like chemical potential, vapor pressure or mass conservation. For the latter case that we will focus on here, C_1 takes the role of a Lagrange multiplier. The choice $C_1 = \partial_h f(h_0)$ ensures the flat film $h(x) = h_0$ to be a solution. Note that Eq. (3.3) also follows directly from the minimization of the energy functional (2.49) when asuring mass conservation. Later we will compute periodic solutions of Eq. (3.3) and parametrize them by their mean film thickness, $\bar{h} = (1/L) \int_0^L h(x)dx$, and period, L.

In a two-dimensional situation Eq. (3.3) is equivalent to the equation of motion for a particle in a potential $V(h) = -f(h) + C_1\, h$. For radial-symmetric solutions in a three-dimensional situation it is equivalent to such an equation of motion including a time-dependent friction term (see Deissler and Oron (1992); Thiele et al. (2002b); Bestehorn et al. (2003)).

Beside the chosen h_0 other flat film solutions or fixed points of Eq. (3.3) $h(x) = h_f$ may exist. They are given by

$$\partial_h f(h_f) = \partial_h f(h_0). \tag{3.4}$$

For the disjoining pressure shown in Fig. 5 [Eq. (2.17)] one finds one or three fixed points depending on the value of b and h_0. The bifurcation points between the two regimes are given by $\partial_{hh} f(h_0) = 0$ and Eq. (3.4). Linearizing Eq. (3.3) at the fixed points one finds that for $\partial_{hh} f(h_f) > 0 (< 0)$ they are saddles (centers). This corresponds to the results of the linear stability analysis for flat films shown next.

In order to determine thickness profiles that are solutions of Eq. (3.3) we multiply by h_x, integrate, and obtain

$$\partial_x h = \sqrt{2}\, \sqrt{f(h) - C_1\, h - C_2}. \tag{3.5}$$

where C_2 is a constant discussed below.

Linear stability of flat films To assess the linear stability of the flat films $h(x) = h_0$ we use a Fourier mode decomposition $h(x) = h_0 + \epsilon \exp(\beta t + ikx)$ where β and k provide the growth rate and the wave number of the disturbances. Linearizing the full time dependent Equation (3.1) in $\epsilon \ll 1$ yields the dispersion relation

$$\beta = -Q(h_0)\, k^2 \left[k^2 + \partial_{hh} f(h_0)\right]. \tag{3.6}$$

The possible outcomes are sketched in Fig. 7. The flat film is unstable for $\beta > 0$, i.e. there exists some range of unstable wavenumbers $0 < k < k_c$ for

$$\partial_{hh} f(h_0) < 0. \tag{3.7}$$

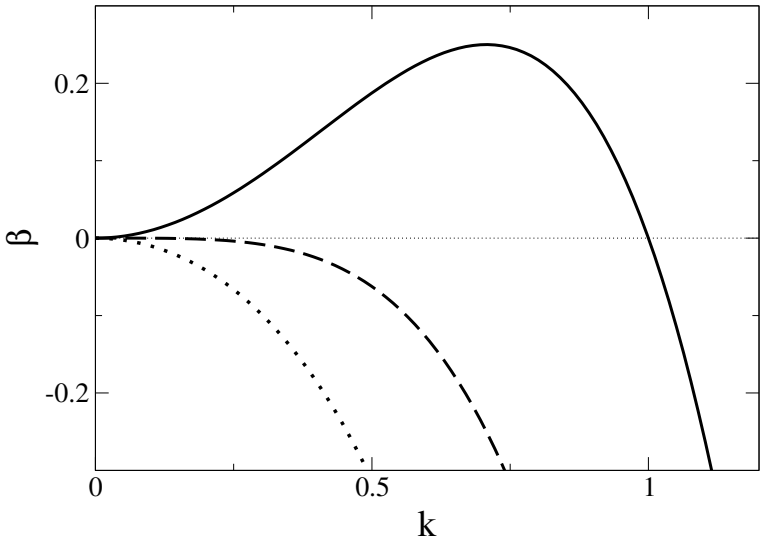

Figure 7. Dispersion relations for a flat film on a horizontal homogeneous substrate. Sketched are the unstable (solid line), marginally stable (dashed line) and linearly stable case (dotted line).

The instability has its onset at $\partial_{hh} f = 0$ with $k_c = 0$. This is also called the marginally or neutrally stable case. Because of the onset at zero wavenumber it is called a long-wave instability. It corresponds to an instability of type II_s in the classification of Cross and Hohenberg (1993) (see their section IV.A.1.b) The critical wave number is

$$k_c \,=\, \sqrt{-\partial_{hh} f(h_0)} \tag{3.8}$$

and the corresponding wavelength is $\lambda_c = 2\pi/k_c$. The thickness profile $h(x) = h_0 + \epsilon \exp(ik_c x)$ is neutrally (or marginally) stable ($\beta = 0$) and represents a small amplitude periodic steady solution of Eq. (3.1).

For a linearly unstable film the fastest growing mode has the wavelength $\lambda_m = \sqrt{2}\lambda_c$ and the growth rate

$$\beta_m \,=\, \frac{1}{4}\, Q(h_0)\, [\partial_{hh} f(h_0)]^2. \tag{3.9}$$

Nonlinear Stability A linearly stable flat film may not be absolutely stable. It can be unstable to finite amplitude disturbances corresponding to a metastable flat film. This may indicate the occurance of a sub-critical instability. Only if, for a given mean film thickness there is no thickness profile with smaller energy the flat film is absolutely stable. To further clarify this issue we assume an infinitely long film of thickness h_0. Only a small part of finite length s has a different thickness h to ensure that the mean film thickness remains h_0. The width of the finite transition region between the two thicknesses is small compared to s, so its energy can be neglected. Now we can calculate

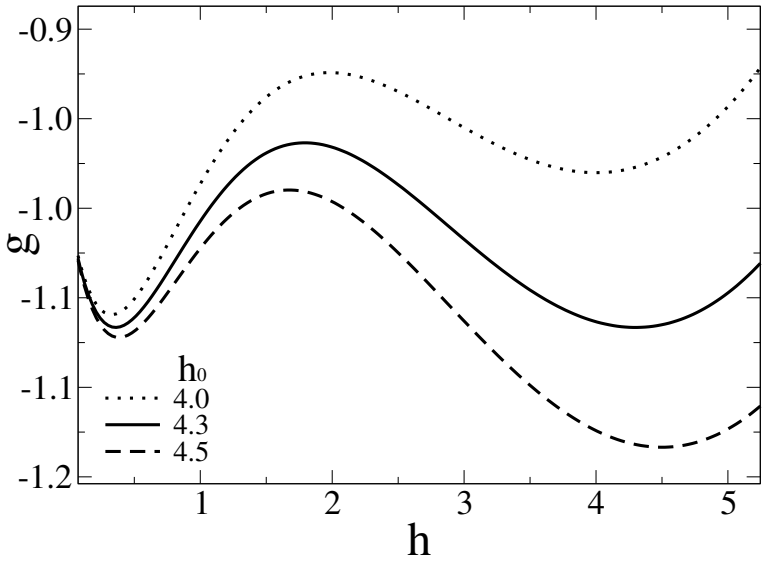

Figure 8. The local energy $g(h) = f(h) - C_1(h_0)\,h$. As an example the dependence is shown for the disjoining pressure (2.50) (see Thiele et al. (2001c)). An equivalent plot for the disjoining pressure (2.51) can be found in Thiele et al. (2001a).

the energy per unit length of the changed part

$$g(h) \;=\; f(h) \;-\; C_1(h_0)\,h. \tag{3.10}$$

The function $g(h)$ is plotted in Fig. 8 for different values of h_0. The two minima represent a lower and an upper linearly stable film thickness. However, only the deeper minimum corresponds to an absolutely stable state, whereas the other one is metastable. The maximum represents a linearly unstable film thickness. There exist an upper and a lower limit of the metastable thickness range, denoted by h_m^u and h_m^d, respectively. They are characterized by minima of equal depth in Fig. 8 and identical $C_1(h_m)$, i.e. by

$$\begin{aligned} \partial_h f|_{h_m^u} &= \partial_h f|_{h_m^d} \\ g(h_m^u) &= g(h_m^d). \end{aligned} \tag{3.11}$$

Note, that Eqs. (3.11) are equivalent to a Maxwell construction (see also Mitlin (1993); Samid-Merzel et al. (1998); Mitlin (2000)).

Using the results for the onset of the linear instability of the flat film Eq. (3.7) and Eqs. (3.11) for its absolute stability one can calculate the stability diagram. An example is given below in Fig. 12. These diagrams are valid for two- and three-dimensional film geometries.

Equilibrium contact angle If Eq. (3.11) yields two equilibrium thicknesses, i.e. binodal thicknesses, one can not define a mesoscopic equilibrium contact angle in an asymp-

totic sense (Pismen and Thiele, 2006) because no solution profile continues towards an infinite height. However one can still define equilibrium contact angles as the slope at the inflection point of the profile. This situation is always encountered for the disjoining pressure derived from diffuse interface theory when including gravity [Eq. (2.50)] and for $b > 8/e^2$ also for the apolar/polar combination Eq. (2.51).

A simpler result is obtained if only one finite equilibrium film thickness exists (the second one is infinite) as for the disjoining pressure (2.51) for $b < 8/e^2$ and always for (2.50) without gravitation. Then a droplet of infinit height coexists with a precursor film of thickness h_p given by $\partial_h f(h_p) = 0$. One also finds $C_1 = 0$ and $C_2 = f(h_p)$ [see Eqs. (3.3) and (3.5)]. Going back to physical (dimensional) scaling the asymptotic equilibrium contact angle given as h_x for $h \to \infty$ results as $\theta_e = \sqrt{-2f(h_p)/\gamma}$.

Periodic solutions In order to study the various non-constant thickness profiles, i.e. periodic (assemblies of drops or holes), homoclinic (single drops or holes) and heteroclinic (fronts) solutions of Eq. (3.5) we choose for the integration constant

$$C_2 = f(h_m) - (\partial_h f(h_0))\, h_m \tag{3.12}$$

where h_m is the maximal or minimal thickness for periodic solutions. For localized solutions is $h_m = h_0 = h_\infty$. Hence, all solutions are parameterized by the pair (h_0, h_m) or (C_1, C_2). Eq. (3.5) allows to plot the solutions in the phase plane (h, h_x) [see Mitlin (1993); Thiele et al. (2001c)]. Three qualitatively different phase portraits (each for fixed C_1) can be observed (see Fig.9). They represent drop, hole and front regime, respectively. In the hole [drop] regime one finds beside periodic solutions a homoclinic solution representing a localized hole [drop] in an infinitely extended flat film (shown on the lower line of Fig. 9). These localized profiles can be found in the metastable range for flat films.

In the front regime, besides the periodic solutions, one also finds two heteroclinic solutions that connect the lowest and the highest fixed point, thus representing localized front or kink solutions that connect two infinitely extended flat films of thicknesses, h_m^d and h_m^u (right image on lower line of Fig. 9). The fronts exist only on the border between metastable and stable flat films.

In the following we concentrate on the periodic solutions. They exist for parameter ranges corresponding to linearly unstable or metastable flat films. Depending on the relevant control parameters, like mean film thickness, Marangoni number and interaction constants one can distinguish three qualitatively different families of solutions. Chosing period as the main control parameter and fixing the mean film thickness their characteristics are sketched in Fig. 10. The solution families are characterized by the amplitude (left) and energy (right) of the solutions. The energy E corresponds to the functional F (Eq. (2.49)) per length normalized by the energy of the flat film.

(a) Deep inside the linear unstable film thickness range there exists only one branch of periodic solutions. It bifurcates supercritically from the flat film solution at $L = \lambda_c = 2\pi/k_c$ (Eq. (3.8)) and continues towards infinite period. Amplitude increases and energy decreases monotonically with increasing period. The energy is always lower than the one of the corresponding flat film.

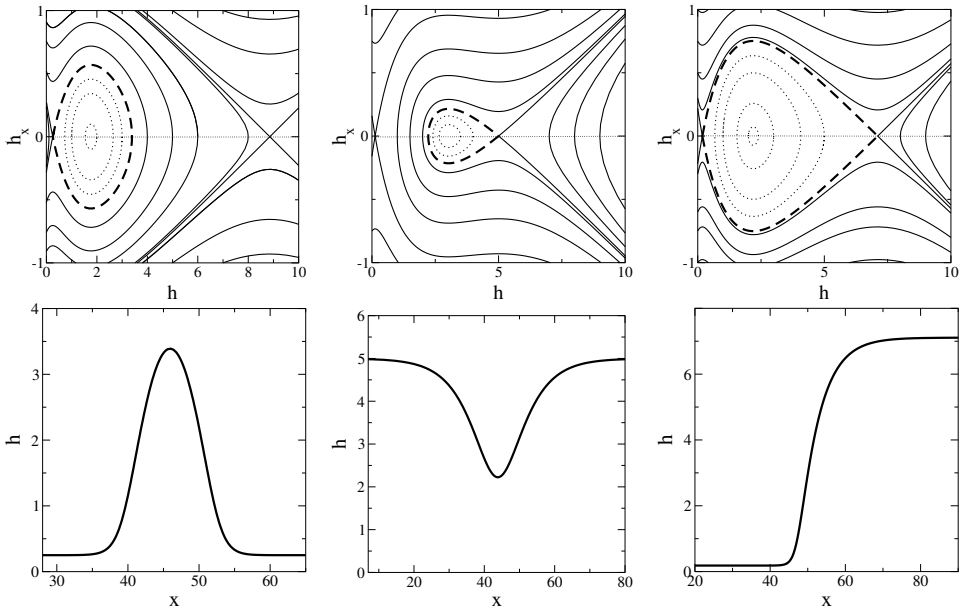

Figure 9. Sketched are qualitatively different phase portraits in the $(h, \partial_x h)$ plane (upper line) and corresponding localized profiles (lower) for drop (left), hole (middle) and front regime (right). For details on the parameters see Thiele et al. (2001c).

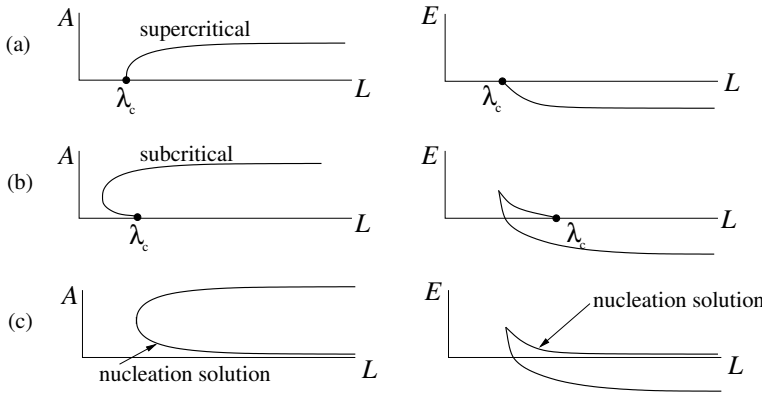

Figure 10. Sketched are the three types of families of periodic solutions. In (a) and (b) a branch bifurcates supercritically and subcritically, respectively, from the unstable flat film solution. In (c) two branches exist that both continue towards infinite period. The flat film is metastable. In (b) and (c) the low-energy branch corresponds to nucleation solutions.

Manuscript —- contact: thiele@pks.mpg.de – http://www.uwethiele.de – 10th March 2006

(b) Closer to the metastable range but still for linearly unstable film thicknesses there exist two branches of solutions. For both, energy decreases with increasing period. The high energy branch bifurcates at $L = \lambda_c$ subcritically from the flat film solution. Its energy is always higher than the one of the flat film. This branch is linearly unstable and represents nucleation solutions that have to be 'overcome' if the film is to break into finite portions with size $p < \lambda_c$. The energy of the lower branch decreases rapidly with increasing period. However, there is a very small range of periods where the flat film has the smallest energy implying its absolute stability for systems of this size. Consequently, for this range the low-energy periodic solution is only metastable.

(c) For metastable flat films there exist two solution branches that both continue towards infinite period. The upper one consists of nucleation solutions of different periods that separate energetically the lower periodic solution from the linearly stable flat film solution.

Linear stability of steady solutions The linear stability of the periodic solutions is assessed by linearizing the full time dependent Eq. (3.1) around the periodic solutions, $h_0(x)$. Using the ansatz

$$h(x,t) = h_0(x) + \epsilon\, h_1(x)\, \exp(\beta t) \tag{3.13}$$

gives a linear eigenvalue problem for the growth rate β and disturbance h_1.

$$\beta h_1(x) \;=\; \mathbf{N_0}[h_0(x)]\, h_1(x) \tag{3.14}$$

with

$$\begin{aligned} \mathbf{N_0} h_1 \quad &= \quad -\partial_x \left\{ Q_h h_1\, \partial_x (\partial_{xx} h_0 - \partial_h f) \right\} \\ &\quad\quad -\partial_x \left\{ Q\, \partial_x (\partial_{xx} h_1 - \partial_{hh} f\, h_1) \right\}. \end{aligned} \tag{3.15}$$

Q and f and their derivatives are functions of $h_0(x)$. To determine $h_1(x)$ and β by continuation one has to follow simultaneously the steady solution $h_0(x)$ of Eq. (3.3) and the solution of Eq. (3.14). Because of the variational structure of the problem all β are real. Therefore the β can be directly determined as branching points (Doedel et al. (1997)). The required extended system consists of 7 first order differential equations (3 for h_0 and 4 for h_1).

After introducing the general approach, next we will present some selected results for the dewetting of ultrathin films on homogeneous substrates (Section 3.2) and for the long-wave Marangoni-Bénard instability of heated thin films (Section 3.3).

3.2 Ultrathin partially wetting films

While hydrodynamical surface instabilities in thin-film flows are investigated since the experiments of the Kapitzas (Kapitza, 1949; Kapitza and Kapitza, 1949), in soft matter physics they became increasingly recognised as important for the structure formation in thin films on solid substrates since the work on dewetting by Reiter only one decade ago (Reiter, 1992). In this paradigmatic experiment a polymer film on a solid substrate

is brought above its glass transition temperature, ruptures, and the formed holes grow resulting in a network of liquid rims. The latter may decay subsequently into small drops[7].

The ongoing pattern formation can be described by Eq. (3.1) using a disjoining pressure $\partial_h f(h)$ appropriate for the combination of materials used and accounting also for eventual coatings. A variety of different combinations of stabilising or destabilising exponentials and power laws are used (Hunter, 1992; Israelachvili, 1992; Teletzke et al., 1988) and still new candidates for underlying physical effects beside dispersion or electrostatic forces are discussed (Pismen and Pomeau, 2000; Schäffer et al., 2003; Schäffer and Steiner, 2002; Ziherl et al., 2000).

One of the questions discussed sometimes controversially (Bischof et al., 1996; Brochard-Wyart and Daillant, 1989; Jacobs et al., 1998; Reiter, 1992; Thiele et al., 1998, 2001a; Xie et al., 1998) concerns the mechanism of the rupture of the initially flat film. Does it occur via *instability* or *nucleation*? Most literature relates the occurrence of surface instability and heterogeneous nucleation at defects to linearly unstable and metastable films, respectively (see Fig. 12 below and the discussion above in Section 3.1).

The importance of this question in dewetting is due to the fact that in most systems the evolution is frozen before mayor coarsening occurs, i.e. the mechanism of the initial rupture still determines the structure. On the contrary, for the decomposition of a binary mixture (as described by the Cahn-Hilliard equation) there is little discussion about this point, what rather interests there is the scaling behaviour of the long-time coarsening, because it gives the evolution of the length scales that can be measured experimentally. For thin films coarsening is up to now only of minor interest (exceptions are Mitlin (2001); Bestehorn et al. (2003); Glaser and Witelski (2003); Pismen and Pomeau (2004), see also Section 3.4) because for the used experimental systems in dewetting the time scale for large-scale coarsening is very large.

Recent work re-evaluated for two-dimensional model systems the two rupture mechanisms starting from an analysis of the solution structure of Eq. (3.1). As elucidated above at Fig. 10 nucleation solutions exist not only in the metastable thickness range but also in a part of the linearly unstable thickness range. These unstable solutions 'organise' the evolution of the thin film by offering a fast track to film rupture that does not exist in their absence.[8]

For a linearly unstable film with a solution structure as in Fig. 10 (b) the nucleation solutions are unstable solutions that have to be overcome to break a film in smaller portions than the critical linear wavelength, λ_c. However, they also influence the local rupture dynamics if there exist localized disturbances of the film surface (defects) with lateral extensions smaller than λ_c. Then, locally the nucleation solutions first attract the evolution to later repel it with a well-defined rate β_{nuc}. The rate can be obtained by

[7] Note, however, that descriptions of the patterns formed in this kind of process can already be found for liquid-liquid dewetting in papers by Tomlinson (Tomlinson, 1870, footnote 18 on p. 40) for turpentine on water and Marangoni (Marangoni, 1871, p. 352f) for oil on water.

[8] For the decomposition of a binary mixture Novick-Cohen (1985) discussed such solutions as an evidence for a smooth transition from spinodal decomposition to nucleation somewhere within the classical spinodal.

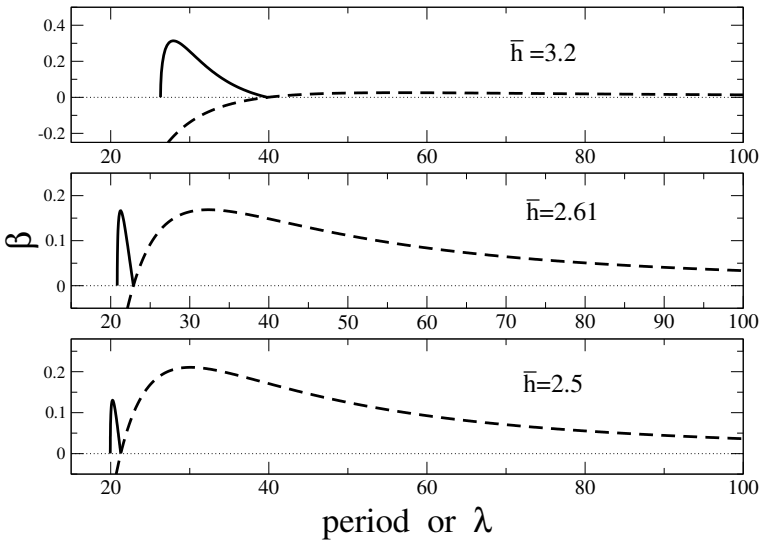

Figure 11. Comparison of the linear growth rates of the surface instability of the flat film (dashed lines) and of the linear unstable nucleation solutions (solid lines). In the first (last) image the nucleation solutions (flat film modes) by dominate whereas in the intermediate image both have equal maximal groeth rate (see Thiele et al. (2001c)).

analysing the linear stability of the nucleation solutions. This property reflects the fact that the nucleation solutions are saddles in the space of all possible surface profiles.

To evaluate the influence of this nucleation solution mediated rupture one has to compare the related rates β_{nuc} and the rates of the 'normal' linear rupture modes of a flat unstable film given by Eq. (3.6). Such comparisons are shown in Fig. 11 for different mean film thicknesses. The heights of the two maxima now allow to predict whether defects have an influence on the resulting morphology or not.

As a result one distinguishes nucleation-dominated and instability-dominated behaviour for linearly unstable films as indicated in Fig. 12 (Thiele et al., 2001a). The new boundary separating the two sub-ranges is defined as the line where the two maxima in Fig. 11 have the same height.

If the behaviour is nucleation-dominated an initial disturbance grows much faster than the also active linear instability of the flat film (Fig. 13 (a)). The produced holes expand and if the dynamically produced surface depression just outside the rim becomes larger than the respective nucleation solution secondary nucleation events occur. The resulting structure is a set of holes with distances unrelated to λ_m. It depends strongly on the properties of the initial defect. If the behaviour is instability-dominated the initial disturbance also starts to grow but rather acts as starting point for the most unstable flat film mode (Fig. 13 (b)). Undulations of period λ_m extend laterally to give finally a periodic set of holes nearly independent of the initial perturbation.

The qualitative result does neither depend on the details of the used disjoining pres-

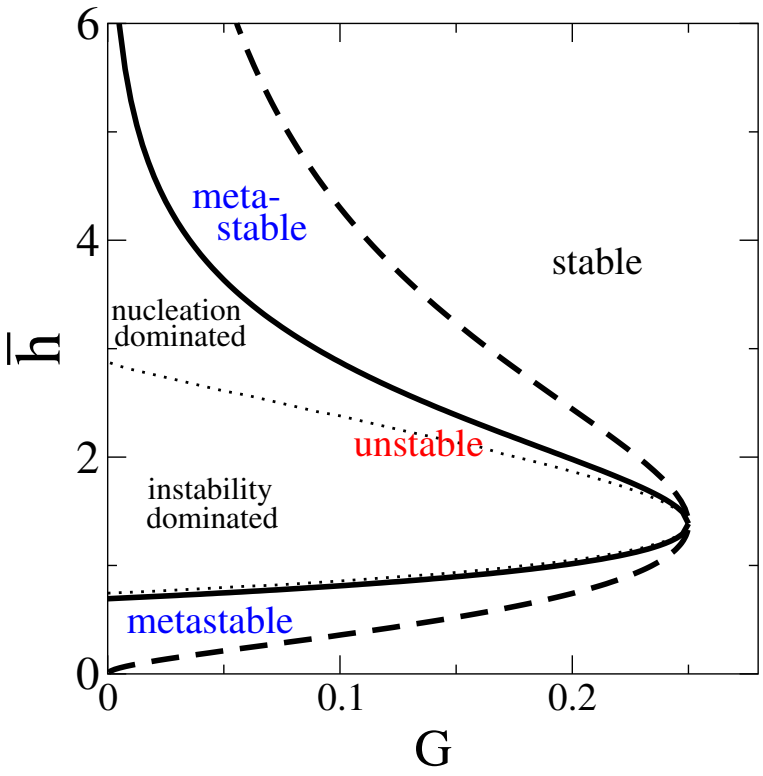

Figure 12. Stability diagram for a thin liquid film including the binodal (dashed line) and the spinodal (solid line) for the disjoining pressure of Eq. (2.50). The dot-dashed line indicates the boundary between nucleation-dominated and instability-dominated sub-ranges within the linearly unstable range.

sure (Thiele et al., 2002b) nor is it expected to be different in three-dimensional systems. Therefore our results (Thiele et al., 2001a) and Thiele et al. (2001c) explain qualitatively *why* the morphological transition occurs that is shown by Becker et al. (2003). For a detailed analysis of the result of Becker et al. (2003) and application of our findings to further experiments (Du et al., 2002; Meredith et al., 2000) see Thiele (2003a,b)[9].

[9]Note that in Seemann et al. (2005) our result was misunderstood (p. S285/S286). The predicted boundary between the two qualitatively different sub-ranges lies well inside the range of linearly unstable film thicknesses, i.e. the film is not metastable as stated there. Our theory even explains why 'this behaviour should be typical for thin films of Newtonian liquids particularly in the unstable state' (Seemann et al., 2005).

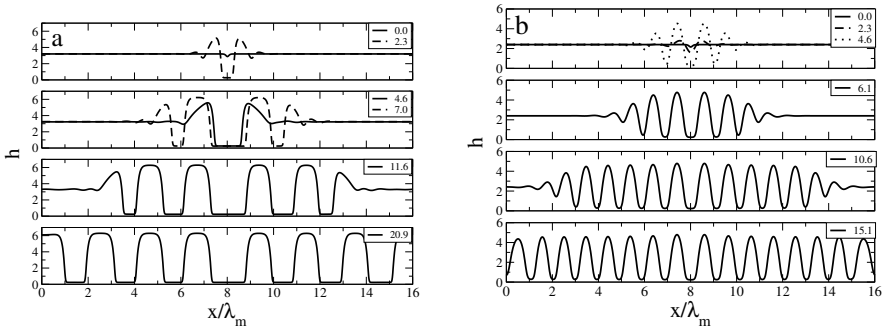

Figure 13. Snapshots of the time evolution in the (a) nucleation-dominated and (b) instability-dominated sub-ranges within the linearly unstable film thickness range. The insets give the evolution time and x is given in units of the fastest growing wavelength (for details see Thiele et al. (2001c)).

3.3 Heated thin films

The second case where the theoretical framework presented in Section 3.1 can be applied are large scale surface deformations of thin liquid films on a smooth solid homogeneously heated substrate. Without heating the film is stable. However, this is no longer the case once thermocapillary (Marangoni) effects are included. The resulting instability evolves according to Eq. (3.1) with the additional pressure given by Eq. (2.52) (Burelbach et al., 1988; Oron and Rosenau, 1992; Thiele and Knobloch, 2004). We consider only parameter regimes where the short-wave convective mode (Davis, 1987; Golovin et al., 1994) does not occur. The details of the thermocapillary instabilities depend on the assumed dependence of the surface tension on temperature (Nepomnyashchy et al., 2002). Usually it is taken to be linear (Deissler and Oron, 1992). A similar equation for a film below an air layer of finite thickness, was given by (VanHook et al., 1997) in connection with their investigation of the formation of dry spots. Work by Boos and Thess followed numerically the evolution of a film profile towards rupture using the full Stokes equation in combination with a linear temperature field (Boos and Thess, 1999), and identified a cascade of consecutive "structuring events" pointing towards the formation of a set of drops as the final state of the system.

In Thiele and Knobloch (2004) we revisit the problem of a heated thin film on a horizontal and a slightly inclined substrate to study the multiplicity of solutions to the nonlinear evolution equation and their stability properties. We also wish to understand the effects of a small inclination of the substrate (see Section 5). The basic behaviour is captured by a simplified model that omits complications due to effective molecular interactions, i.e. a model without disjoining pressure. One finds that the possible steady two-dimensional solutions of Eq. (3.1) can be determined independently of the fact that they cannot be reached from the initial condition of a flat film by integration in time. As for the ultrathin films studied above in Section 3.2, one encounters unstable nucleation solutions and drop-like solutions. A difference is, that the primary instability is always

subcritical, i.e. defects always play an important role.

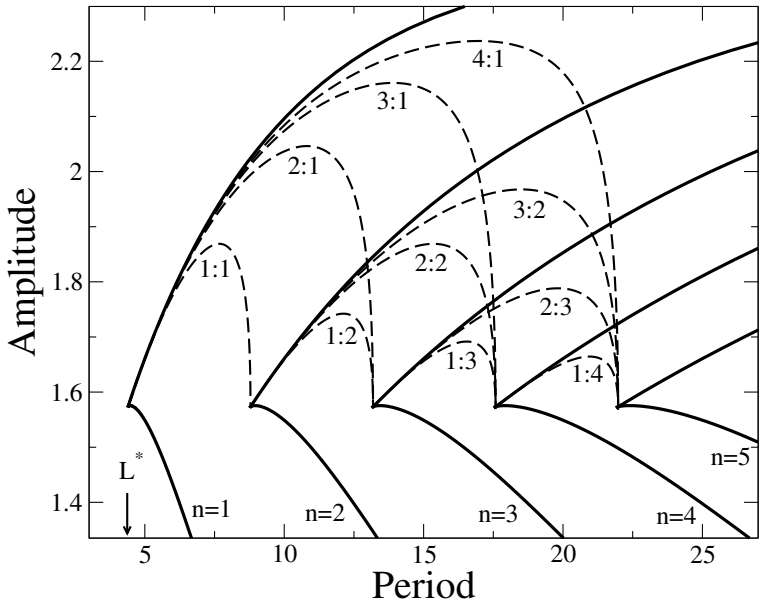

Figure 14. The amplitude $\Delta h \equiv h_{max} - h_{min}$ along single drop and multidrop branches with microscopic contact angle $\theta_0 = 0$ as a function of period L. They are steady solutions of Eq. (3.3) with (2.52) with Ma = 3.5, Bi = 0.5 and Bo = 1.0. The solid lines show the primary $n = 1, \ldots, 5$ branches where n gives the number of drops per period. They consist of periodic nucleation solutions (lower part) and the periodic drop solutions (upper part). The dashed lines show the different possible multidrop branches with maximal internal symmetry (i.e. branch $i : j$ has i identical drops of one type and j identical drops of another type) and no dry holes. Multidrop solutions with broken internal symmetry are present between these multidrop branches as described by Thiele and Knobloch (2004). Every multidrop solution of this type in turn represents the starting point for $i + j$ branches containing finite dry holes.

There is a vast family of solutions that represents drops of different sizes separated by dry regions of different lengths. In Thiele and Knobloch (2004) we describe and illustrate a construction that generates all such solutions. An example for the hierarchical structure that such families form is given in Fig. 14.

All of these solutions are nominally linearly stable, i.e. no coarsening can occur, since drops separated by truly dry regions do not interact if no non-hydrodynamic interaction is included. In the formulation without disjoining pressure the solutions with zero microscopic contact angle are energetically favored. However, the inclusion of a disjoining pressure selects a certain contact angle and removes the degeneracy. In Section 5 we discuss how the solution landscape collapses once the substrate is inclined.

In most works like, for instance, by Oron and Rosenau (1992); Thiele and Knobloch

(2004) the temporal evolution of the pattern is restricted by rupture, i.e. it is limited to the short-time evolution, leaving the long-time limit un-investigated. In Bestehorn et al. (2003) a precursor film is stabilized by introducing a van der Waals term as disjoining pressure. The model then consists of the three-dimensional version of Eq. (3.1), the additional pressure Eq. (2.52), and the first term of Eq. (2.51). Linear stability analysis, the determination of nonlinear steady solutions, as well as three-dimensional time dependent numerical solutions reveal a rich scenario of possible structures.

Using Maxwell-type constructions on calculates the existence regions of drops, holes, or fronts with respect to the applied substrate temperature and the mean film thickness. On very thin films drops should always evolve at onset whereas for thicker films, the formation of holes is predicted. Drops, or at least one big drop on a rather thick film was found in the experiment by VanHook et al. for an air layer, instead of holes for a helium gas layer above a silicone film (VanHook et al., 1997). The thermal properties of the gas layer influence the Biot number and also the Marangoni number. It seems possible that the Helium experiment was performed closer to threshold than the one with the air layer. According to the stability analysis in Bestehorn et al. (2003) this would explain the patterns observed in this experiment.

3.4 Coarsening

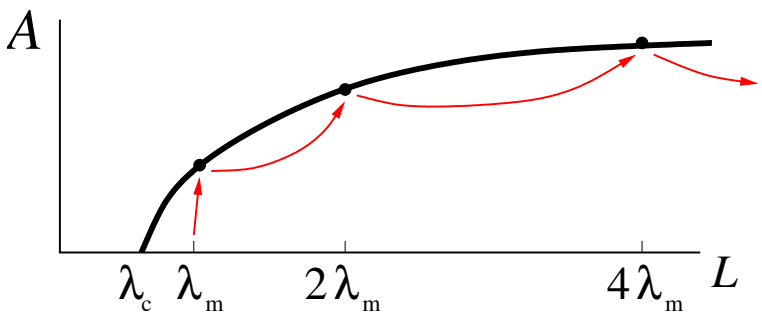

Figure 15. Schematic of the time evolution of a thin film. In the short-time evolution the flat film ruptures, the system approaches the large-amplitude branch. In the long-time evolution coarsening sets in and the system moves towards structures of larger length scales.

Up to here our presentation has mainly focused on the short-time evolution, i.e. the initial structuring process leading to the evolution of large amplitude structures from the initial flat film state. The time and length scales of the short-time evolution are determined by the linear modes of the flat film as sketched in Fig. 15. In a first approximation the length scale is given by the wave length of the fastest growing linear mode [Eq. (3.9)] and the time scale by $\tau_m = 1/\beta_m$ [Eq. (3.9)]. A nonlinear rupture time can also be determined (Sharma and Jameel, 1993), but is normally of the same order of magnitude as the linear one.

However, all the large-amplitude periodic drops and holes are only stable when the

analysis of their stability is restricted to instability modes of the same period. They are all unstable to modes of larger period, so-called coarsening modes. In the long-time evolution a coarsening process then leads in consecutive steps to the appearance of larger and larger structures as sketched in Fig. 15. Only a structure of system size is absolutely stable. An example of part of such a process is illustrated below by an energy-time plot (see below Fig.21, solid line). Note, that practically the coarsening process may be stopped by small substrate heterogeneities (see below Section 4).

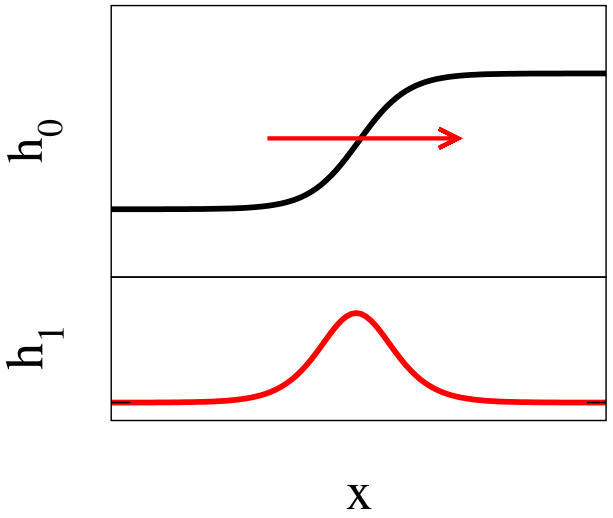

Figure 16. Sketch of the steady solution h_0 and the translational symmetry mode $h_1(x) = \partial_x h_0(x)$ for a liquid front.

In a system where the basic structure consists of drops, in the course of time droplets merge into larger droplets. Thereby the system moves along the low-energy branch of periodic solutions (Fig. 10) towards states of lower energy. The pathway of the coarsening, i.e. the detailed properties of the active coarsening modes can be understood from an analysis of the linear stability of the steady solutions on the low-energy branch. The important modes are related to the symmetry modes of the system. In general, each continuous symmetry is connected with a marginally stable symmetry mode, i.e. with a linear mode $h_1(x)$ that fulfills Eq. (3.14) with $\beta = 0$. For instance, situations involving a homogeneous horizontal substrate are translationally invariant. The related symmetry mode is the translation mode with $h_1(x) = \partial_x h_0(x)$ where h_0 is the steady solution. For a liquid front both are sketched in Fig. 16.

To introduce the symmetry modes for a single droplet on a horizontal homogeneous substrate we assume that the left and the right side of the droplet are nearly decoupled allowing to see them as two individual fronts. Then we combine the symmetry modes of the two fronts. We obtain a translational mode when both fronts move in the same direction and a volume mode when they move in opposite directions (see Fig. 17).

The two symmetry modes of a single droplet can be combined in the same spirit as

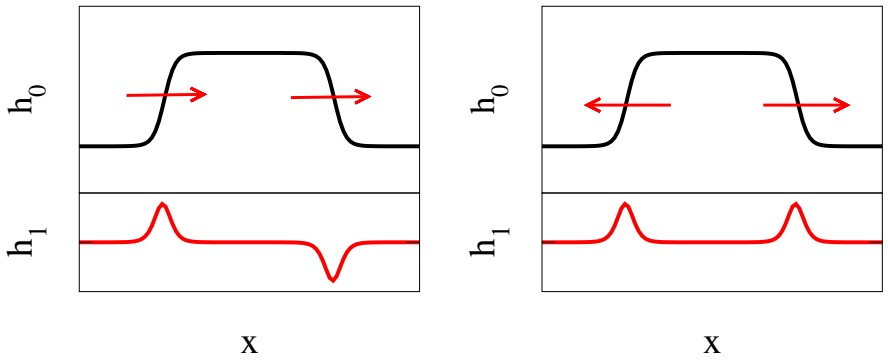

Figure 17. Symmetry modes for a single droplet on a horizontal substrate. Translation mode (left) and volume mode (right) are both obtained as a linear combination of translation modes for the two individual fronts.

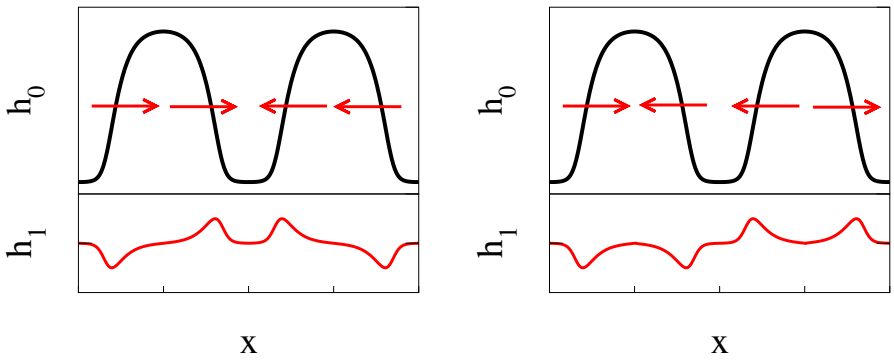

Figure 18. Coarsening modes correspond to combinations of symmetry modes for individual droplets. Shown are translation mode (left) and mass transfer mode (right).

above to obtain the two relevant coarsening modes for a pair of droplets. One mode results as a combination of a leftwards and a rightwards translation of the two respective drops (left part of Fig. 18). This leads to coarsening by translation. The other mode combines a negative (inward) and a positive (outward) volume mode, i.e. one droplet grows at the cost of the other one (right part of Fig. 18). This is the mass transfer mode of coarsening. The material may be transported through the precursor film or through evaporation/condensation. Assuming the transport equation (3.1) excludes the latter.

For unstable heated films a van der Waals interaction may stabilize a precursor film and avoid true rupture (Bestehorn et al., 2003). A numerical study then reveals the long-time behavior of such a system. The overall coarsening behaviour is well characterized by a scaling law $k \sim t^{-\nu}$ for the dependence of the typical length-scale $1/k$ on time t. We found an independent scaling factor with respect to the Hamaker constant close to threshold. First results give a tendency for the scaling exponent as $\nu = 0.21 \pm 0.01$. This

indicates that the coarsening is slower than in spinodal decomposition, where $\beta = 1/3$ as given by the Lifshitz-Slyozov-Wagner theory (see for example Langer (1992)). The inclusion of hydrodynamic effects in the description of spinodal decomposition gives even larger exponents for the long time limit (in two dimensions $\beta = 1/2$ viscosity controlled, $\beta = 2/3$ inertia controlled (Podariu et al., 2000)). The scaling behaviour is in general not yet well studied. We are still far from a detailed understanding (but see Mitlin (2001); Bestehorn et al. (2003); Glaser and Witelski (2003); Pismen and Pomeau (2004)). This is also true for two-layer films where a variety of scaling exponents is reported Merkt et al. (2005).

4 Horizontal inhomogeneous substrate

Several recent experiments (Karim et al., 1998; Rehse et al., 2001; Rockford et al., 1999; Sehgal et al., 2002) involve dewetting of thin films on inhomogeneous substrates. Mostly they aim at arranging soft matter in a regular manner as determined by the physically and/or chemically patterned substrates. In nearly all experiments the (strong) heterogeneity imposes itself on the dewetting film if the length scale of the pattern is similar to the intrinsic scale of dewetting. This corresponds to theoretical results of a variety of groups (Lenz and Lipowsky, 1998; Bauer et al., 1999; Bauer and Dietrich, 2000; Kargupta et al., 2000, 2001; Kargupta and Sharma, 2001; Brinkmann and Lipowsky, 2002) based on a static approach using energy minimisation or a dynamic approach using a long wave equation like Eq. (3.1) but with strong stepwise wettability contrasts (for a discussion see Thiele (2003a)). Deposited liquid volume, chemical potential or the size of the heterogeneous patches are used as control parameters to derive morphological phase diagrams. However, special care has to be taken using stepwise wettability patterns in dynamical studies because Eq. (3.1) is a long wave equation. In its derivation it is assumed that *all* relevant length scales parallel to the substrate are large as compared to the film thickness. This is not the case for a stepwise wettability contrast.

To understand the influence of a heterogeneous substrate in detail it is convenient to regard dewetting on a smoothly patterned substrate using the wettability contrast as a control parameter (Thiele et al., 2003). A film on a striped substrate is modelled using Eqs. (3.1) and (2.50) replacing the constant κ by the heterogeneity

$$\kappa(x) \;=\; \kappa_0 \left[1 \;+\; \epsilon \cos\left(\frac{2\pi x}{P_{het}}\right)\right] \tag{4.1}$$

thereby modulating the wettability of the substrate sinusoidally. κ_0 is then absorbed into the scaling. The parameters ϵ and P_{het} correspond to the maximal wettability contrast and the period of the stripe-like heterogeneities.

Again continuation is used to determine all the stable and unstable steady solutions. Thereby solutions determined for the homogeneous substrate or analytic solutions obtained for small ϵ are used as starting solutions, then ϵ is increased to get the basic bifurcation diagram for the transition from homogeneous to inhomogeneous substrates and in consequence also the characteristics of the transition between coarsening and pinning (ideal templating) in its dependence on heterogeneity strength, heterogeneity

period and film thickness. Taking two periods of the heterogeneity as the system size one obtains, for instance, the bifurcation diagram given in Fig. 19.

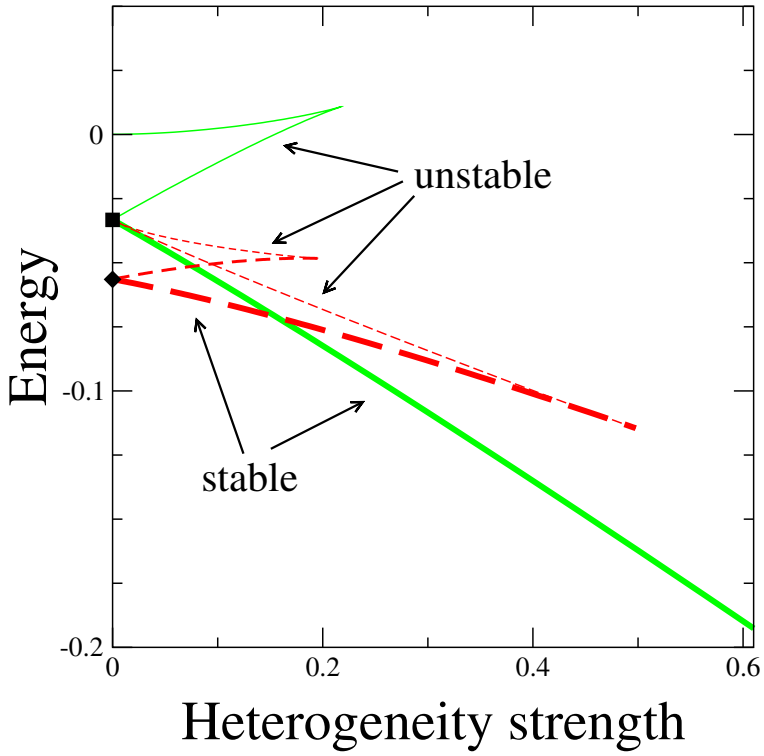

Figure 19. Energy of steady solutions to Eq. (3.3) with (4.1) for system size $L = P_{het}$ and $L = 2P_{het}$ versus the wettability contrast ϵ. Square and diamond denote the periodic solutions in the homogeneous case. Solid curves correspond to $L = P_{het}$ and dashed curves to $L = 2P_{het}$. Stable (unstable) solutions are marked by thick (thin) lines. The disjoining pressure (2.50) is used and the parameters are $\bar{h} = 2.5$, $P_{het} = 50$ and $G = 0.1$ (for details see Thiele et al. (2003)).

We start the analysis with the shortest system of size $L = P_{het}$. Switching on the heterogeneity implies that the flat film is no longer a solution of Eq. (3.3) with (4.1). The flat film solution is replaced by a periodic solution that can be given analytically in the limit of weak heterogeneity $\epsilon \ll 1$. Writing the heterogeneity as $\epsilon \cos(kx) = \epsilon/2(e^{ikx} - c.c.)$ with $k = 2\pi/P$ where $c.c.$ stands for complex conjugate, the volume conserving ansatz for the film thickness

$$h(x) = \bar{h} + \frac{\delta}{2}(e^{i\tilde{k}x} - c.c.) \tag{4.2}$$

is inserted into Eq. (3.3). This gives for $\delta \sim O(\epsilon)$ and neglecting terms of higher order

in ϵ solutions with $\tilde{k} = k$ and

$$\delta = \frac{M(\bar{h})}{k_c^2 - k^2}\,\epsilon \tag{4.3}$$

where M is the κ-dependend part of the disjoining pressure. The condition $\delta \ll 1$ is only fulfilled if P is well separated from λ_c. For Eq. (2.50), $M(\bar{h})$ is always positive, hence for $k_c > k$ ($\lambda_c < P$) the solution is modulated in phase with the heterogeneity, i.e., the film is thicker on the less wettable parts of the substrate. These small amplitude solutions are linearly unstable like the flat film of the corresponding thickness without heterogeneity. However, if the critical period is larger than the period of the heterogeneity ($\lambda_c > P$) this solution has a phase shift of π with respect to the heterogeneity, i.e., the film is thinner on the less wettable parts of the substrate. This is also the case if the flat film of thickness $\bar{h}$ is linearly stable because there $k_c^2 < 0$. These small amplitude solutions are linearly stable.

Restricting our attention to linearly unstable film thicknesses we use the weakly modulated solution Eqs. (4.2) and (4.3) as starting solution for the continuation procedure (Doedel et al., 1997) and compute steady solutions with period $L = P_{het}$ as ϵ is increased. The flat film and periodic solution at $\epsilon = 0$ give rise to one and two solution branches, respectively. Fig. 19 shows the corresponding bifurcation diagram. The branch emerging from the flat film solution is for small ϵ well approximated by the analytical result Eq. (4.3). The solutions on this branch are indeed in phase with the heterogeneity whereas the branch of lowest energy (thick solid line emerging from the square at $\epsilon = 0$) that corresponds to large amplitude solutions possesses a phase shift, as one would expect from physical considerations: the drops concentrate on the more wettable patches. The middle branch is in phase with the heterogeneity and terminates together with the small amplitude branch in a saddle-node bifurcation. In the regarded small system with $L = P_{het}$, the entire thick solid branch in Fig. 19 is linearly stable whereas the other two solid branches are linearly unstable.

New solutions appear as we double the system size to $L = 2\,P_{het}$. Beside the already discussed solutions with period P_{het} there exist also solutions with period $2P_{het}$ (dashed lines in Fig. 19). At $\epsilon = 0$ they are denoted by a diamond.

Although the solutions discussed above for system size $L = P_{het}$ are still solutions, their period is now smaller than the system size and they may be unstable to coarsening. At least for $\epsilon = 0$ this is known from Section 3.4. Let us focus on the solutions on the thick solid branch that we will call the pinned solutions because they image the heterogeneity in an ideal way. For $\epsilon = 0$ the solution possesses two positive eigenvalues corresponding to the coarsening modes of translation and mass transfer discussed above (Section 3.4). As ϵ departs from zero the heterogeneity counteracts the coarsening and the two modes are subsequently stabilized. For the present choice of parameters in Fig. 19 the translational mode becomes stable at smaller ϵ values than the mass transfer mode implying that the mass transfer is the dominant coarsening process. As ϵ increases, both eigenvalues become negative, implying the linear stability of the pinned solution for larger ϵ. At the two points where the eigenvalues cross the zero, period doubling bifurcations occur where steady solutions of period $2P_{het}$ emerge from the thick solid line. The two bifurcations are both subcritical hence the emerging solutions inherit the respective instability of the unstable solutions at smaller ϵ (cp. Guckenheimer and Holmes (1993)).

Manuscript —- contact: thiele@pks.mpg.de – http://www.uwethiele.de – 10th March 2006

The four branches of solutions of period $2P_{het}$ shown in Fig. 19 have the following linear stability. The upper thin dashed branch carries two positive eigenvalues and is itself a saddle in function space that divides evolutions by mass transfer towards the lower thin dashed branch and the branch of pinned solutions. The lower thin dashed branch still has one positive eigenvalue that leads to a shift of the pattern towards solutions of the thick dashed branch. The upper dashed branch emerging from the diamond has one positive eigenvalue and is a saddle that divides evolutions by translation of two droplets towards the thick dashed branch and the branch of pinned solutions. The entire thick dashed branch is linearly stable and represents the coarse solution competing with the pinned pattern.

Extracting the results on the stability of the pinned and the coarse solution one can generally state that for a wettability contrast ϵ below a first threshold value ϵ_1 the coarse solution is the only stable one and also has the lowest energy. For $\epsilon > \epsilon_1$ one has multistability between the pinned and the coarse solution. In consequence initial conditions and noise become very important for the evolution of the dewetting process. At $\epsilon = \epsilon_2$ the energies of both linearly stable solutions are equal. Above that value the pinned pattern has lowest energy. Finally at the threshold ϵ_3 the coarse solution ceases to exist and for $\epsilon > \epsilon_3$ the pinned solution is the only possible one.

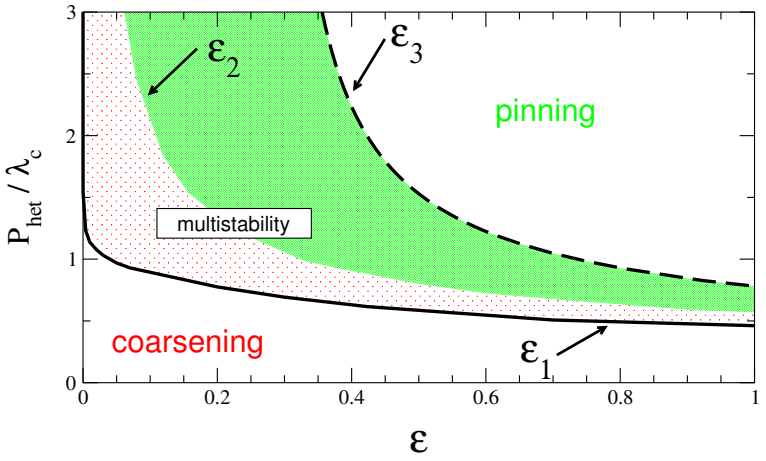

Figure 20. Morphological phase diagram of templating shows parameter regions in the $(\epsilon, P_{het}/\lambda_c)$ plane with different behavior of the thin film on a heterogeneous substrate. The shaded area separates the parameter region of coarsening from the one of pinning. Inside the shaded band multistability is present with the pinned pattern having the minimal energy inside the dark shaded area. The threshold values ϵ_i are indicated. Parameters are $\bar{h} = 2.5$ and $G = 0.1$ (for details see Thiele et al. (2003)).

Repeating the above analysis for the full range of P_{het} results in the morphological phase diagram Fig. 20 where we indicate the relation of the different borders with the above defined ϵ_i. At low values of ϵP_{het} coarsening prevails while for large values the pattern is pinned to the heterogeneity. At intermediate values (shaded area) the initial

condition selects the asymptotic state due to multistability. In particular, it is not possible to pin a pattern to a heterogeneity that is much smaller than the critical wavelength λ_c for the surface instability of the corresponding flat film on the homogeneous substrate. Similar phase diagrams are also obtained for stepwise wettability contrast (Kargupta and Sharma, 2001, 2002). This suggests that the actual functional form of the heterogeneity is much less important than its length scale and strength.

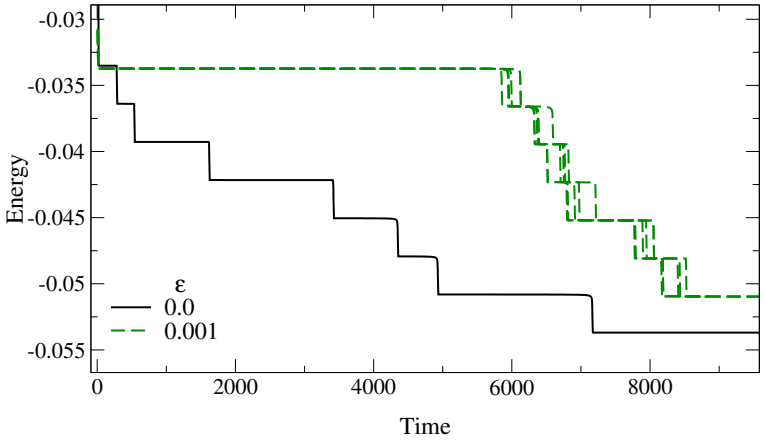

Figure 21. Energy for the long-time evolution for the homogeneous substrate (solid lines) and a slightly heterogeneous substrate (dashed lines, $\epsilon = 0.001$). The various dashed lines stand for evolutions with different realizations of noise with an amplitude of 0.001. The remaining parameters are $\bar{h} = 2.5$, $P_{het} = 50$ and $G = 0.1$ (see Thiele et al. (2003)).

The bifurcation and stability analysis of the possible liquid ridge solutions reveal parameter ranges where pinning or coarsening ultimately prevail, but also allows to establish the existence of a large hysteresis between pinned and coarse solutions, i.e. a large range where both morphologies correspond to local minima of the energy. This characterises the pinning-coarsening transition as a first order phase transition. In the resulting metastable range, the selected pattern depends sensitively on the initial conditions and potential finite perturbations (noise) in the system as illustrated with numerical integrations in time in (Thiele et al., 2003). Fig. 21 shows that compared to the homogeneous system a weak heterogeneity slows down the onset of coarsening but accelerates the coarsening in the nonlinear regime. Recently, Grün et al. (2005) derived a stochastic evolution equation for a thin film on a heterogeneous substrate from the Navier-Stokes equations using long wave approximation and Fokker-Planck-type arguments.

5 Inclined homogeneous substrate

5.1 General analysis

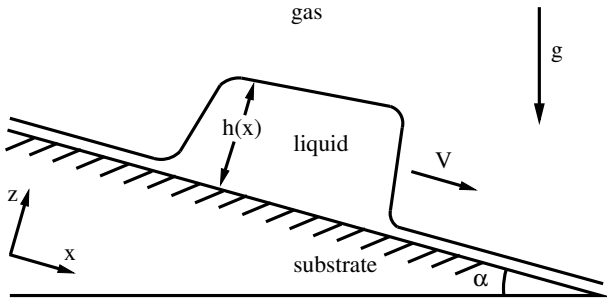

Figure 22. Sketch of a sliding drop on an inclined homogeneous substrate.

For a film on an inclined substrate we are interested in stationary moving solutions for the film thickness profile $h(x,t)$. We use the comoving coordinate system $x' = x - vt$, where v is the dimensionless velocity. Replacing in Eq. (2.47) the time derivative $\partial_t h$ by $-v\partial_{x'}h$ and integrating yields after dropping the dash

$$0 \;=\; Q(h)(\partial_{xxx}h \;-\; \partial_{hh}f\,\partial_x h) \;+\; \chi(h) \;-\; v\,h - C_0. \tag{5.1}$$

Note, that the v is the phase velocity of the profile not the mean velocity of the liquid (cf. surface waves). In contrast to the reflection symmetric problem of a film on a horizontal homogeneous substrate (Section 3) here we cannot set the integration constant C_0 to zero. Consequentely one cannot integrate another time. Writing Eq. (5.1) in the form $C_0 = (\Gamma - vh)$ tells that for all stationary solutions the flow in the comoving frame $\Gamma - vh$ is constant but not the flow in the laboratory frame Γ. The choice of the constant of integration,

$$C_0 \;=\; (\Gamma_0 - vh_0) \;=\; -\chi(h_0) \;+\; v\,h_0, \tag{5.2}$$

introduces a flat film solution of thickness h_0. This corresponds to prescribing the liquid volume (see Scheid et al. (2005) for prescription of the flow rate).

Beside the flat film solution given by the choice of h_0 there may exist other film thicknesses, h_i, that give the same flow in the comoving frame, $C_0 = \Gamma_i - vh_i = \Gamma_0 - vh_0$. These flat film solutions correspond to the fixed points of Eq. (5.1), seen as a dynamical system. Taking, for instance, $\chi(h) = \alpha h^3$ there exist for a given h_0 two more flat film solutions

$$h_{1,2} \;=\; h_0\left(-\frac{1}{2} \;\pm\; \sqrt{\frac{v}{\alpha h_0^2} \;-\; \frac{3}{4}}\right) \tag{5.3}$$

Because the film thickness has to be positive everywhere one has to choose the positive sign in (5.3). This solution is positive for $v/\alpha h_0^2 > 1$, i.e. a second flat film solution exists (called conjugate solution in, for instance, Nguyen and Balakotaiah (2000)). Note, that the flat film solutions do not depend on the disjoining pressure $\Pi(h)$. However, they are

entirely determined by $\Pi(h)$ in the limiting case $\alpha = 0$ (see Eq. (3.4). The consequences are discussed by Thiele et al. (2001c).

A linear stability analysis of the flat film yields the dispersion relation

$$\beta \;=\; -Q(h_0)\,k^2\left(k^2 \;+\; \partial_{hh} f(h_0)\right) - i\,\partial_h \chi(h_0) k. \tag{5.4}$$

The real and imaginary parts of $\beta(k)$ give the respective growth rate and downwards phase velocity of the mode with wavenumber k.

In contrast to the existence of flat film solutions their stability does not depend on the dynamical aspect of the problem (inclination angle and velocity), but only on $\partial_{hh} f(h_0)$ as for a flat film on a horizontal substrate (Section 3.1). In the limit of vanishing influence of the disjoining pressure this corresponds to the fact that we only regard Stokes flow, i.e. without the disjoining pressure the flat film is linearly stable for all inclination angles. All linear modes propagate downwards with the velocity $v = -\mathrm{Im}\beta/k$, corresponding to the fluid velocity at the surface of the unperturbed flat film.

Given a flat film in the linearly unstable thickness range, it will start to evolve in time. This may lead to stationary film profiles of finite amplitude, i.e. to sliding drops or nonlinear surface waves. They can be determined as periodic solutions of Eq. (5.1) using continuation methods (Doedel et al., 1997) starting from small amplitude analytic solutions.

5.2 Isothermal partially wetting case

Experiments on liquid films or droplets moving down an inclined plate study, for instance, the formation of surface waves (Kapitza and Kapitza, 1949), localized structures and their interaction (Liu and Gollub, 1994), or shape transitions of sliding drops (Podgorski et al., 2001). Thereby, most studies on surface waves focus on structure formation caused by inertia measured by the Reynolds number and modelled by Benney-type equations (Benney, 1966; Joo et al., 1991; Scheid et al., 2005). However, because there the base flow and the 'structuring influences' have different orders in the smallness parameter (see Section 2.7) this type of description can normally not be applied to very thin films or to sliding drops.

Other studies that regard the evolution of falling sheets or ridges on an inclined 'dry' substrate encounter the problem of the moving three-phase contact line (Huppert, 1982; Silvi and Dussan, 1985) discussed above in Section 2.4. There the classical no-slip boundary condition at the liquid-solid interface has to be relaxed to permit movement of the contact line. This is normally done by introducing explicitely a very thin precursor film, or by allowing for slip near the contact line, or introducing an effective molecular interaction between the substrate and liquid into the hydrodynamic model (de Gennes, 1985; Dussan, 1979; Greenspan, 1978; Hocking, 1977; Huh and Scriven, 1971). Most work on moving liquid sheets and ridges uses one of the first two options. Both prescriptions avoid divergence problems at the contact line, but introduce ad hoc parameters into the theory. These parameters, namely the slip length or the precursor film thickness, influence the base state profile and also the characteristics of transverse front instabilities (Bertozzi and Brenner, 1997; Hocking and Miksis, 1993; Kataoka and Troian, 1997; Spaid and Homsy, 1996). Moreover, the equilibrium and dynamic contact angles have to be

fixed independently when introducing the slip condition (Greenspan, 1978; Hocking, 1990; Moyle et al., 1999). In contrast, in the absence of motion the precursor film models require that the contact angle be zero, although once the film is in motion the dynamic contact angle depends on the velocity of the advancing front.

Furthermore, most works (Hocking, 1990; Huppert, 1982; Troian et al., 1989) on liquid sheets or ridges flowing down an inclined plane analyse separately the three regions (1) upstream end, (2) central part and (3) downstream end of the ridge. Similarity solutions in the regions (1), (2) and (3) are matched together. The power-law dependence on time in these models is due to the fact that the situations studied are a superposition of spreading and sliding going on forever. However, recent experiments studied stationary drops that slide down a plate without changing their shape (Podgorski, 2000).

The explicit introduction of molecular interactions between the film surface and the substrate into the hydrodynamic formalism by means of a disjoining pressure (Section 2.4) can resolve the divergence problem at the moving contact line (Eres et al., 2000; Bestehorn and Neuffer, 2001; Thiele et al., 2001b, 2002a). Depending on the particular problem treated, this disjoining pressure may incorporate long-range van der Waals and/or various types of short-range interaction terms Teletzke et al. (1988); Hunter (1992); Israelachvili (1992). Because these interactions are essential for the process of dewetting, studies of dewetting of a thin liquid film on a substrate generally involve a disjoining pressure (see Section 3). This allows to connect the normally well separated fields of pattern formation on horizontal and inclined substrates.

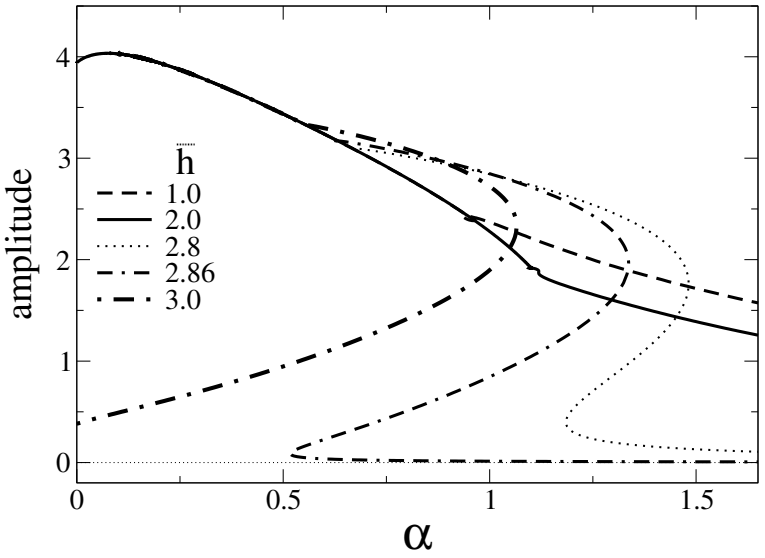

Figure 23. Characterization of stationary travelling periodic solutions. Shown is the dependence of the amplitude on period, L, for different mean film thicknesses, $\bar{h}$ as given in the legend. $G = 0.1$ and $\alpha = 0.1$ (for details see Thiele et al. (2001b)).

However, only a few studies have adopted such an approach despite the fact that

such an approach predicts all the ad hoc parameters of the slip or precursor models (i.e., the static and dynamic contact angle, drop velocity, and the drop and precursor film thickness). The necessary input is a description of the wetting properties of the liquid in terms of the parameters characterizing the disjoining pressure.

In the following we present some basic results for sliding drops and surface waves as stationary solutions of Eq. (3.1). Specifically, we present solutions of Eq. (5.1) for different mean film thicknesses and inclination angles. In general one distinguishes large amplitude drop-like solutions found for small inclination angles and small amplitude surface waves found for large inclinations. The solution families are presented for different mean film thicknesses in Fig. 23 in the form of an inclination-amplitude plot. There the upper (lower) branches stand for drop-like (surface wave) solutions. Note, that for small inclinations the drop-like solutions all converge to an 'universal' curve (solid line). Drops along this line have a velocity and amplitude that are independent of their volume.

On the 'universal' curve the film profile converges to a common shape: a flat drop with a capillary ridge at the advancing front, an upper plateau of arbitrary extension and a non-oscillatory receding front. The drops slide on a very thin precursor film (lower plateau). Only the length of the upper plateau depends on the mean film thickness. Choosing one of the two plateau thicknesses as h_0, the other plateau thickness is given by Eq. (5.3). The velocity of the flat drops is determined by the dynamic equilibrium between the overall forces of gravity acting on the liquid and viscous friction. The equilibrium does not depend on the liquid volume because both forces are proportional to the length of the flat drop.

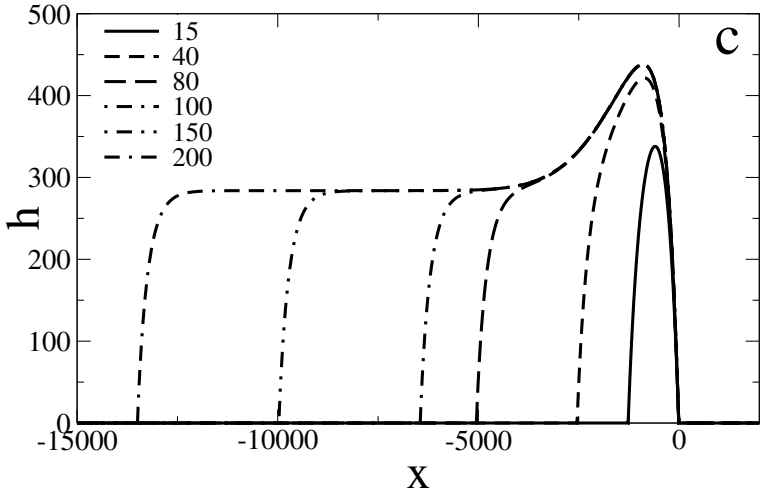

Figure 24. Profiles for different drop volume for a period of $L = 100000$, $G = 10^{-5}, and \alpha = 0.2$. The mean film thickness is increased (values given in legend, for details see Thiele et al. (2002a)).

Fig. 24 shows the related transition, for fixed inclination angle and interaction parameters, from small (asymmetric) cup-like drops to large flat drops as the volume increases.

Manuscript —- contact: thiele@pks.mpg.de – http://www.uwethiele.de – 10th March 2006

The two-dimensional cup-like drops correspond to cross-sections of ridge-like solutions that are independent of the coordinate y transverse to the flow. The flat drops correspond to cross-sections of liquid sheets of finite longitudinal extent.

Using the models that incorporate a disjoining pressure allows to study the dependence of the advancing and receding dynamic contact angles on the drop velocity. We define the contact angle as the absolute value of the slope of the profile at its inflection point. The drop has two dynamic contact angles, the advancing angle at its downstream front, θ_a, and the receeding angle upstream, θ_r. The differences between these angles and the equilibrium or static contact angle, θ_e, obtained for $\alpha = 0$ are shown in Figs. 9 and 10 of Thiele et al. (2001b), respectively[10] The receeding angle is always smaller than θ_e and in the velocity range studied here the absolute value of the difference between both angles increases linearly with increasing velocity. However, it was found that the difference between the advancing angle and θ_e changes non-monotonically with increasing velocity (Thiele et al., 2001b).

For a detailed analysis of the 'non-universal' part of the curves in Fig. 23 we refer the reader to Thiele et al. (2001b, 2002a). Let us mention that the study of the non-universal solutions has revealed a hysteresis effect, when jumps between small and large amplitude solutions occur that both exist for a certain range of inclination angles for some mean film thicknesses (cp. Fig. 23). The transition between the two branches may be called a *dynamical wetting transition with hysteresis*. Such a dynamical wetting transition is now reasonably well understood (Blake and Ruschak, 1979; Podgorski, 2000; Pomeau, 2000; Ben Amar et al., 2001; Eggers, 2004): at the macro scale it would occur when the contact angle vanishes at finite velocity. However, as far as we know, no hysteresis has been predicted and/or observed although it does not seem to be excluded at all from first principles.

5.3 Heated inclined substrate

In Section 3.3 we already discussed the vast family of drop solutions that can be constructed for a heated horizontal substrate. Next we sketch how the solution landscape collapses once the substrate is inclined, i.e. using Eq. (2.47) with (2.52) and $\chi \neq 0$ (Thiele and Knobloch, 2004). On an inclined substrate the dry spots are replaced by regions of ultrathin film, and the array of drops slides downwards. This precursor film is not the usual static one but is dynamically produced by the 'first' drop. Its thickness depends on the dynamics of the system. This corresponds to the dependence of the lower plateau thickness on sliding velocity mentioned above in Section 5.2. In Thiele and Knobloch (2004) it is demonstrated that sliding trains of drops can be stable with respect to longitudinal perturbations, i.e. with respect to coarsening modes. This corresponds to similar results obtained for convective Cahn-Hilliard models (Golovin et al., 2001).

Because of the enormous degeneracy of solutions in the horizontal case there is a very large number of slowly drifting drop-like states once the substrate is slightly inclined. In this regime one can locate intervals in the spatial period containing no stable simple

[10] Note, that the results for the contact angles in lubrication approximation have to be seen as corrections to the usually obtained proportionality $v \sim \theta^3$ (de Gennes, 1985) that is already absorbed into the scaling.

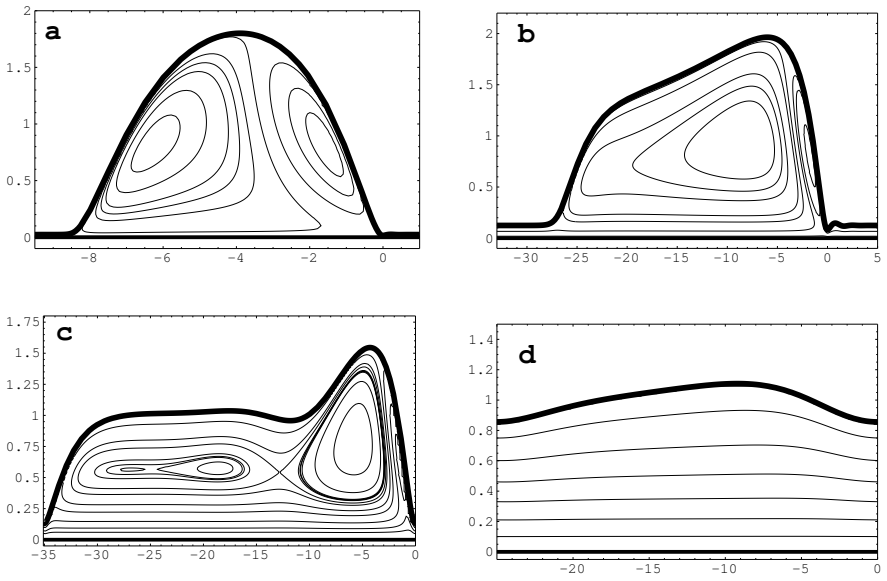

Figure 25. Comoving streamlines for different inclination angles and periods when Ma = 3.5, Bi = 0.5 and Bo = 0.5. (a) $\alpha = 0.08$, $L = 10$ and $v = 0.021$; (b) $\alpha = 0.08$, $L = 40$ and $v = 0.053$; (c) $\alpha = 0.215$, $L = 35$ and $v = 0.09$; (d) $\alpha = 0.215$, $L = 25$ and $v = 0.21$. The last panel shows a solution on the small amplitude surface wave branch formed when the primary bifurcation becomes supercritical (for details see Thiele and Knobloch (2004)).

traveling wave solutions. Here one expects states with complex time-dependence, but perhaps more than that, since the profusion of unstable states suggests that the system may wander among these states, exhibiting very long transients even when stable states are available. At larger inclination the drift associated with finite inclination starts to dominate the dynamics, and the primary branches become supercritical with the resulting solutions resembling the traveling wavetrains familiar from the Kuramoto-Sivashinsky equation. As an illustration Fig. (25) presents a selection of stationary profiles for cap-like and flat drops and surface waves. The flow field in the comoving system is represented by streamlines.

The main conclusion is that the degeneracy of the horizontal case influences the inclined problem only for quite small values of the inclination angle where the dynamics is still Cahn-Hilliard-like. For larger inclinations the system behaves much more like the falling films under the influence of inertia studied, for example, in Benney (1966); Joo et al. (1991) even though the theory does not retain inertial effects. Such films behave much like the Kuramoto-Sivashinsky equation, and Thiele and Knobloch (2004) can be viewed as a quantification of the range of applicability of this equation to thin films on an inclined plane.

6 Transversal instability

In the final section on systems described by the single film evolution equation (2.47) we will focus on the transversal stability of liquid ridges on horizontal homogeneous, horizontal heterogeneous and inclined homogeneous substrates. Thereby we follow in part Thiele and Knobloch (2003) where the linear stability of liquid ridges on horizontal and inclined substrates is studied as a function of their volume and the inclination. The aim is on the one hand to understand the transition between the various instability modes for liquid ridges on a horizontal substrate (Davis, 1980; Roy and Schwartz, 1999; Sekimoto et al., 1987) and on an inclined plane (Hocking, 1990; Hocking and Miksis, 1993), and on the other hand to relate these findings to results for falling semi-infinite sheets (Bertozzi and Brenner, 1997; de Bruyn, 1992; Eres et al., 2000; Huppert, 1982; Kalliadasis, 2000; Spaid and Homsy, 1996; Troian et al., 1989; Veretennikov et al., 1998; Ye and Chang, 1999).

In the latter case the leading front advances onto the 'dry' substrate and may initiate a fingering instability. It develops into an array of fingers advancing faster than the original front. A related transverse (or span-wise) instability occurs on a liquid front that advances as a result of a Marangoni flow induced by a longitudinal (i.e., stream-wise) temperature gradient (Bertozzi et al., 1998; Kataoka and Troian, 1998). In both cases the instabilities are due to differences in the mobility of the thinner and thicker parts of the capillary ridge at the advancing front.

6.1 Linear stability analysis of a liquid ridge

We have shown in the preceding sections that continuation is a very effective method to determine stable and unstable stationary solutions and their bifurcations by following them through parameter space using Newton's method (Doedel et al., 1991a,b). Here, we also apply it to study the linear stability of the found solutions with respect to transversal disturbances (Thiele and Knobloch, 2003). There one has to continue simultaneously the stationary solution of Eq. (2.47), i.e. the profile $h_0(x)$ and the velocity v of the ridge, and the solution of Eq. (2.47) linearized around $h_0(x)$. Using the ansatz

$$h(x,y,t) = h_0(x) + \epsilon\, h_1(x)\, \exp(iky + \beta t) \tag{6.1}$$

to linearize Eq. (2.47) gives the linear eigenvalue problem for the growth rate β and disturbance h_1 as

$$\beta h_1(x) \;=\; \mathbf{S}[k, h_0(x)]\, h_1(x) \qquad \text{with} \qquad \mathbf{S}h_1 \;=\; \mathbf{N}_0 h_1 + k^2 \mathbf{N}_2 h_1 + k^4 \mathbf{N}_4 h_1 \tag{6.2}$$

with

$$\begin{aligned} \mathbf{N}_0 h_1 &= -\left\{Q_h h_1\, [(\partial_{xx} h_0 - \partial_h f)_x]\right\}_x , \\ &\quad -\left\{Q\,(\partial_{xx} h_1 - \partial_{hh} f h_1)_x\right\}_x \\ \mathbf{N}_2 h_1 &= \left\{Q\, h_{1x}\right\}_x + Q\,(\partial_{xx} h_1 - \partial_{hh} f h_1), \\ \mathbf{N}_4 h_1 &= -Q\, h_1 . \end{aligned} \tag{6.3}$$

The solution of Eq. (6.2) for the (complex) disturbance mode $h_1(x)$, transversal wavenumber k and the (complex) eigenvalue β has to be continued in parameter space together

with the stationary solution $h_0(x)$. This is done using a three step procedure. First, h_0 and v are calculated by continuation starting from analytically known small amplitude solutions. The eigenvalue problem is then discretized in space and solved numerically. However, the necessary equidistant discretisation can be used in a small parameter range only. These restricted results are, in the third step, used as starting solutions for continuation of both h_0 and v, *and* of the solutions to the eigenvalue problem for any set of parameter values. The required extended system consists of 11 first order differential equations (3 for h_0 and 4 each for the real and imaginary parts of h_1). Furthermore, points of special interest such as the zeros or the maxima of the dispersion relation or the transition between real and complex eigenvalues can be followed through parameter space (Thiele and Knobloch, 2003).

6.2 Horizontal homogeneous substrate

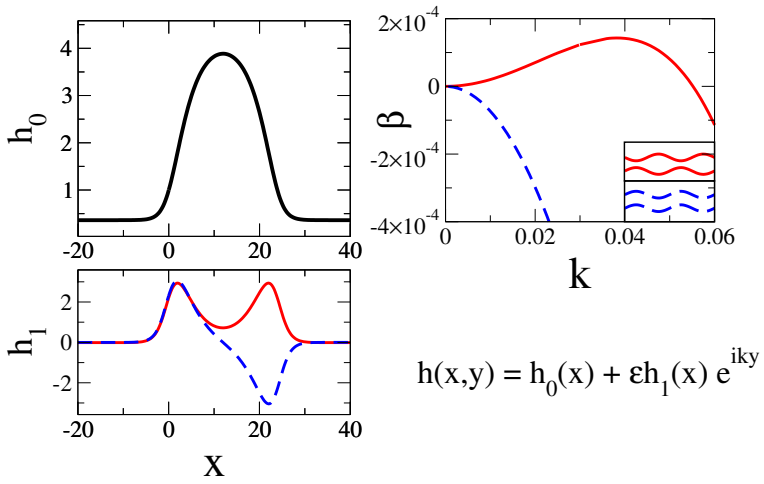

Figure 26. Overview for the transverse stability of a ridge on a horizontal substrate: (a) Steady ridge profile $h_0(x)$; (b) Dispersion relation $\beta(k)$ for the two transverse modes: the unstable varicose mode (solid) and the stable zigzag mode (dashed). Top views of the corresponding modes are sketched in the inset. (c) The eigenmodes $h_1(x)$ with line styles corresponding to (b). For details see Thiele and Knobloch (2003).

First we consider the homogeneous horizontal substrate. Remember that in this case the problem is variational implying that all eigenvalues β and eigenfunctions h_1 are real. This simplifies the above explained proceedure to the continuation of 7 first order differential equations. An individual liquid ridge is always transversally unstable with respect to a varicose mode that emerges from the zero-eigenvalue at $k = 0$ connected to the volume mode for a single two-dimensional drop (cp. Section 3.4, especially Fig. 17 (right)). It is reminiscent of the Rayleigh instability known from liquid jets (Chandrasekhar, 1992; Eggers, 1997). Fig. 26 shows the cross section of such a ridge in (a), the dispersion rela-

tions in (b), and the relevant eigenmodes $h_i(x)$ in (c). The second important eigenmode is a zigzag mode emerging from the zero-eigenvalue at $k = 0$ representing the translation mode for a single two-dimensional drop (cp. Fig. 17 (left)) It is always linearly stable on the horizontal substrate but becomes important for inclined substrates. Note, that the two modes correspond to transversally modulated volume (varicose) and translation (zigzag) modes of two-dimensional drops (see section 3.4, Fig. 17.

6.3 Horizontal striped substrate

On a striped substrate the wettability contrast not only stabilizes the system with respect to coarsening as detailed above in Section 4 but also stabilizes the transversal varicose instability (Gau et al., 1999; Thiele et al., 2003). However, having in mind the sinusoidal form of the used heterogeneity (4.1) one cannot decouple individual ridges because their width is of the order of their distance. The interaction of the ridges influences also the transversal stability of an array of ridges. For details of the different mode types see Thiele et al. (2003). For instance, the varicose instability can take two forms: the instabilities of two neighbour ridges may be transversally in-phase or anti-phase. The in-phase combination is a periodic continuation of the varicose instability of an individual ridge and has the same dispersion relation. The growth rate goes to zero as the wavenumber approaches zero and the eigenmode at $k = 0$ corresponds to the volume mode. However, this is not the case for the anti-phase mode. For $k = 0$ it corresponds to the longitudinal coarsening mode by mass transfer between the two ridges as discussed in Section 3.4. For the zigzag mode one finds that the in-phase mode is stable as for an individual ridge, but the anti-phase mode has a small band of unstable wavenumbers around $k = 0$.

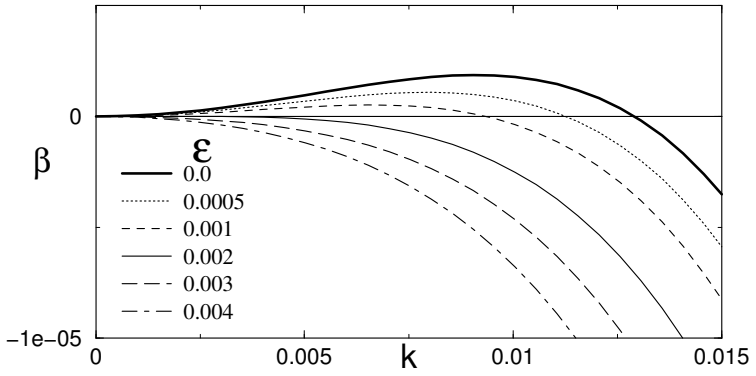

Figure 27. The largest eigenvalues β versus wavenumber k of transversal perturbations on a striped substrate. With increasing wettability contrast ϵ the range of unstable wave numbers becomes smaller and finally vanishes (for details see Thiele et al. (2003)).

For the parameter values studied by Thiele et al. (2003) the in-phase varicose mode is the most important one for a transversal modulation of the ridges. Its stabilisation with

increasing wettability contrast is illustrated in Fig. 27. On heterogeneous substrates all growth rates decrease monotonously with increasing strength of the heterogeneity. This leads first to a shrinkage of the band of unstable wavenumbers and then to the complete stabilisation of the transversal instabilities. Already at small wettability contrast ϵ the length scale of the transversal instability is much larger than the longitudinal period. For $\epsilon = 0.001$, for instance, the fastest growing mode has a wavelength of about 1000 corresponding to twenty times P_{het}. The critical heterogeneity where the band of unstable varicose modes vanishes is only slightly larger than the value ϵ_1 where the longitudinal coarsening mode is stabilised (see Fig. 20). The unstable zigzag mode stabilises at smaller ϵ than the varicose modes.

Sliding ridge on inclined substrate The physical situation changes once the substrate is inclined as a consequence of the broken symmetry $x \to -x$. As a result the ridges become asymmetric and slide down the substrate (Thiele et al., 2001b)). When $\alpha = 0$ the variational structure of Eq. (2.47) implies that $v = C_0 = 0$. As a result the equation is invariant under both translations in x and changes in volume (or $\bar{h}$). In particular for each set of parameter values there is a two-parameter family of solutions. In contrast, when $\alpha \neq 0$ the stationary solutions are described by Eq. (5.1) with α, v, and C_0 all nonzero. The resulting equation is still invariant under translation but no longer under volume change. This is because a change in volume also changes the velocity v. As a result only the translational neutral mode remains, i.e., only one mode with zero growth rate exists at zero wavenumber, in contrast to the two modes for the horizontal substrate plotted in Fig. 26. This implies that the two leading eigenmodes of the transverse stability problem, i.e., the equivalents of the varicose and zigzag modes for the inclined case are either no longer independent at $k = 0$ or only one has a zero growth rate at $k = 0$. In fact we find that the first hypothesis is true: the two modes coincide at $k = 0$ forming the translational neutral mode, but are distinct whenever $k \neq 0$ being mapped into one another by the transformation $k \to -k$.

The disperion relation $\beta(k)$ undergoes dramatic changes when either increasing the ridge volume or the inclination of the substrate (Fig. 28). Using as example the increase of the inclination the different regimes are

(i) For very small inclination a varicose instability involving asymmetrically both edges of the ridge is still the dominant transversal instability mode. The zigzag mode is stable. Note that the character of the mode changes along the dispersion curve. In the following we refer to the character at the maxima.

(ii) For slightly larger inclination the most unstable mode corresponds to an asymmetric zigzag type [Fig. 28 (a)].

(iii) The dispersion curves of the zigzag and varicose modes couple resulting in complex modes for an intermediate wavenumber range [Fig. 28 (b) and (c)]. Two maxima evolve.

(iv) The two modes decouple again and represent spatially decoupled instabilities of the advancing and the receding front having different growth rates and fastest growing wavenumbers ($k_{adv} < k_{rec}$). They are illustrated in a time simulation in Fig. 29.

In the transition region between the instabilities (ii) - (iv) oscillatory instabilities are present in a certain wavenumber range. However, in the cases studied the oscillatory

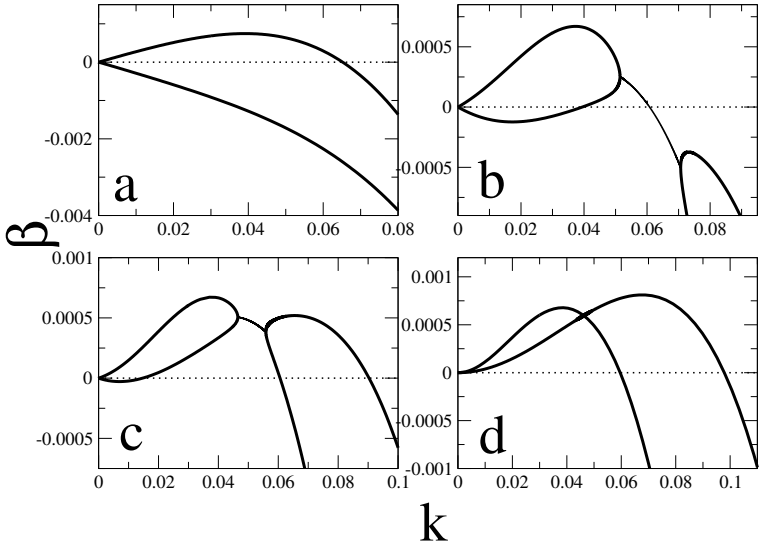

Figure 28. Sketch of the different dispersion relations obtained for increasing ridge volume or increasing inclination angle. Thick (thin) lines indicate real (complex) modes (for details see Thiele and Knobloch (2003)).

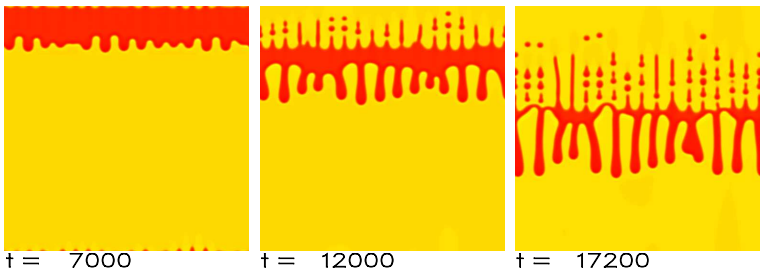

Figure 29. Time simulation of a sliding ridge. Both, the advancing and the receding front, get unstable to a periodic transverse instabilities and fingering can be observed. $G = 0.2$, 512×512 points, $\alpha = 0.1$ and domain size 1900 (Thiele et al., 2002a).

modes were never dominant, and may therefore be seen only when the corresponding wavenumber is selected by the experimental apparatus.

The physical mechanism responsible for contact line instabilities can be studied using the method of energy analysis (Spaid and Homsy, 1996; Matar and Troian, 1997; Skotheim et al., 2003; Thiele and Knobloch, 2003). The growth rate β of an unstable mode is interpreted as an energy production rate and contributions to it from the individual terms of the linearized problem can be connected to underlying physical mechanisms (Spaid and Homsy, 1996). The decoupled instabilities of advancing and receding fronts are driven by gravity and by the destabilising disjoining pressure, respectively (Thiele and Knobloch, 2003).

We close this Section with a speculation on the transversal instability found for dewetting. There holes often grow in a stable way (Redon et al., 1991; Reiter, 2001; Seemann et al., 2005), however, in a number of systems a transversal front instability of the receding dewetting front is observed. One can distinguish: (i) thickness modulations of the outward moving liquid rim around the growing hole (Brochard-Wyart and Redon, 1992; Masson et al., 2002; Meredith et al., 2000; Sharma and Reiter, 1996), (ii) development of relatively stable fingers that stay behind the outward moving rim (Herminghaus et al., 2000; Reiter, 1993; Thiele, 1998), and (iii) an emanation of a structured field of small droplets from the moving rim (Elbaum and Lipson, 1994; Kim et al., 1999; Reiter, 1993; Reiter and Sharma, 2001; Sharma and Reiter, 1996; van der Wielen et al., 2000). Not much is known on the exact conditions for the instability to occur and to have appearance (i), (ii) or (iii). For the type (i) instability it was proposed (Brochard-Wyart and Redon, 1992) that it is very similar to the Rayleigh instability of immobile rims as studied by (Sekimoto et al., 1987). Type (ii) or (iii) instabilities were attributed (Reiter and Sharma, 2001) to a combination of a Rayleigh mechanism and dissipation due to slip (see also Thiele (1998)). The results of Thiele and Knobloch (2003) point to the destabilising effect of the disjoining pressure, i.e. the effective interaction with the substrate that is responsible for the dewetting itself. Moreover, one may argue that the sequence of asymmetric varicose instability, asymmetric zigzag instability and decoupled front and back instability found when increasing the driving also gives a first hint on the mechanisms behind the change from instability type (i) to types (ii) and (iii) in dewetting. So give Figs. 6 and 5 of Brochard-Wyart and Redon (1992) a rough indication for a change from varicose to zigzag instability when increasing the driving force. A stronger zigzag instability leading to finger formation is also seen in Fig. 14 of Reiter (1993).

7 Beyond the single evolution equation

Finally, we introduce thin film systems that can not be described by a single evolution equation for the film thickness profile, i.e. by an evolution equation for a single conserved order parameter field. In the simplest case the description has then to be based on two coupled evolution equations. For systems involving a thin film with a free surface one equation will again describe the dynamics of the film thickness profile representing a conserved order parameter field. However, the second equation can model a conserved *or* a non-conserved order parameter field.

We focus on two physical situations representing the respective two cases. In Sec-

Manuscript —- contact: thiele@pks.mpg.de – http://www.uwethiele.de – 10th March 2006

tion 7.1 we study ultrathin two-layer systems (Pototsky et al., 2004, 2005). There, the two mean interface heights are conserved, i.e. the two interface profiles correspond to the two conserved fields. In Section 7.2 we investigate chemically driven self-propelled running droplets (Thiele et al., 2004; John et al., 2005). There, the film thickness and the substrate adsorbate coverage correspond to the conserved and the non-conserved order parameter field, respectively.

Note, however, that we do not cover the extensive work on thin films covered by a layer of non-soluble surfactant that belongs to the first class, i.e. its dynamics is described by two coupled evolution equations of conserved order parameter fields (see Oron et al. (1997) and references therein).

7.1 Two-layer thin films

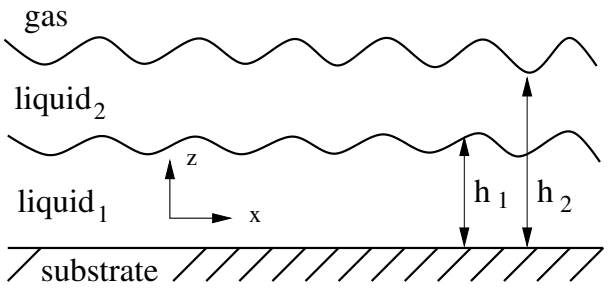

Figure 30. Geometry of the two-layer system.

Little is known about the behaviour of two stacked ultrathin layers of soft matter on a solid substrate (see Fig. 30). Such a two-layer film in a open geometry[11] allows for richer dynamics than the one-layer system because, both, the free liquid-liquid and the free liquid-gas interface evolve in a coupled way. The evolution is driven by the effective molecular interactions between *all* the three interfaces separating the four material layers: substrate, liquid 1, liquid 2 and ambient gas. Although experimental studies investigate different aspects of dewetting for two-layer films like interface instabilities or the growth of holes (David et al., 1998; Faldi et al., 1995; Lambooy et al., 1996; Morariu et al., 2003; Pan et al., 1997; Renger et al., 2000; Sferrazza et al., 1997, 1998) up to now the interface dynamics has not been studied in detail.

The most intricate question for the first stage of dewetting of a two-layer system is *which* interface will become unstable and *where* does the film rupture. This will determine the final morphology of the film. Experiments found roughening of the liquid-liquid interface (Sferrazza et al., 1998) or an instability of the liquid-gas interface (Faldi et al., 1995; Morariu et al., 2003). Holes that evolve solely in the upper layer were also studied (Lambooy et al., 1996; Pan et al., 1997).

[11] In the open geometry the system has two free interfaces. On the contrary in a bounded geometry the two layers are enclosed by two solid substrates. Then the evolution of the single free interface can still be described by a single thin film equation (Merkt et al., 2005).

Evolution equations for the film thicknesses h_1 and h_2 can be obtained by simplifying the Navier-Stokes equations employing long-wave approximation along the lines sketched above in Section 2 for a single layer. One obtains

$$\begin{aligned} \frac{\partial h_1}{\partial t} &= \partial_x \left(Q_{11} \partial_x \frac{\delta F}{\delta h_1} + Q_{12} \partial_x \frac{\delta F}{\delta h_2} \right) \\ \frac{\partial h_2}{\partial t} &= \partial_x \left(Q_{21} \partial_x \frac{\delta F}{\delta h_1} + Q_{22} \partial_x \frac{\delta F}{\delta h_2} \right), \end{aligned} \tag{7.1}$$

where $\delta F/\delta h_i$ with $i = 1, 2$ denotes functional derivatives of the total energy of the system

$$F = \int [\rho_{\mathrm{S}} + \rho_{\mathrm{VW}}] \, dx \tag{7.2}$$

and the Q_{ik} are the positive elements of the symmetric mobility matrix. The energy F contains the densities of the surface energy and of the energy for the van der Waals interaction (Pototsky et al., 2004). Inclusion of other interactions, like for instance, a stabilising short-range interaction, is straightforward (Pototsky et al., 2005). Related models were derived, for instance, assuming a lower liquid layer that is much thicker than the upper layer (Brochard-Wyart et al., 1993), and for two-layer systems with surfactants (and non-Newtonian behaviour) (Zhang et al., 2003; Craster and Matar, 2000; Matar et al., 2002) or including evaporation (Danov et al., 1998a,b; Paunov et al., 1998). A two-layer system under the solely influence of long-range molecular interactions is studied by Bandyopadhyay et al. (2005).

The system (7.1) represents the most general form of coupled evolution equations for two conserved order parameter fields in a relaxational situation and is apt to describe a broad variety of experimentally studied two-layer systems.

Studying Eqs. (7.1) by means of linear analysis one distinguishes two different types of unstable modes, namely, varicose and zigzag modes that also determine the non-linear evolution. In the model without stabilising short-range interactions studied in Pototsky et al. (2004) they lead to rupture at the substrate or at the liquid-liquid interface. Both modes are asymmetric since the deflection amplitudes of the two interfaces are normally different. The mobilities have no influence on the stability threshold, but determine mode type and the length and time scales of the dynamics.

Furthermore, the simultaneous action of the van der Waals forces between the three interfaces allows for dispersion relations with two maxima. An experimental system showing this unusual form of $\beta(k)$ can be realized with a substrate that is less polarisable than both layers of soft matter. If the two maxima are of equal height two modes of different wavelength may evolve at the two interfaces, respectively. Different types of dispersion relations and snapshots of respective time evolutions are given in Fig. 31. For more details see Pototsky et al. (2004).

The system presented here is strongly restricted by the sole inclusion of a destabilizing interaction. Every unstable evolution terminates with a rupture event. To be able to study different pathways of coarsening that may occur in the long-time evolution one has to include a stabilizing short-range interaction. In this way thin precursor films are stabilized and a rich coarsening dynamics is found (Pototsky et al., 2005).

Manuscript —- contact: thiele@pks.mpg.de – http://www.uwethiele.de – 10th March 2006

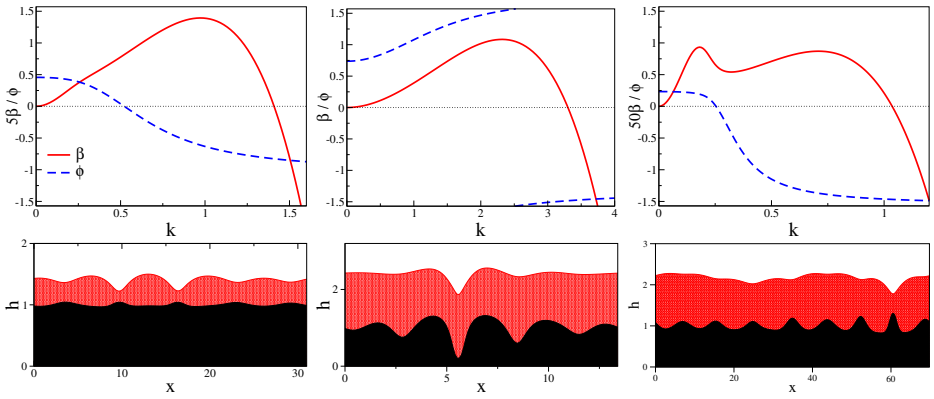

Figure 31. Shown are the growth rate γ (solid lines) and the mode type ϕ (dashed lines) of the leading eigenmode. (a) A varicose mode from the one-mode region at $d_1 = 30$, $d_2 = 47$ and $\sigma = \mu = 1$, (b) a zigzag mode from the one-mode region at $d_1 = 15$, $d_2 = 40$ and $\sigma = \mu = 1$. Panel (c) gives γ and ϕ for d_1 and d_2 as in (b) but for $\mu = 0.1$. For convenience we plot in (b) 10γ and in (a) 20γ. Snapshots from time evolutions of a two-layer film for a Si/PMMA/PS/air system at dimensionless times (in units of $\tau_{\rm up}$) as shown in the insets. (a) At $d = 1.4$ a varicose mode evolves leading to rupture of the upper layer at the liquid-liquid interface. The ratio of the time scales derived from upper and lower effective one-layer system is $\tau_{\rm up}/\tau_{\rm low} = 0.066$. (b) At $d = 2.4$ a zigzag mode evolves and rupture of the lower layer occurs at the substrate ($\tau_{\rm up}/\tau_{\rm low} = 34.98$). The domain lengths are 5 times the corresponding fastest unstable wave length and $\mu = \sigma = 1$ (for details see Pototsky et al. (2004)).

7.2 Chemically driven running drops

It is generally known that drops can move in externally given gradients like, for instance, in a temperature or chemical gradient (Brochard, 1989) or most simply on an inclined plate as discussed above in Section 5. However, drops may also move in an initially gradientless surrounding if they themselfes change the surrounding and thereby produce a gradient that drives their motion.

Recent experiments found such droplets on solid substrates that are chemically changed by the droplets. A driving wettability gradient is produced by an adsorption or desorption reaction at the substrate underneath the drop (Bain et al., 1994; Domingues Dos Santos and Ondarçuhu, 1995; Lee et al., 2002; Sumino et al., 2005a,b).

In these experiments, a small droplet of solvent is put on a partially wettable substrate. A chemical dissolved in the droplet reacts with the substrate resulting in the deposition of a less wettable coating. Likewise, it may also dissolve a wettable coating exposing the less wettable bare substrate. In both cases, the substrate below becomes less wettable than the substrate outside the droplet. Because of the radial symmetry it is still in an equilibrium position. However, it becomes more and more unstable. Eventually, the symmetry is broken by fluctuations and the drop starts to move, thereby changing the

substrate and leaving a less wettable trail behind (see Fig. 32). Similar phenomena can be seen in reactive (de)wetting (Zheng et al., 1998), in camphor boats (Hayashima et al., 2002), and in the migration of reactive islands in alloying (Schmid et al., 2000).

A simple theoretical argument (Brochard-Wyart and de Gennes, 1995), predicts a monotone increase of the droplet velocity with the droplet length and the reaction rate, in line with early experimental observations (Domingues Dos Santos and Ondarçuhu, 1995). Recent experiments (Lee et al., 2002) show also the opposite trend; the velocity decreases with increasing drop sizes and reaction rate.

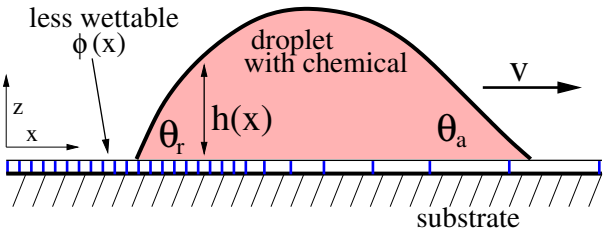

Figure 32. Sketch of a right moving droplet driven by a self-produced chemical gradient.

Recently we proposed and analysed dynamical models for self-propelled running droplets (Thiele et al., 2004; John et al., 2005). Here we introduce these models using the one that only accounts for an adsorption reaction underneath the droplets but not for a recovery of the substrate. The model consists of coupled evolution equations describing the interdependent spatiotemporal dynamics of the film thickness h and of the concentration of an adsorbate ϕ that decreases the substrate wettability. The model equations in dimensionless form are

$$\partial_t h = -\nabla \left\{ h^3 \nabla \left[\Delta h - \partial_h f(h,\phi) \right] \right\} \tag{7.3}$$

$$\partial_t \phi = R(h,\phi) + d\,\Delta\phi. \tag{7.4}$$

The first equation describes the evolution of the film thickness profile. It is based on Eq. (2.47) with $\chi = 0$, and incorporates a disjoining pressure following Eq. (2.51) (with the positive sign). However, the short-range part of the disjoining pressure depends not only on h but changes linearly with the adsorbate concentration ϕ

$$\partial_h f(h,\phi) = -\frac{b}{h^3} + \left(1 + \frac{\phi}{g}\right) e^{-h} \tag{7.5}$$

The scaled equilibrium contact angle θ_e is given by $\cos\theta_e = \hat{S} + 1$, where $\hat{S}$ is the dimensionless (negative) spreading coefficient (Sharma, 1993b) and $1/g$ defines the magnitude of the wettability gradient. With Eq. (7.5), $\hat{S} = b - 1 - \phi/g$ and $b \geq 0$, implying that θ_e increases with increasing ϕ, i.e. the coated substrate is less wettable.

The second equation (7.4) models the evolution of the chemical concentration of the adsorbate using a reaction-diffusion equation. The function $R(h,\phi)$ describes the reaction that changes the wettability of the substrate and the second term allows for a (usually

small) diffusion of the chemical species along the substrate. The main results, however, are obtained without diffusion. As reaction term we choose

$$R(h,\phi) \;=\; r\Theta(h-h_0)\;(1-\phi) \tag{7.6}$$

where r defines the time scale of the reaction. It is assumed that the reaction at the substrate occurs only underneath the droplet as modelled by the step function $\Theta(h-h_0)$, and that it saturates at a value $\phi_{max}=1$. The value of h_0 is chosen slightly larger than the thickness of the precursor film.

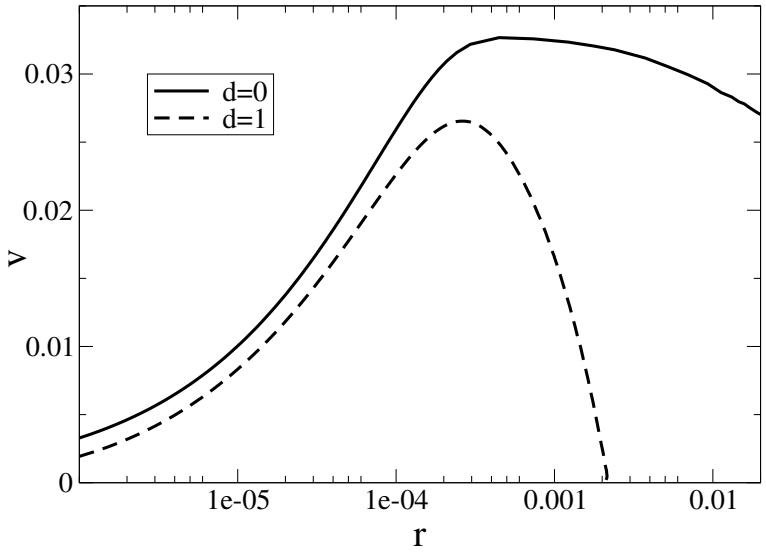

Figure 33. Characterization of running droplets stationary in a comoved frame. Shown is the velocity v in dependence of the reaction rate r (logarithmic scale) without ($d=0$, solid line) and with ($d=1.0$, dotted line) diffusion.; The remaining parameters are $g=1.0, d=0.0, b=0.5$ and the droplet volume is 30000 (for details see Thiele et al. (2004)).

The model Eqs. (7.3) and (7.4) is capable of reproducing the different experimentally found regimes. In particular, varying the reaction rate or drop volume we identify two distinct regimes of running drops as shown in Fig. 33. For small reaction rate (or droplet size), the chemical gradient in the drop is limited by the progress of reaction. In contrast for a fast reaction (or large droplets), the chemical concentration at the receding end saturates at the maximum value. The velocity of reaction-limited droplets increases, while the velocity of saturated droplets decreases with increasing reaction rate or droplet size. Specifically, the velocity of the droplets may increase (Domingues Dos Santos and Ondarçuhu, 1995) or decrease (Lee et al., 2002) with their volume. If we take into account fast diffusion of the adsorbate along the substrate the droplet velocity in the saturated regime decreases much faster and only steady sitting drops are found at large reaction rates.

In addition, we find that the dynamic contact angles at the advancing and receding edges of the droplets differ substantially. The differences between the static and the dynamic contact angles at the front and the rear are one order of magnitude smaller than the difference between the two static contact angles. This challenges the assumption of equal dynamic contact angles at the front and the rear that was used by de Gennes (1998) and Brochard-Wyart and de Gennes (1995) to develop a simple description of self-propelled running droplets. A simple quantitative theory should instead be based on the assumption that the respective dynamic contact angles equal the different static contact angles at the front and rear.

An extension of the model presented here describes also experiments (Sumino et al., 2005a,b) where the substrate recovers its original state behind the droplet through an adsorption from a surrounding medium (John et al., 2005). This allows, for instance, for a periodic droplet movement on circular or finite stripe-like substrates.

8 Outlook

We have given an overview of some recent developments in the description of pattern formation in thin liquid films. Althought we have tried to allow glimpses on the general developments of the field the presentation of the derivation and analysis of thin film equations focused mainly on our own results. The outcome is a text that has in part introductory and in part review character.

Specifically, on the one hand, we have focused on the common mathematical framework behind all thin film systems involving a single layer of liquid. Thereby, we have emphasised the advantages of studying the transitions between the different geometries, i.e. from homogeneous to inhomogeneous, or from horizontal to inclined substrates. On the other hand, we have introduced the physical questions posed by the individual systems detailing our contributions to them and their relation with the literature. We summarise here a selection of main results for single layers of liquid:

- For the initial film rupture in the process of dewetting one has to distinguish nucleation-dominated and instability-dominated behaviour for linearly unstable films.
- For heated films on a horizontal substrate we have discussed nucleation and drop solutions. It is also shown that it is possible to construct all drop solutions separated by dry regions.
- Incorporating a disjoining pressure in the study of heated thin films on horizontal substrates has allowed to study the long-time coarsening behaviour of the evolving pattern.
- For dewetting on an inhomogeneous substrate we describe a pinning-coarsening transition with a large range of multistability, implying a large hysteresis and strong dependence on initial conditions and noise.
- Studying sliding drops on an inclined homogeneous substrate by using a model that incorporates a disjoining pressure has allowed to calculate from surface chemistry the usual ad-hoc parameters of models for moving contact lines.

Manuscript —- contact: thiele@pks.mpg.de – http://www.uwethiele.de – 10th March 2006

- For heated films on slightly inclined plates we have described a very involved transition from a Cahn-Hilliard-like to a Kuramoto-Sivashinsky-like dynamics occurring at small inclination angles.
- Investigating the transversal instabilities of liquid ridges on homogeneous and striped horizontal substrates and for a sliding liquid ridge on an inclined substrate we have indicated that the mode type of the instability changes with increasing inclination from a symmetric varicose mode (horizontal substrate) via an asymmetric varicose mode via an asymmetric zigzag mode to decoupled front and back modes.

Finally, we have shown two possible ways to extend the study of thin film systems beyond the case of a single evolution equation. Especially, we have introduced models describing:

- The dynamics of a two-layer thin film that may follow different pathways of dewetting;
- Self-propelled droplets driven by a chemical reaction at the substrate.

These models describe some experiments out of a large class that have to be modelled by coupled evolution equations. Beside the cases studied here, the evolution of the film thickness can be accompanied by phase changes as observed, for example, for liquid crystals, block copolymers or polymer melts (Demirel and Jerome, 1999; Yerushalmi-Rozen et al., 1999; Knoll et al., 2002; Schlagowski et al., 2002) or by density variations as discussed in Sharma and Mittal (2002). To describe the observed phenomena involving complex fluids it will in the future be necessary to derive coupled evolution equations for the film thickness and fields describing the involved inner degrees of freedom.

Bibliography

D. M. Anderson, G. B. McFadden, and A. A. Wheeler. Diffuse-interface methods in fluid mechanics. *Ann. Rev. Fluid Mech.*, 30:139–165, 1998.

C. D. Bain, G. D. Burnetthall, and R. R. Montgomerie. Rapid motion of liquid-drops. *Nature*, 372:414–415, 1994.

N. J. Balmforth, R. V. Craster, and R. Sassi. Dynamics of cooling viscoplastic domes. *J. Fluid Mech.*, 499:149–182, 2004.

D. Bandyopadhyay, R. Gulabani, and A. Sharma. Stability and dynamics of bilayers. *Ind. Eng. Chem. Res.*, 44:1259–1272, 2005.

S. G. Bankoff. Significant questions in thin liquid-film heat-transfer. *J. Heat Transf.-Trans. ASME*, 116:10–16, 1994.

C. Bauer and S. Dietrich. Phase diagram for morphological transitions of wetting films on chemically structured substrates. *Phys. Rev. E*, 61:1664–1669, 2000.

C. Bauer, S. Dietrich, and A. O. Parry. Morphological phase transitions of thin fluid films on chemically structured substrates. *Europhys. Lett.*, 47:474–480, 1999.

J. Becker, G. Grün, R. Seemann, H. Mantz, K. Jacobs, K. R. Mecke, and R. Blossey. Complex dewetting scenarios captured by thin-film models. *Nature Mat.*, 2:59–63, 2003.

M. Ben Amar, L. Cummings, and Y. Pomeau. Singular points of a moving contact line. *C R Acad. Sci. Ser. IIB*, 329:277–282, 2001.

H. Bénard. Les tourbillons cellulaires dans une nappe liquide. *Rev. Gén. Sci. Pures Appl.*, 11:1261–1271, 1900.

T. B. Benjamin. Wave formation in laminar flow down an inclined plane. *J. Fluid Mech.*, 2:554, 1957.

D. J. Benney. Long waves on liquid films. *J. Math. & Phys.*, 45:150–155, 1966.

A. L. Bertozzi and M. P. Brenner. Linear stability and transient growth in driven contact lines. *Phys. Fluids*, 9:530–539, 1997.

A. L. Bertozzi, A. Münch, X. Fanton, and A. M. Cazabat. Contact line stability and "undercompressive shocks" in driven thin film flow. *Phys. Rev. Lett.*, 81:5169–5173, 1998.

M. Bestehorn and K. Neuffer. Surface patterns of laterally extended thin liquid films in three dimensions. *Phys. Rev. Lett.*, 87:046101,1–4, 2001.

M. Bestehorn, A. Pototsky, and U. Thiele. 3D large scale Marangoni convection in liquid films. *Eur. Phys. J. B*, 33:457–467, 2003.

J. Bischof, D. Scherer, S. Herminghaus, and P. Leiderer. Dewetting modes of thin metallic films: Nucleation of holes and spinodal dewetting. *Phys. Rev. Lett.*, 77:1536–1539, 1996.

T. D. Blake and K. J. Ruschak. A maximum speed of wetting. *Nature*, 282:489–491, 1979.

W. Boos and A. Thess. Cascade of structures in long-wavelength Marangoni instability. *Phys. Fluids*, 11:1484–1494, 1999.

M. Brinkmann and R. Lipowsky. Wetting morphologies on substrates with striped surface domains. *J. Appl. Phys.*, 92:4296–4306, 2002.

F. Brochard. Motions of droplets on solid-surfaces induced by chemical or thermal-gradients. *Langmuir*, 5:432–438, 1989.

F. Brochard-Wyart and J. Daillant. Drying of solids wetted by thin liquid films. *Can. J. Phys.*, 68:1084–1088, 1989.

F. Brochard-Wyart and P.-G. de Gennes. Spontaneous motion of a reactive droplet. *C. R. Acad. Sci. Ser. II*, 321:285–288, 1995.

F. Brochard-Wyart, P. Martin, and C. Redon. Liquid/liquid dewetting. *Langmuir*, 9: 3682–3690, 1993.

F. Brochard-Wyart and C. Redon. Dynamics of liquid rim instabilities. *Langmuir*, 8: 2324–2329, 1992.

F. Brochard-Wyart, C. Redon, and C. Sykes. Dewetting of ultrathin liquid films. *C. R. Acad. Sci.*, 314 II:19–24, 1992.

J. P. Burelbach, S. G. Bankoff, and S. H. Davis. Nonlinear stability of evaporating/condensing liquid films. *J. Fluid Mech.*, 195:463–494, 1988.

J. P. Burelbach, S. G. Bankoff, and S. H. Davis. Steady thermocapillary flows of thin liquid layers. II. Experiment. *Phys. Fluids A*, 2:321–333, 1990.

J. W. Cahn. Phase separation by spinodal decomposition in isotropic systems. *J. Chem. Phys.*, 42:93–99, 1965.

J. W. Cahn and J. E. Hilliard. Free energy of a nonuniform system. 1. Interfacual free energy. *J. Chem. Phys.*, 28:258–267, 1958.

S. Chandrasekhar. *Hydrodynamic and Hydromagnetic Stability*. Clarendon Press, Oxford, 1992.

H.-C. Chang. Wave evolution on a falling film. *Ann. Rev. Fluid Mech.*, 26:103–136, 1994.

R. V. Craster and O. K. Matar. Surfactant transport on mucus films. *J. Fluid Mech.*, 425:235–258, 2000.

M. C. Cross and P. C. Hohenberg. Pattern formation out of equilibrium. *Rev. Mod. Phys.*, 65:851–1112, 1993.

K. D. Danov, V. N. Paunov, N. Alleborn, H. Raszillier, and F. Durst. Stability of evaporating two-layered liquid film in the presence of surfactant - I. The equations of lubrication approximation. *Chem. Eng. Sci.*, 53:2809–2822, 1998a.

K. D. Danov, V. N. Paunov, S. D. Stoyanov, N. Alleborn, H. Raszillier, and F. Durst. Stability of evaporating two-layered liquid film in the presence of surfactant - ii. linear analysis. *Chem. Eng. Sci.*, 53:2823–2837, 1998b.

M. O. David, G. Reiter, T. Sitthai, and J. Schultz. Deformation of a glassy polymer film by long-range intermolecular forces. *Langmuir*, 14:5667–5672, 1998.

S. H. Davis. Moving contact lines and rivulet instabilities. Part 1. The static rivulet. *J. Fluid Mech.*, 98:225–242, 1980.

S. H. Davis. Thermocapillary instabilities. *Ann. Rev. Fluid Mech.*, 19:403–435, 1987.

J. R. de Bruyn. Growth of fingers at a driven three–phase contact line. *Phys. Rev. A*, 46:R4500–R4503, 1992.

P.-G. de Gennes. Wetting: Statistics and dynamics. *Rev. Mod. Phys.*, 57:827–863, 1985.

P.-G. de Gennes. The dynamics of reactive wetting on solid surfaces. *Physica A*, 249: 196–205, 1998.

R. J. Deissler and A. Oron. Stable localized patterns in thin liquid films. *Phys. Rev. Lett.*, 68:2948–2951, 1992.

A. L. Demirel and B. Jerome. Restructuring-induced dewetting and re-entrant wetting of thin glassy films. *Europhys. Lett.*, 45:58–64, 1999.

B. V. Derjaguin, N. V. Churaev, and V. M. Muller. *Surface Forces*. Consultants Bureau, New York, 1987.

E. Doedel, H. B. Keller, and J. P. Kernevez. Numerical analysis and control of bifurcation problems (I) Bifurcation in finite dimensions. *Int. J. Bif. Chaos*, 1:493–520, 1991a.

E. Doedel, H. B. Keller, and J. P. Kernevez. Numerical analysis and control of bifurcation problems (II) Bifurcation in infinite dimensions. *Int. J. Bif. Chaos*, 1:745–72, 1991b.

E. J. Doedel, A. R. Champneys, T. F. Fairgrieve, Y. A. Kuznetsov, B. Sandstede, and X. J. Wang. *AUTO97: Continuation and bifurcation software for ordinary differential equations*. Concordia University, Montreal, 1997.

F. Domingues Dos Santos and T. Ondarçuhu. Free-running droplets. *Phys. Rev. Lett.*, 75:2972–2975, 1995.

B. Y. Du, F. C. Xie, Y. J. Wang, Z. Y. Yang, and O. K. C. Tsui. Dewetting of polymer films with built-in topographical defects. *Langmuir*, 18:8510–8517, 2002.

E. B. Dussan. On the spreading of liquids on solid surfaces: Static and dynamic contact lines. *Ann. Rev. Fluid Mech.*, 11:371–400, 1979.

I. E. Dzyaloshinskii, E. M. Lifshitz, and L. P. Pitaevskii. Van der Waals forces in liquid films. *Sov. Phys. JETP*, 37:161, 1960.

J. Eggers. Nonlinear dynamics and breakup of free-surface flows. *Rev. Mod. Phys.*, 69: 865–929, 1997.

J. Eggers. Hydrodynamic theory of forced dewetting. *Phys. Rev. Lett.*, 93:094502, 2004.

M. Elbaum and S. G. Lipson. How does a thin wetted film dry up? *Phys. Rev. Lett.*, 72:3562–3565, 1994.

M. H. Eres, L. W. Schwartz, and R. V. Roy. Fingering phenomena for driven coating films. *Phys. Fluids*, 12:1278–1295, 2000.

A. Faldi, R. J. Composto, and K. I. Winey. Unstable polymer bilayers. 1. Morphology of dewetting. *Langmuir*, 11:4855, 1995.

H. Gau, S. Herminghaus, P. Lenz, and R. Lipowsky. Liquid morphologies on structured surfaces: From microchannels to microchips. *Science*, 283:46–49, 1999.

D. P. III Gaver and J. B. Grotberg. The dynamics of a localized surfactant on a thin film. *J. Fluid Mech.*, 213:127–148, 1990.

B. Gjevik. Occurrence of finite-amplitude surface waves on falling liquid films. *Phys. Fluids*, 13:1918–1925, 1970.

K. B. Glaser and T. P. Witelski. Coarsening dynamics of dewetting films. *Phys. Rev. E*, 67:016302, 2003.

A. A. Golovin, A. A. Nepomnyashchy, S. H. Davis, and M. A. Zaks. Convective Cahn-Hilliard models: From coarsening to roughening. *Phys. Rev. Lett.*, 86:1550–1553, 2001.

A. A. Golovin, A. A. Nepomnyashchy, and L. M. Pismen. Interaction between short-scale Marangoni convection and long-scale deformational instability. *Phys. Fluids*, 6:34–48, 1994.

H. P. Greenspan. On the motion of a small viscous droplet that wets a surface (relevant to cell movement). *J. Fluid Mech.*, 84:125–143, 1978.

G. Grün, K. Mecke, and M. Rauscher. Thin film flow influenced by thermal noise. *preprint*, 2005. submitted.

J. Guckenheimer and P. Holmes. *Nonlinear Oscillations, Dynamical Systems and Bifurkations of Vector Fields*, volume 42 of *Applied Mathematical Sciences*. Springer-Verlag, Berlin, 1993.

W. B. Hardy. Historical notes upon surface energy and forces of short range. *Nature*, 109:375–378, 1922.

F. Hauksbee. Several experiments touching the seeming spontaneous ascent of water. *Phil. Trans.*, 26:258–266, 1708.

F. Hauksbee. An account of an experiment touching the direction of a drop of oil of oranges, between two glass planes, towards any side of them that is nearest press'd together. *Phil. Trans.*, 27:395–396, 1710.

Y. Hayashima, M. Nagayama, Y. Doi, S. Nakata, M. Kimura, and M. Iida. Self-motion of a camphoric acid boat sensitive to the chemical environment. *Phys. Chem. Chem. Phys.*, 4:1386–1392, 2002.

S. Herminghaus, A. Fery, S. Schlagowski, K. Jacobs, R. Seemann, H. Gau, W. Mönch, and T. Pompe. Liquid microstructures at solid interfaces. *J. Phys.-Condes. Matter*, 12:A57–A74, 2000.

L. M. Hocking. A moving fluid interface. II. The removal of the force singularity by a slip flow. *J. Fluid Mech.*, 79:209–229, 1977.

L. M. Hocking. Spreading and instability of a viscous fluid sheet. *J. Fluid Mech.*, 211: 373–392, 1990.

L. M. Hocking and M. J. Miksis. Stability of a ridge of fluid. *J. Fluid Mech.*, 247:157–177, 1993.

C. Huh and L. E. Scriven. Hydrodynamic model of steady movement of a solid / liquid / fluid contact line. *J. Colloid Interface Sci.*, 35:85–101, 1971.

R. J. Hunter. *Foundation of Colloid Science*, volume 1. Clarendon Press, Oxford, 1992.

H. E. Huppert. Flow and instability of a viscous current down a slope. *Nature*, 300: 427–429, 1982.

J. N. Israelachvili. *Intermolecular and Surface Forces*. Academic Press, London, 1992.

K. Jacobs, S. Herminghaus, and K. R. Mecke. Thin liquid polymer films rupture via defects. *Langmuir*, 14:965–969, 1998.

K. John, M. Bär, and U. Thiele. Self-propelled running droplets on solid substrates driven by chemical reactions. *Eur. Phys. J. E*, 18:183–199, 2005.

S. W. Joo, S. H. Davis, and S. G. Bankoff. Long-wave instabilities of heated falling films: Two-dimensional theory of uniform layers. *J. Fluid Mech.*, 230:117–146, 1991.

O. A. Kabov and I. V. Marchuk. Infrared study of the liquid film flowing on surface with nonuniform heat flux distribution. *Heat Transfer Research*, 29:544–562, 1998.

S. Kalliadasis. Nonlinear instability of a contact line driven by gravity. *J. Fluid Mech.*, 413:355–378, 2000.

P. L. Kapitza. Waveflow of thin layers of a viscous fluid: I. The free flow. *Zh. Exp. Teor. Fiz.*, 18:3–18, 1949.

P. L. Kapitza and S. P. Kapitza. Waveflow of thin layers of a viscous fluid: III. Experimental study of undulatory flow conditions. *Zh. Exp. Teor. Fiz.*, 19:105–120, 1949.

K. Kargupta, R. Konnur, and A. Sharma. Instability and pattern formation in thin liquid films on chemically heterogeneous substrates. *Langmuir*, 16:10243–10253, 2000.

K. Kargupta, R. Konnur, and A. Sharma. Spontaneous dewetting and ordered patterns in evaporating thin liquid films on homogeneous and heterogeneous substrates. *Langmuir*, 17:1294–1305, 2001.

K. Kargupta and A. Sharma. Templating of thin films induced by dewetting on patterned surfaces. *Phys. Rev. Lett.*, 86:4536–4539, 2001.

K. Kargupta and A. Sharma. Creation of ordered patterns by dewetting of thin films on homogeneous and heterogeneous substrates. *J. Colloid Interface Sci.*, 245:99–115, 2002.

A. Karim, J. F. Douglas, B. P. Lee, S. C. Glotzer, J. A. Rogers, R. J. Jackman, E. J. Amis, and G. M. Whitesides. Phase separation of ultrathin polymer-blend films on patterned substrates. *Phys. Rev. E*, 57:R6273–R6276, 1998.

D. E. Kataoka and S. M. Troian. A theoretical study of instabilities at the advancing front of thermally driven coating films. *J. Colloid Interface Sci.*, 192:350–362, 1997.

D. E. Kataoka and S. M. Troian. Stabilizing the advancing front of thermally driven climbing films. *J. Colloid Interface Sci.*, 203:335–344, 1998.

I. G. Kevrekidis, B. Nicolaenko, and J. C. Scovel. Back in the saddle again - a computer-assisted study of the Kuramoto-Sivashinsky equation. *SIAM J. Appl. Math.*, 50: 760–790, 1990.

H. S. Kheshgi and L. E. Scriven. Dewetting: Nucleation and growth of dry regions. *Chem. Eng. Sci.*, 46:519–526, 1991.

H. I. Kim, C. M. Mate, K. A. Hannibal, and S. S. Perry. How disjoining pressure drives the dewetting of a polymer film on a silicon surface. *Phys. Rev. Lett.*, 82:3496–3499, 1999.

A. Knoll, A. Horvat, K. S. Lyakhova, G. Krausch, G. J. A. Sevink, A. V. Zvelindovsky, and R. Magerle. Phase behavior in thin films of cylinder-forming block copolymers. *Phys. Rev. Lett.*, 89:035501, 2002.

R. Konnur, K. Kargupta, and A. Sharma. Instability and morphology of thin liquid films on chemically heterogeneous substrates. *Phys. Rev. Lett.*, 84:931–934, 2000.

S. Krishnamoorthy, B. Ramaswamy, and S. W. Joo. Spontaneous rupture of thin liquid films due to thermocapillarity: A full-scale direct numerical simulation. *Phys. Fluids*, 7:2291–2293, 1995.

Y. Kuramoto and T. Tsuzuki. Persistent propagation of concentration waves in dissipative media far from thermal equilibrium. *Prog. Theor. Phys.*, 55:356–369, 1976.

P. Lambooy, K. C. Phelan, O. Haugg, and G. Krausch. Dewetting at the liquid-liquid interface. *Phys. Rev. Lett.*, 76:1110–1113, 1996.

J. S. Langer. *An introduction to the kinetics of first-order phase transitions*, chapter 3, pages 297–363. Cambridge University Press, 1992.

P. S. Laplace. Sur l'action capillaire. *Suppl. au livre X, Traité de Mécanique Céleste*, page 349, 1806.

S. W. Lee, D. Y. Kwok, and P. E. Laibinis. Chemical influences on adsorption-mediated self-propelled drop movement. *Phys. Rev. E*, 65:051602, 2002.

P. Lenz and R. Lipowsky. Morphological transitions of wetting layers on structured surfaces. *Phys. Rev. Lett.*, 80:1920–1923, 1998.

S. P. Lin. Finite amplitude side-band instability of a viscous film. *J. Fluid Mech.*, 63: 417–429, 1974.

S. P. Lin and H. Brenner. Tear film rupture. *J. Colloid Interface Sci.*, 89:226–231, 1982.

J. Liu and J. P. Gollub. Solitary wave dynamics of film flows. *Phys. Fluids*, 6:1702–1712, 1994.

C. G. Marangoni. Ueber die Ausbreitung der Tropfen einer Flüssigkeit auf der Oberfläche einer anderen. *Ann. Phys. (Poggendorf)*, 143:337–354, 1871.

J. L. Masson, O. Olufokunbi, and P. F. Green. Flow instabilities in entangled polymer thin films. *Macromolecules*, 35:6992–6996, 2002.

O. K. Matar, R. V. Craster, and M. R. E. Warner. Surfactant transport on highly viscous surface films. *J. Fluid Mech.*, 466:85–111, 2002.

O. K. Matar and S. M. Troian. Linear stability analysis of an insoluble surfactant monolayer spreading on a thin liquid film. *Phys. Fluids*, 9:3645–3657, 1997.

J. C. Meredith, A. P. Smith, A. Karim, and E. J. Amis. Combinatorial materials science for polymer thin-film dewetting. *Macromolecules*, 33:9747–9756, 2000.

D. Merkt, A. Pototsky, M. Bestehorn, and U. Thiele. Long-wave theory of bounded two-layer films with a free liquid-liquid interface: Short- and long-time evolution. *Phys. Fluids*, 17:064104, 2005.

E. C. Millington. Studies in capillarity and cohesion in the eighteenth century. *Annals of Science*, 5:352–369, 1945.

V. S. Mitlin. Dewetting of solid surface: Analogy with spinodal decomposition. *J. Colloid Interface Sci.*, 156:491–497, 1993.

V. S. Mitlin. Dewetting revisited: New asymptotics of the film stability diagram and the metastable regime of nucleation and growth of dry zones. *J. Colloid Interface Sci.*, 227:371–379, 2000.

V. S. Mitlin. Numerical study of Lifshitz-Slyozov-like metastable dewetting model. *J. Colloid Interface Sci.*, 233:153–158, 2001.

M. D. Morariu, E. Schäffer, and U. Steiner. Capillary instabilities by fluctuation induced forces. *Eur. Phys. J. E*, 12:375–379, 2003.

D. T. Moyle, M.-S. Chen, and G. M. Homsy. Nonlinear rivulet dynamics during unstable wetting flows. *Int. J. Multiphase Flow*, 25:1243–1262, 1999.

A. Münch. Dewetting rates of thin liquid films. *J. Phys.-Condes. Matter*, 17:S309–S318, 2005.

A. A. Nepomnyashchy, M. G. Velarde, and P. Colinet. *Interfacial phenomena and convection*. Chapman & Hall/CRC, Boca Raton, 2002.

I. Newton. *Opticks*. G. Bell & Sons LTD., London, 1730. (reprinted 4th ed. 1931).

L. T. Nguyen and V. Balakotaiah. Modeling and experimental studies of wave evolution on free falling viscous films. *Phys. Fluids*, 12:2236–2256, 2000.

A. Novick-Cohen. The nonlinear Cahn - Hilliard equation: Transition from spinodal decomposition to nucleation behavior. *J. Stat. Phys.*, 38:707–723, 1985.

A. Oron. Three-dimensional nonlinear dynamics of thin liquid films. *Phys. Rev. Lett.*, 85:2108–2111, 2000.

A. Oron, S. H. Davis, and S. G. Bankoff. Long-scale evolution of thin liquid films. *Rev. Mod. Phys.*, 69:931–980, 1997.

A. Oron and P. Rosenau. Formation of patterns induced by thermocapillarity and gravity. *J. Physique II France*, 2:131–146, 1992.

Q. Pan, K. I. Winey, H. H. Hu, and R. J. Composto. Unstable polymer bilayers. 2. The effect of film thickness. *Langmuir*, 13:1758–1766, 1997.

V. N. Paunov, K. D. Danov, N. Alleborn, H. Raszillier, and F. Durst. Stability of evaporating two-layered liquid film in the presence of surfactant - iii. non-linear stability analysis. *Chem. Eng. Sci.*, 53:2839–2857, 1998.

L. M. Pismen. Nonlocal diffuse interface theory of thin films and the moving contact line. *Phys. Rev. E*, 6402:021603, 2001.

L. M. Pismen and Y. Pomeau. Disjoining potential and spreading of thin liquid layers in the diffuse interface model coupled to hydrodynamics. *Phys. Rev. E*, 62:2480–2492, 2000.

L. M. Pismen and Y. Pomeau. Mobility and interactions of weakly nonwetting droplets. *Phys. Fluids*, 16:2604–2612, 2004.

L. M. Pismen and U. Thiele. Asymptotic theory for a moving droplet driven by a wettability gradient. *Phys. Fluids*, 2006. (submitted).

J. A. F. Plateau. *Statique Expérimentale et Théorique des Liquides Soumis aux Seules Forces Moléculaires*. Gauthier-Villars, Paris, 1873.

I. Podariu, Z. Y. Shou, and A. Chakrabarti. Viscous flow and coarsening of microdomains in diblock copolymer thin films. *Phys. Rev. E*, 62:R3059–R3062, 2000.

T. Podgorski. Ruisselement en condition de mouillage partiel, 2000. PhD Thesis (U. Paris 6).

T. Podgorski, J.-M. Flesselles, and L. Limat. Corners, cusps, and pearls in running drops. *Phys. Rev. Lett.*, 87:036102, 2001.

Y. Pomeau. Représentation de la ligne de contact mobile dans les équations de la mécanique des fluides. *C. R. Acad. Sci. Ser. II-B*, 328:411–416, 2000.

A. Pototsky, M. Bestehorn, D. Merkt, and U. Thiele. Alternative pathways of dewetting for a thin liquid two-layer film. *Phys. Rev. E*, 70:025201(R), 2004.

A. Pototsky, M. Bestehorn, D. Merkt, and U. Thiele. Morphology changes in the evolution of liquid two-layer films. *J. Chem. Phys.*, 122:224711, 2005.

R. F. Probstein. *Physicochemical Hydrodynamics*. Wiley, New York, 2. edition, 1994.

A. Pumir, P. Manneville, and Y. Pomeau. On solitary waves running down an inclined plane. *J. Fluid Mech.*, 135:27–50, 1983.

D. Quéré, M. J. Azzopardi, and L. Delattre. Drops at rest on a tilted plane. *Langmuir*, 14:2213–2216, 1998.

J. W. S. Rayleigh. On convective currents in a horizontal layer of fluid, when the higher temperature is on the under side. *Phil. Mag. S.6*, 32:529–546, 1916.

C. Redon, F. Brochard-Wyart, and F. Rondelez. Dynamics of dewetting. *Phys. Rev. Lett.*, 66:715–718, 1991.

N. Rehse, C. Wang, M. Hund, M. Geoghegan, R. Magerle, and G. Krausch. Stability of thin polymer films on a corrugated substrate. *Eur. Phys. J. E*, 4:69–76, 2001.

G. Reiter. Dewetting of thin polymer films. *Phys. Rev. Lett.*, 68:75–78, 1992.

G. Reiter. Unstable thin polymer films: Rupture and dwetting. *Langmuir*, 9:1344, 1993.

G. Reiter. Dewetting of highly elastic thin polymer films. *Phys. Rev. Lett.*, 87:186101, 2001.

G. Reiter and A. Sharma. Auto-optimization of dewetting rates by rim instabilities in slipping polymer films. *Phys. Rev. Lett.*, 8716:166103, 2001.

C. Renger, P. Müller-Buschbaum, M. Stamm, and G. Hinrichsen. Investigation and retardation of the dewetting on top of highly viscous amorphous substrates. *Macromolecules*, 33:8388–8398, 2000.

O. Reynolds. On the theory of lubrication and its application to Mr. Beauchamp Tower's experiments, including an experimental determination of the viscosity of olive oil. *Phil. Trans. Roy. Soc.*, 177:157–234, 1886.

L. Rockford, Y. Liu, P. Mansky, T. P. Russell, M. Yoon, and S. G. J. Mochrie. Polymers on nanoperiodic, heterogeneous surfaces. *Phys. Rev. Lett.*, 82:2602–2605, 1999.

R. V. Roy and L. W. Schwartz. On the stability of liquid ridges. *J. Fluid Mech.*, 391: 293–318, 1999.

E. Ruckenstein and R. K. Jain. Spontaneous rupture of thin liquid films. *J. Chem. Soc. Faraday Trans. II*, 70:132–147, 1974.

T. R. Salamon, R. C. Armstrong, and R. A. Brown. Traveling waves on vertical films: Numerical analysis using the finite element method. *Phys. Fluids*, 5:2202–2220, 1994.

N. Samid-Merzel, S. G. Lipson, and D. S. Tannhauser. Pattern formation in drying water films. *Phys. Rev. E*, 57:2906–2913, 1998.

E. Schäffer, S. Harkema, M. Roerdink, R. Blossey, and U. Steiner. Morphological instability of a confined polymer film in a thermal gradient. *Macromolecules*, 36:1645–1655, 2003.

E. Schäffer and U. Steiner. Acoustic instabilities in thin polymer films. *Eur. Phys. J. E*, 8:347–351, 2002.

B. Scheid, A. Oron, P. Colinet, U. Thiele, and J. C. Legros. Nonlinear evolution of nonuniformly heated falling liquid films. *Phys. Fluids*, 14:4130–4151, 2002.

B. Scheid, C. Ruyer-Quil, U. Thiele, O. A. Kabov, J. C. Legros, and P. Colinet. Validity domain of the Benney equation including Marangoni effect for closed and open flows. *J. Fluid Mech.*, 527:303–335, 2005.

S. Schlagowski, K. Jacobs, and S. Herminghaus. Nucleation-induced undulative instability in thin films of nCB liquid crystals. *Europhys. Lett.*, 57:519–525, 2002.

A. K. Schmid, N. C. Bartelt, and R. Q. Hwang. Alloying at surfaces by the migration of reactive twodimensional islands. *Science*, 290:1561–1564, 2000.

L. E. Scriven and C. V. Sternling. Marangoni effects. *Nature*, 187:186–188, 1960.

R. Seemann, S. Herminghaus, and K. Jacobs. Dewetting patterns and molecular forces: A reconciliation. *Phys. Rev. Lett.*, 86:5534–5537, 2001a.

R. Seemann, S. Herminghaus, and K. Jacobs. Shape of a liquid front upon dewetting. *Phys. Rev. Lett.*, 87:196101, 2001b.

R. Seemann, S. Herminghaus, C. Neto, S. Schlagowski, D. Podzimek, R. Konrad, H. Mantz, and K. Jacobs. Dynamics and structure formation in thin polymer melt films. *J. Phys.-Condes. Matter*, 17:S267–S290, 2005.

A. Sehgal, V. Ferreiro, J. F. Douglas, E. J. Amis, and A. Karim. Pattern-directed dewetting of ultrathin polymer films. *Langmuir*, 18:7041–7048, 2002.

K. Sekimoto, R. Oguma, and K. Kawasaki. Morphological stability analysis of partial wetting. *Ann. Phys.*, 176:359–392, 1987.

M. Sferrazza, M. Heppenstall-Butler, R. Cubitt, D. Bucknall, J. Webster, and R. A. L. Jones. Interfacial instability driven by dispersive forces: The early stages of spinodal dewetting of a thin polymer film on a polymer substrate. *Phys. Rev. Lett.*, 81:5173–5176, 1998.

M. Sferrazza, C. Xiao, R. A. L. Jones, D. G. Bucknall, J. Webster, and J. Penfold. Evidence for capillary waves at immiscible polymer/polymer interfaces. *Phys. Rev. Lett.*, 78:3693–3696, 1997.

A. Sharma. Equilibrium contact angles and film thicknesses in the apolar and polar systems: Role of intermolecular interactions in coexistence of drops with thin films. *Langmuir*, 9:3580, 1993a.

A. Sharma. Relationship of thin film stability and morphology to macroscopic parameters of wetting in the apolar and polar systems. *Langmuir*, 9:861–869, 1993b.

A. Sharma and A. T. Jameel. Nonlinear stability, rupture and morphological phase separation of thin fluid films on apolar and polar substrates. *J. Colloid Interface Sci.*, 161:190–208, 1993.

A. Sharma and J. Mittal. Instability of thin liquid films by density variations: A new mechanism that mimics spinodal dewetting. *Phys. Rev. Lett.*, 89:186101, 2002.

A. Sharma and G. Reiter. Instability of thin polymer films on coated substrates: Rupture, dewetting and drop formation. *J. Colloid Interface Sci.*, 178:383–399, 1996.

A. Sharma and E. Ruckenstein. Mechanism of tear film rupture and its implications for contact-lens tolerance. *Amer. J. Optom. Physiol. Opt.*, 62:246–253, 1985.

W. Ya. Shkadov. Wave conditions in the flow of a thin layer of a viscous liquid under the action of gravity. *Izv. Akad. Nauk SSSR, Mekh. Zhidk. Gaza*, 1:43–51, 1967.

N. Silvi and V. E. B. Dussan. The rewetting of an inclined solid surface by a liquid. *Phys. Fluids*, 28:5–7, 1985.

G. I. Sivashinsky. Non-linear analysis of hydrodynamic instability in laminar flames. 1. Derivation of basic equations. *Acta Astronaut.*, 4:1177–1206, 1977.

J. M. Skotheim, U. Thiele, and B. Scheid. On the instability of a falling film due to localized heating. *J. Fluid Mech.*, 475:1–19, 2003.

A. Sommerfeld. Zur hydrodynamischen Theorie der Schmiermittelreibung. *Z. Math. Phys.*, 50:97–155, 1904.

M. A. Spaid and G. M. Homsy. Stability of Newtonian and viscoelastic dynamic contact lines. *Phys. Fluids*, 8:460–478, 1996.

Y. Sumino, N. Magome, T. Hamada, and K. Yoshikawa. Self-running droplet: Emergence of regular motion from nonequilibrium noise. *Phys. Rev. Lett.*, 94(6):068301, 2005a.

Y. Sumino, M. Nagayama, H. Kitahata, S.-i.M. Nomura, N. Magome, Y. Mori, and K. Yoshikawa. Chemo-sensitive running droplet. *arXiv:nlin.AO/0505006*, 2005b.

M. J. Tan, S. G. Bankoff, and S. H. Davis. Steady thermocapillary flows of thin liquid layers. I. Theory. *Phys. Fluids A*, 2:313–321, 1990.

G. F. Teletzke, H. T. Davis, and L. E. Scriven. Wetting hydrodynamics. *Rev. Phys. Appl.*, 23:989–1007, 1988.

U. Thiele. Entnetzung von Kollagenfilmen, 1998. PhD-thesis, Dresden.

U. Thiele. Open questions and promising new fields in dewetting. *Eur. Phys. J. E*, 12: 409–416, 2003a.

U. Thiele. Tentative interpretation of the dewetting morphologies presented by Tsui et al. *Eur. Phys. J. E*, 12:427–430, 2003b.

U. Thiele, L. Brusch, M. Bestehorn, and M. Bär. Modelling thin-film dewetting on structured substrates and templates: Bifurcation analysis and numerical simulations. *Eur. Phys. J. E*, 11:255–271, 2003.

U. Thiele, K. John, and M. Bär. Dynamical model for chemically driven running droplets. *Phys. Rev. Lett.*, 93:027802, 2004.

U. Thiele and E. Knobloch. Front and back instability of a liquid film on a slightly inclined plate. *Phys. Fluids*, 15:892–907, 2003.

U. Thiele and E. Knobloch. Thin liquid films on a slightly inclined heated plate. *Physica D*, 190:213–248, 2004.

U. Thiele, M. Mertig, and W. Pompe. Dewetting of an evaporating thin liquid film: Heterogeneous nucleation and surface instability. *Phys. Rev. Lett.*, 80:2869–2872, 1998.

U. Thiele, K. Neuffer, M. Bestehorn, Y. Pomeau, and M. G. Velarde. Sliding drops on an inclined plane. *Colloid Surf. A*, 206:87–104, 2002a.

U. Thiele, K. Neuffer, Y. Pomeau, and M. G. Velarde. On the importance of nucleation solutions for the rupture of thin liquid films. *Colloid Surf. A*, 206:135–155, 2002b.

U. Thiele, M. G. Velarde, and K. Neuffer. Dewetting: Film rupture by nucleation in the spinodal regime. *Phys. Rev. Lett.*, 87:016104, 2001a.

U. Thiele, M. G. Velarde, K. Neuffer, M. Bestehorn, and Y. Pomeau. Sliding drops in the diffuse interface model coupled to hydrodynamics. *Phys. Rev. E*, 64:061601, 2001b.

U. Thiele, M. G. Velarde, K. Neuffer, and Y. Pomeau. Film rupture in the diffuse interface model coupled to hydrodynamics. *Phys. Rev. E*, 64:031602, 2001c.

J. Thomson. On certain curious motions observable at the surface of wine and other alcoholic liquors. *Phil. Mag. Ser. 4*, 10:330–333, 1855.

W. Thomson. On the division of space with minimum partitional area. *Acta Math.*, 11: 121–134, 1887.

C. Tomlinson. On the motion of certain liquids on the surface of water. *Phil. Mag. Ser. 4*, 39:32–48, 1870.

S. M. Troian, E. Herbolzheimer, S. A. Safran, and J. F. Joanny. Fingering instabilities of driven spreading films. *Europhys. Lett.*, 10:25–30, 1989.

M. W. J. van der Wielen, E. P. I. Baars, M. Giesbers, M. A. C. Stuart, and G. J. Fleer. The effect of substrate modification on the ordering and dewetting behavior of thin liquid-crystalline polymer films. *Langmuir*, 16:10137–10143, 2000.

S. J. VanHook, M. F. Schatz, W. D. McCormick, J. B. Swift, and H. L. Swinney. Long-wavelength instability in surface-tension-driven Bénard convection. *Phys. Rev. Lett.*, 75:4397–4400, 1995.

S. J. VanHook, M. F. Schatz, J. B. Swift, W. D. McCormick, and H. L. Swinney. Long-wavelength surface-tension-driven Bénard convection: Experiment and theory. *J. Fluid Mech.*, 345:45–78, 1997.

I. Veretennikov, A. Indeikina, and H.-C. Chang. Front dynamics and fingering of a driven contact line. *J. Fluid Mech.*, 373:81–110, 1998.

A. Vrij. Possible mechanism for the spontaneous rupture of thin free liquid films. *Disc. Faraday Soc.*, 42:23–33, 1966.

R. Xie, A. Karim, J. F. Douglas, C. C. Han, and R. A. Weiss. Spinodal dewetting of thin polymer films. *Phys. Rev. Lett.*, 81:1251–1254, 1998.

Y. Ye and H.-C. Chang. A spectral theory for fingering on a prewetted plane. *Phys. Fluids*, 11:2494–2515, 1999.

R. Yerushalmi-Rozen, T. Kerle, and J. Klein. Alternative dewetting pathways of thin liquid films. *Science*, 285:1254–1256, 1999.

C. S. Yih. Stability of liquid flow down an inclined plane. *Phys. Fluids*, 6:321–334, 1963.

T. Young. An essay on the cohesion of fluids. *Phil. Trans. R. Soc.*, 95:65–87, 1805.

Y. L. Zhang, O. K. Matar, and R. V. Craster. Analysis of tear film rupture: effect of non-newtonian rheology. *J. Colloid Interface Sci.*, 262:130–148, 2003.

D. W. Zheng, W. Wen, and K. N. Tu. Reactive wetting- and dewetting-induced diffusion-limited aggregation. *Phys. Rev. E*, 57:R3719–R3722, 1998.

P. Ziherl, R. Podgornik, and S. Zumer. Pseudo-casimir structural force drives spinodal dewetting in nematic liquid crystals. *Phys. Rev. Lett.*, 84:1228–1231, 2000.